IN VITRO MINERALIZATION MODELS: EXAMINING THE FORMATION OF CALCIUM PHOSPHATES IN A HYDROGEL BASED DOUBLE DIFFUSION SYSTEM

A Dissertation

Presented to the Faculty of the Graduate School

of Cornell University

In Partial Fulfillment of the Requirements for the Degree of

Doctor of Philosophy

by

Jason Richard Dorvee

January 2012

IN VITRO MINERALIZATION MODELS: EXAMINING THE FORMATION OF CALCIUM PHOSPHATES IN A HYDROGEL BASED DOUBLE DIFFUSION SYSTEM

Jason Richard Dorvee, Ph. D.

Cornell University 2012

In biomineralization, both crystal nucleation and growth are under tight regulation. The components required for biomineralization are: the controlled delivery of reagents required for crystal growth to the site of mineralization, a nucleating substrate, a growth medium (often a hydrogel-like matrix), and growth-modifying elements (often acidic biomacromolecules). Using synthetic analogs of components found in biology, *in vitro* models can be created to study various aspects of biomineralization. Depending on what one wants to model, the type of in vitro system can vary greatly: from solution growth of hydroxyapatite using a constant composition set-up, to *in vitro* mineralization using cells, to synthetic growth in hydrogels. Traditionally, crystal growth in hydrogels is a technique used by crystallographers to grow large crystals. For those seeking to model biomineralization, hydrogels are also excellent models of the extracellular matrix (ECM) microenvironment.

In this thesis, I use an optimized hydrogel-based double diffusion system (DDS) (Chapt. 1) to explore interesting questions in biomineralization such as: What are the effects of various types of hydrogels (in which ions have different diffusivities) on both the crystal morphology and degree of mineralization in an environment where the rate of diffusion is controlled by changing the experimental setup (Chap. 2)? What

is the role of substrates in mineralization within an ECM-like matrix, and how can such a substrate be fabricated and introduced into a hydrogel-based DDS (Chap. 3)? What are the effects regulating gradients of inhibitors, using enzymes strategically placed in a DDS, on mineral formation within an ECM-like environment (Chap. 4)?

By evaluating the DDS in the context of classical diffusion theory, an optimized system was designed and tested (Chap. 1). Using an innovative layered hydrogel design, differences in ion diffusivities within different hydrogels were eliminated. These experiments showed that both collagen and gelatin gels produce similar crystal morphology, while both agarose and collagen have increased mineral content over that of gelatin (Chap. 2). Placing porous silicon substrates into the DDS, revealed that cooperative behavior of proteins and substrates has an effect on both the morphology and the quantity of mineral in the hydrogel (Chap. 3). Finally, by modulating a gradient of mineral inhibitors, mineral gradients within the hydrogel are formed. The resulting "sharpness" in the mineral/hydrogel interface is proportional to the steepness of the inhibitor gradient (Chap. 4). Taken together these results provide insight into the formation of calcium phosphate in biological systems.

BIOGRAPHICAL SKETCH

Jason Richard Dorvee was born in Glens Falls NY on November 24, 1979, and was raised in Carlsbad, CA. Jason graduated from Guajome Park Academy in Vista CA, in 1998, as salutatorian and president of his high school senior class. In the fall of 1998 Jason started his long college career at the University of California San Diego where for his undergraduate thesis he wrote *A Getting-Started-Guide For Project Management & Systems Engineering In Space Science and Engineering* under the mentorship of Dr. James Arnold. In 2003 he obtained a BS in Biochemistry and a BA in Space Science and Systems Engineering, from UC San Diego. Jason continued his studies at UC San Diego in the department of chemistry under Dr. Michael Sailor, and received an MS in Chemistry in 2005 where the focus of his thesis was on *Digital Microfluidics Based on Magnetic, Amphiphilic 1-D Porous Silicon Photonic Crystal Microparticles*. Jason also obtained three patents during this period. In 2005 Jason began attending Cornell University and joined the Estroff Group in the department of material science and engineering. In 2009 Jason received his second MS this time in Material Science and Engineering and in August 2011 Jason defended his dissertation for a PhD in Material Science and Engineering, specializing in studies in biomineralization. Jason has received and post-doctoral fellowship at Northwestern University's Feinberg School of Medicine under Dr. Arthur Veis. At Northwestern Jason will be the last post-doctoral fellow to participate in the NIH funded 2R01DE001374-50, Matrix Component Interactions in Bone, Dentin and Invertebrate Mineral, from the National Institute for Dental and Craniofacial Research, which has had the distinction of having the longest record of continuous NIDCR support.

ACKNOWLEDGMENTS

To my Mom (Barabara Dorvee) and Dad (Louis Caterina) for all their support and advice for each and every avenue I have decided to pursue in life. And to Massimo and Atrina, for their comfort and support all through the writing process.

I'd like to thank Dr. Lara Estroff and Dr. Adele Boskey for guidance, mentorship and funding for these six long years.

I'd also like to thank the following agencies for support and funding for these projects: NBTC Seed Grants (NSF-STC), Cornell Center for Materials Research Seed Grant (NSF-DMR), J.D. Watson Young Investigator Award (NYSTAR) and the Weill-Ithaca Seed Funding.

TABLE OF CONTENTS

LIST OF FIGURES

LIST OF TABLES

LIST OF ABBREVIATIONS

AA = Atomic Absorption

ACP = Amorphous Calcium Phosphate

BSP = Bone-Sialoprotein

BSA = Bovine Serum Albumin

cm = centimeter

CPPx = Calcium Pyrophosphate Hydrate

DD = Double Diffusion

DDS = Double Diffusion System

DI = Deionized

ECM = Extracellular Matrix

FE-SEM = Field Emission Scanning Electron Microscope

FTIR-ATR = Fourier Transform InfraRed Attenuated Total Reflectance

HA = Hydroxyapatite

hr = hours

Hz = Hetz

ICP-AES= Ion Coupled Plasma-Atomic Emission Spectrometry

ID = Inside Diameter

kV = KiloVolts

L = liter

pXRD = Powder X-ray Diffraction

mA = milliAmperes

microCT or μCT = Micron resolution Computer Aided Tomography

min = minutes

mL = milliliter

mm = millimeter

mM = millimolar

mmol = millimol

mol = mole

OCP = Octacalcium Phosphate

OD = Outside Diameter

OPN = Osteopontin

Pi = Inorganic Phosphate

PPi = Pyrophosphate

ppm = parts-per-million

pSi = Porous Silicon

PVC = Poly-Vinyl Chloride

SAMs = Self-Assembled Monolayers

SBF = Simulated Body Fluid

SD = Single Diffusion

SDS = Single Diffusion System

Tris = tris(hydroxymethyl)aminomethane

LIST OF SYMBOLS

D = Diffusivity or Diffusion Constant

°C = Degrees in celcius

c = concentration

c_0 = concentration

Δc_0 = starting concentration

IP = Ion-product

k_B = Boltzmann's constant

Ksp = dissolution/solubility constant defined at solid product over the reactants

L = pathlength

pH = -log of the concentration of hydrogen ions as measured in moles/liter

s = seconds

σ = supersaturation as determined by the natural log of the ion-product over the Ksp

T = Temperature in Kelvin

t = time

t_0 = start-time

Δt_0 = change in the start-time

μ = chemical potential

$\Delta\mu$ = change in chemical potential

x = a location

x_0 = starting location

Δx_0 = change starting location

PREFACE

Biomineralization is the formation of a mineral by an organism. The intervention of the organism in selecting, acquiring and sequestering ions, ultimately leads to the control of the: size shape, crystal structure and mechanical properties of the particular mineral formed.[1] Formation of biominerals take place in a controlled environment where ions and growth modifiers are delivered to a site of nucleation, dictating the phase, habit and morphology of the mineral being formed. The organic components responsible for the nucleation and directed growth of these minerals can become occluded into the mineral, creating composite materials. The resulting phase, morphology and hierarchal structure of these organic-mineral composites have specific structural and mechanical properties. These specific mechanical properties lead to specified functional roles for these biological composites. In much the same way that the underlying property of materials, in general, are the result bond-types dictating structure, structure dictating function and function dictating application/use; in biological systems the mineralizing environment, be it cellular or extracellular, dictates structure which ultimately dictates function and the application of the material by the organism.

An example of biology's role as a materials engineer can be seen in the construction of tissues such as bone and teeth. The feline (mammalian) tooth is an example of a discontinuous reinforced biological composite. Discontinuous reinforced composites offer a high degree of latitude in changing the component geometry and

dimensions, thus allowing the material to respond to changing environments. In a brief examination of a feline incisor where the surface mineral of the tooth is quickly etched in 0.8 M HNO_3 solution for 15 to 20 seconds, the differences in the underlying structure of this biological composite can be seen. Both the enamel layer (covering of the exposed tooth) and the dentin layer (inside of the tooth) have differing fundamental structures (Fig. 0.1). As can be seen (Fig. 0.1), the covering of the exposed tooth or working end of the tooth is mostly mineral (96-98 wt%). The mineral component is shaped into elongated prismatic-like structures (sometimes characterized as fiber-like) with high aspect ratios and very little organic material, which results in a Mohs hardness ~5. The covering of the exposed tooth, the enamel component is responsible for the tooth's ability to cut, crush, tear and generally interact with the environment in which the organism exists. In contrast, the inside of the tooth, the dentin component, is composed of a network of collagen fibers loosely packed together and mineralized throughout, with more organic content than what is found in enamel (30-40 wt%), yield a Mohs hardness of 3 to 4. In each region, the morphology of the hydroxyapatite (HA) mineral is also different, with the crystals in the enamel layer having prismatic character and the crystals imbedded in the collagen fibers of the dentin layer having a more plate-like character, which is similar to bone. Though the stark contrast of mineral morphology and mineralized structure seen in the tooth is not commonly found in other mineralized tissues, the discontinuous composite design is the principle design in most mineral tissues (such as bone) found in vertebrates.

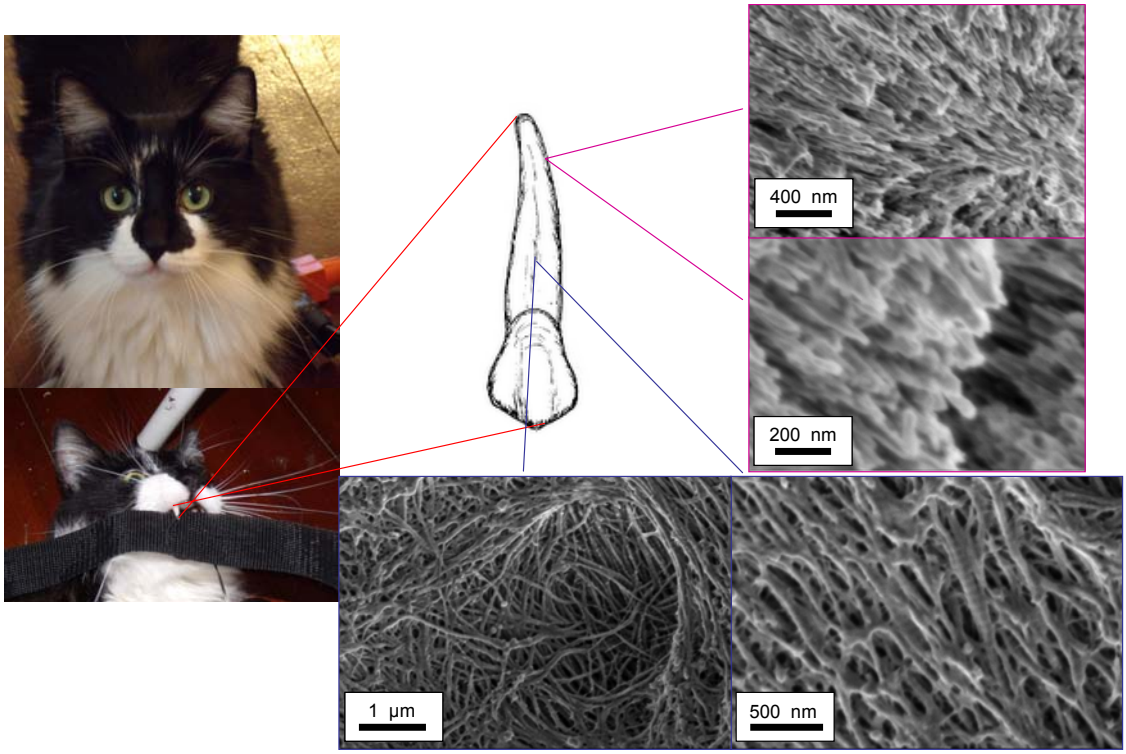

Figure 0.1 Photographic, schematic and (a-d) FE-SEM of a images domestic feline, incisor tooth. The (a. & b.) acid etched enamel layer shows a sires of HA prisms stacked together to form the stiff outer layer of the tooth. The (c. & d.) acid etched dentin layer reveals a different structure than the enamel layer, with network of collagen fibers that are mineralized to form the support structure of the tooth and a relatively more compliant inner layer.

The fabrication of these mineralized structures, which dictate the function of the mineralized tissue/material, is determined by the specialized nature of the extracellular-matrix (ECM) in which they are formed. Both dentin and enamel for example, are formed in their own ECM, other tissues such as bone are also formed in their own specialized ECM. The ECM, by definition, is the environment in which the cell exists. It is in this microenvironment in which the cell acts and works, creating the tissue vital to the existence and survival of the organism as a whole.

In terms of the role of the ECM in directing mineralization, the following sequence of events occurs:

1. Individual/aggregates of cells control their immediate environment making use of biomacromolecules such as: proteoglycans, collagen, acidic proteins, fibronectin etc. as an external extension of their intracellular matrix.

2. The structured matrix created by the cell(s) defines the space/microenvironment to be mineralized, providing both a nucleating substrate and medium in which the mineral can grow.

3. The microenviroment is then "activate" to initialize some sort of construction/transformation, in the case of mineralization, these activators come in the form of matrix and/mineral interactive molecules. These molecules trigger crystal nucleation and subsequently the same and/or additional molecules facilitate and/or modify crystal growth.

4. Mineral ions for crystal growth are introduced into the microenvironment via diffusion (single ions or ion clusters), matrix vesicles (packets of ions or clusters), etc. These ions then nucleate to form mineral, and ions subsequently added to the system are added to the growing mineral.

5. Finally, crystal shape, size and the mineralized tissue boundaries are restricted by either compartment walls or the introduction of inhibitors to crystal growth; to halt or define the edge of the mineralized tissue region.

The specifics for each tissue, each mineral and each organism of course vary, but the generalized components remain. Much, however, remains unknown about the role of the ECM in directly biomineralization. For example: What is it about this specialized environment that facilitates the fabrication of mineral and mineralized tissues? How are the nutrients/ions of mineral formation delivered? How does mineralization start? What dictates the morphologies of the mineralized structures? How is mineralization stopped? What regulates which areas mineralize and which areas do not?

Discerning both the role and the combined effects of these various specific extracellular components for a given system and a given mineral is the goal of this thesis. Previous works have isolated and focused on the contribution individual components with regards to their inhibition or promotion of mineralization. The aim of this thesis is to combine various, well-studied, and already established components and synthetic analogs into *in vitro* models to examine how these components come together and affect mineralization

CHAPTER 1

(Planned for submission to CrystEngComm as a Higlight article 2011/2012)

1 Rediscovering Hydrogel-Based Double-Diffusion Systems for Studying Biomineralization

1.1 Introduction

A challenge in the field of biomineralization is identifying the appropriate *in vitro* model for studying a particular mineralization phenomenon. Depending on what aspects of the process one wants to model, the type of *in vitro* system can vary greatly: from solution growth of hydroxyapatite (HA) using a constant composition set-up,[2, 3] to *in vitro* mineralization using cells,[4] to growth in hydrogels.[5-7] Traditionally, crystal growth in hydrogels is a technique used by crystallographers to grow large crystals [8]and to study how those crystals grow within a hydrogel matrix, sometimes as a function of time.[9] For those seeking to model biomineralization, hydrogels are excellent models of the extracellular matrix (ECM) microenvironment. For example, when proteins are incorporated into gel-based assays, their function can more closely mimic the behavior found in a biological system, as compared to more standard solution-based assays.[7] In one example, the introduction of recombinant amelogenin, a protein found in immature enamel, into a hydrogel matrix led to the growth of high-aspect ratio octacalcium phosphate (OCP) crystals, which were elongated in the direction of ion flow.[10, 11] In other reports, the integration of ostepontin (OPN) into a gelatin hydrogel revealed that both the concentration of OPN and the degree of phosphorylation of OPN, affected the protein's role as either an inhibitor or a promoter of mineralization.[7, 12, 13]

Finally, the mineralization activity of bone-sialoprotein (BSP) was compared with that of a modified BSP, which lacked the collagen binding domain.[14] The unmodified BSP was a stronger promoter of hydroxyapatite (HA) formation in a collagen hydrogel, suggesting that the binding of BSP to collagen contributed to its function in mineralization. All of these examples demonstrate the potential of hydrogel-based systems for developing *in vitro* models of the biomineralization processes in bone and teeth.

We have recently sought to expand the diversity of experiments that can be performed using a double diffusion system (DDS) to study the mineralization in an ECM-like environment.[15] In our explorations we quickly discovered, as with most *in vitro* models for mineralization, the challenge and complexity[16] in creating and building such a system. We also discovered the difficulty in trying to use these types of systems for applications beyond their original purpose. It is this very issue that has motivated this "highlight" and the experimental results presented herein.

Several different hydrogel-based DDSs for studying the formation of calcium phosphate minerals have been described in the literature,[7, 9, 17-20] and their results have been reviewed elsewhere.[7] It is difficult, however, to compare the performances of these systems because of a lack of information in the literature with regards to the design specifications of each system, and how or why these DDSs and their applications differ from each other. Furthermore, not all designs detail the relationships among the specific components of each system and the corresponding diffusion theory or why those components were chosen for a given experimental application. In addition, there are unexplained variations in the reaction times for each system, as well as how each system is used in its application.[7] Here, we demonstrate that when four representative systems

are examined in the context of fundamental diffusion theory,[21-24] even though they differ in their specific application, there is no difference in the techniques required to evaluate them. By identifying and understanding the diffusion theory that is common to all systems, we can now compare and evaluate these systems across the different designs, applications, and fundamental research objectives. In addition to analyzing examples from the literature, we conclude by presenting a series of evaluation strategies for the design and testing of DDSs for future studies in biomineralization.

1.2 Types of Hydrogel-Based Double Diffusion Systems

In this work we focus on passive DDSs, i.e., systems that rely on differences in chemical potential for diffusion. Passive DDSs can be separated into two categories: static and dynamic (Table 1.1). The primary variable between these two categories is the length of the gel and it's relation to the timescale of the experiment. We will describe the construction of both types of systems and their respective advantages and disadvantages for a range of applications. It should be noted that any of these passive systems can be modified to perform as active diffusion systems with the introduction of external forces such as an electric field.[25-27]

In general, the main components of any hydrogel-based DDS are a hydrogel and opposing sources (reservoirs) of ions on either side of the gel. The hydrogel becomes the medium through which ions diffuse (creating an ion gradient), and in which mineralization takes place (Figure 1.1). The physical details of a system (e.g., the path length, the capacity of the reservoirs, the reagent concentrations) all contribute to defining the boundary conditions (Table 1.1). Differences in boundary conditions and system variables change how a particular diffusion system is evaluated (mathematically)

Table 1-1: The key physical differences between static and dynamic. See Fig. 1.1 for further details.

Elements	Static Diffusion System	Dynamic Diffusion System
Path Length of hydrogel (*L*)	*L* is sufficiently small that steady state is reached relatively quickly.	*L* is sufficiently large that steady state is not reached within the time frame of the experiment.
Reagent Concentrations	Concentration *c* of reagents in the hydrogel is constant at a given point *x* for all time $t >> L^2/D$. The flux *j* of reagents through the hydrogel is constant.	Concentration *c* of reactants in the hydrogel is always changing for a given point *x* for all time *t*. The flux *j* of the reagents through the is not constant
Reservoirs	Since the concentration *c* of reagents at any point in the hydrogel is constant, the reservoirs act as "reserves" for the reagents in the hydrogel.	Since the *c* of reagents at any point in the hydrogel is always changing, the reservoirs act as sources of reagents moving into the hydrogel.
Supersaturation Threshold	Operates at either sub or super threshold.	Operates through the threshold window.
Concentration Gradients	Steady state flux *j* provides a linear concentration gradient of reactants throughout the gel that does not change with time.	Concentration gradients of the reactants within the hydrogel are dynamic (flux *j* of reactants in, out and throughout the hydrogel is not constant) and changes with time.

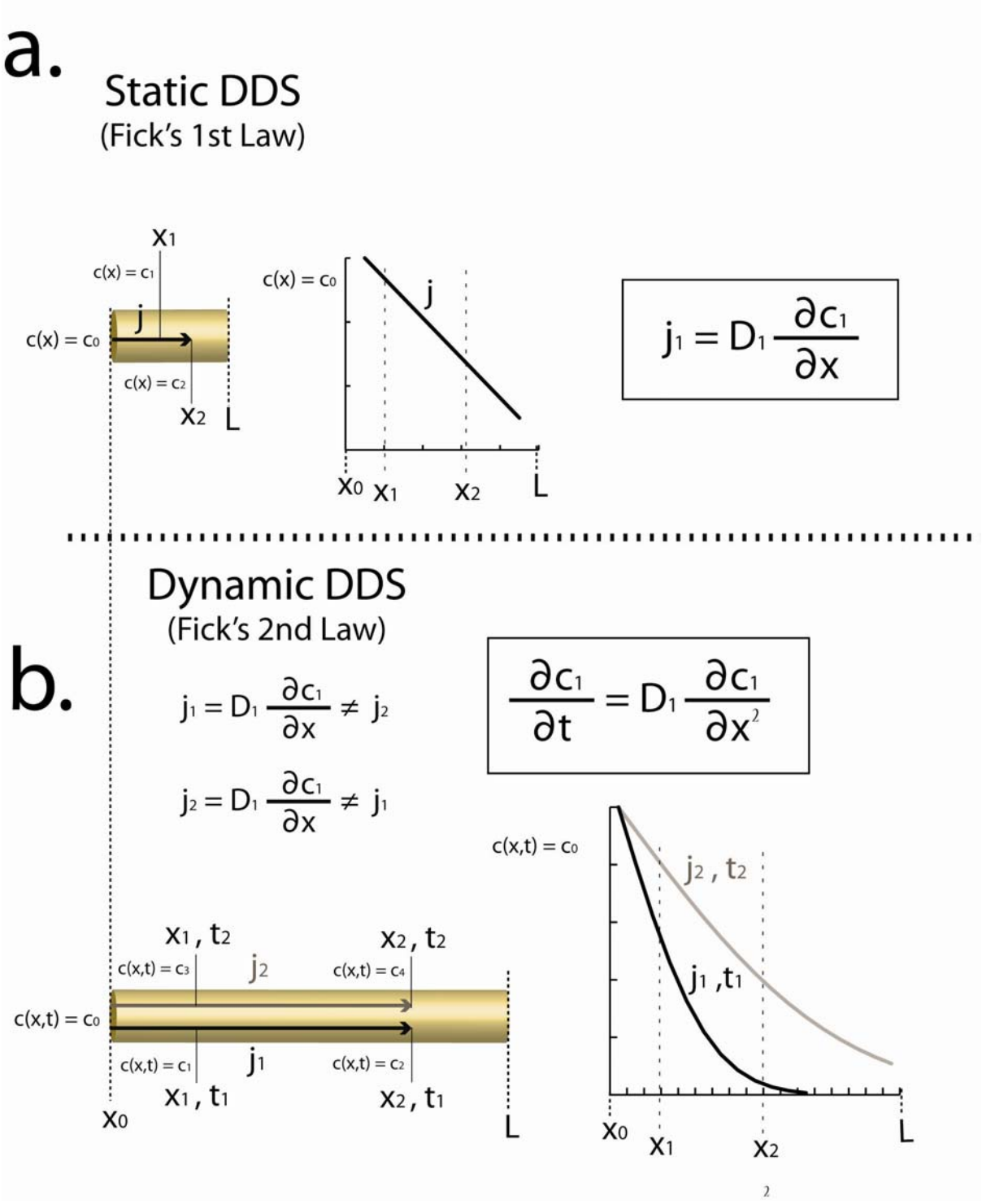

Figure 1.1 Representative illustrations of gels used in both static and dynamic double diffusion systems (DDS), the corresponding Fickian relations, and the characteristic plots of concentration *c* vs. position *x*. a) Static DDSs utilize Fick's 1st law, where the flux *j* of ions is constant and the concentration *c* only varies with the position *x*. b) Dynamic DDSs utilize Fick's 2nd law, where the flux changes with time and therefore the concentration *c* changes with both the position *x* and the time *t*.

and how a diffusion system is used (experimentally). As we go through each example from the literature, we will highlight both the mathematical and experimental treatment of the system.

1.2.1 Static Systems

Static diffusion systems, such as those employed by Ijima and Oldak [18, 28-31] and Hunter and Goldberg,[5, 6, 18, 28-31] rely on the hydrogel being immediately brought to equilibrium (from the start of, or early in the timeframe of the experiment) with the ion(s) kept in reserve in the reservoirs (Fig. 1.1a). In other words, the flux of ions into and out of the gel reaches a steady or static state. [18, 19, 24, 28-31] One of the keys to creating a static DDS is restricting the length of the gel to a size such that the time it takes to reach a steady state condition, with respect to ion diffusion, is reached relatively quickly with respect to the overall time frame of the experiment. The defining moment when steady state is achieved occurs when the relaxation time τ (in seconds) is much greater than the length of the sample L squared (in centimeters) divided by the minimum diffusivity (Eq. 1.1).[24, 32]

$$\tau >> L^2/D_{min} \quad \text{(Eq. 1.1)}$$

Since the value of D for small ions in gels is typically on the order of 10^{-5}-10^{-6}cm^2/s, [5-7, 12, 13, 17, 18, 29-31, 33-38] only L can be varied such that the time τ required to reach steady state becomes very small.

The governing law for the movement of materials in a static diffusion system is Fick's 1st Law (Eq. 1.2); time is not a factor because steady state is reached early on in the experiment. As such, the flux j is dependent simply on the diffusivity, D, of the

diffusing species and the change in concentration, c, over the change in distance from the source, x (Fig. 1.1a and Eq. 1.2).

$$j_1 = -D_1 \frac{\partial c_1}{\partial x} \qquad \text{(Eq. 1.2)}$$

Accordingly, the value of c only changes within the hydrogel with distance from the source, not with time (Fig. 1.1a). The steepness of the resulting linear concentration gradient is dependent on the total length of the hydrogel from x_0 to L. The longer the length of the gel the more gradual the concentration gradient becomes. In contrast, the shorter the gel the steeper the concentration gradient will be. There are cases of static DDSs where the path length of the gel is so small that there is essentially no flux through the gel, because the concentration of ions in the gel has reached the same concentration of ions in the reservoir.

If x is sufficiently small (and D of an ion within the hydrogel is smaller than D of an ion outside the hydrogel) the system reaches equilibrium quickly and the flux of reactant, j throughout the length of the gel from x_0 to L becomes zero. In cases where the source concentration of the diffusing species is exceptionally high and the length of the gel is exceptionally small:

- flux into the gel is zero (flux j from $x < x_0$ to $x = x_0$ is zero)
- flux through the gel is zero (flux j from $x = x_0$ to $x = L$ is zero)
- flux out of the gel is high (flux j from $x = L$ to $x > L$ is not zero).

In this sense the small value of L for the system allows for the gel to be treated as a membrane.[23]

Precipitation in a static DDS can occur at either sub-threshold or super-threshold

levels, depending on how the system is designed and whether nucleation or growth is being studied. A sub-threshold level[6] is when the supersaturation, with respect to precipitation in the gel, is so low that it can be used to study heterogeneous nucleation and growth. A sub-threshold level can be described as a pre-nucleation supersaturation, where homogeneous (spontaneous) nucleation is not the governing nucleation mechanism and only mineralization promoters can trigger nucleation. In contrast, a super-threshold level[6] is achieved when the supersaturation with respect to precipitation in the gel is high enough that it can be used to study the growth of crystals by providing a system where they are guaranteed to nucleate and grow, without the need for seed crystals or mineralization promoters. Since at a super-threshold level, nucleation always occurs, only the degree of mineralization and the effects of additives on growth modification can be observed.

1.2.1.1 The Dual-Membrane Nested Tube Static DDS

The Dual-Membrane Nested Tube static DDS (Fig. 1.2) was designed to study the effects of ionic flow on crystal growth.[11, 39, 40] By using a cation selective membrane on one side of the gel chamber, directional ion flow is obtained. In the absence of any additives, elongated OCP crystals form with their long-axis parallel to the direction of the ionic flow.[41] The same system was later adopted to study the effects of small quantities of proteins and gels on crystal growth, without first inoculating the gel with seed crystals.[10, 11, 19, 41-46] For example, the system was used to study the effects of recombinant amelogenins on the crystal morphology of OCP. Amelogenins were found to limit the growth in the *ab* directions, leading to rod-like, as compared to plate-like, OCP crystals. It is important to note that the final crystal morphology is a result of both the membrane- directed ion flow, which gives elongated crystals, and the hydrogels or the

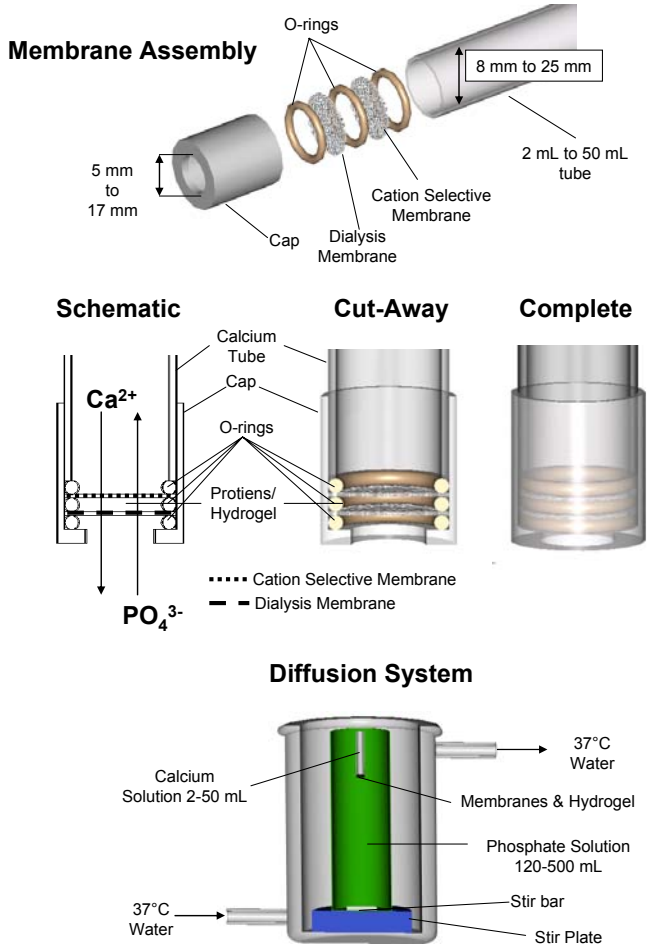

Figure 1.2 The Static Dual-Membrane Nested Tube DDS is used to study the effect various hydrogels have on the growth of calcium phosphate crystals. The nested tube design has a calcium reservoir nested within a phosphate reservoir, with the 15µL hydrogel separated from the two reservoirs by a dialysis or ion-exchange membrane. Both reservoirs are set at a fixed volume and concentration (5-10mM) at the beginning of the experiment, while the reaction occurs at 37°C. The concentrations of the reservoirs are set at levels such that the supersaturation threshold condition is exceeded. The types of gels used in this system have included: Gelatin (bovine skin collagen, Type B 75 Bloom), Bovine Serum Albumin, Polyacryl-amide, Agarose, Enamel matrix proteins (1,5,10% amelogenins in solution)[10, 11, 19, 39-42, 44-46]

proteins, which are responsible for modifications of the relative dimensions of the crystals.

From an engineering perspective, the design of the Dual-Membrane Nested Tube static DDS is relatively straightforward. At its core, the design is simply a tube placed inside a larger tube with an end of the smaller tube capped by a gel encased between two

different membranes. The membranes are held in place with silicone o-rings and a plastic cap that locks the membranes in place. The larger tube is filled with phosphate and the smaller tube is filled with calcium. The specific system used by Iijima and Oldak [10, 40, 42, 44-46] to study amelogenin gels is a bit more intricate and includes: a dialysis membrane (phosphate side), a cation-selective membrane (calcium side), a jacket on the larger tube to maintain a specific temperature, a stir bar in the larger tube (120 mL bottle) to create turbulent mixing, and a floating, smaller tube (2 mL bottle) inside the larger tube, much like a dialysis cassette in a large beaker. Some important points to consider that may affect mineralization studies in this system:

1. Since the system operates at super-threshold conditions, mineral formation is not confined to the gel. Mineral can and does form on the exterior of the membranes.
2. As a result of the design one or both of the ion reservoirs must be considered finite, creating an "infinite" reservoir source with this design is difficult to achieve (Section 1.3.3.2).
3. Since the gel is only 15 μL in volume:
    i. Only a small amount of mineral is available for study.
    ii. The resulting path length (300-750 microns) is so small that it is difficult to discern if a precipitation has taken place.
4. The solution concentrations/ratios and pH conditions used by Ijima and Oldak only facilitate the formation of OCP and do not readily allow for the creation of HA in this system.

1.2.1.2 The Flowing Infinite Reservoir Static DDS

The Flowing Infinite Reservoir static DDS (Fig. 3), is a modified version of the

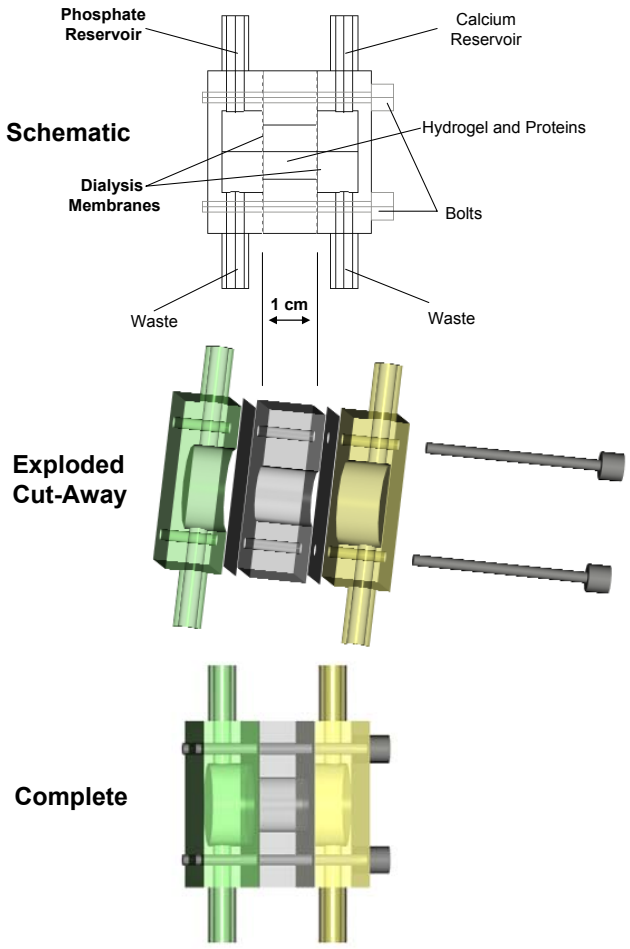

Figure 1.3 The Flowing Infinite Reservoir DDS is used to study the effects extracellular matrix molecules on the nucleation of hydroxyapatite crystals. With an infinite reservoir design both the phosphate and calcium reservoirs are cycled using peristaltic pumps (1 per set of 3 assemblies) along the opposite boundaries of three separate 1 cm long hydrogels. As the solution from the reservoirs flow past the hydrogel interface they empty into a waste collector at 1mL/h per gel. The hydrogel is maintained in a steady state condition by the two reservoirs with a calcium concentration of 5.5-7.5mM and a phosphate concentration of 5.5-7.5mM. The interface between the hydrogel and the reservoirs is separated by dialysis membranes to keep target proteins within the hydrogel. The reaction takes place over the course of 5 days at pH 7.4 (Tris-buffer) and at 37°C.[18, 29-31]

design by De Jong et al.[47] where the acrylamide film (using in the original design) is replaced by a hydrogel. Since the diffusing solutions are maintained at constant composition by using a flow-through, rather than a circulating reservoir design, this type

of DDS is most closely related to the constant composition systems used for solution-based mineralization studies.[2, 3] This type of system is used to determine whether or not particular extracellular matrix molecules promote or inhibit mineralization in various kinds of hydrogels.[18, 28-31] Utilizing two different hydrogels (agarose and collagen) with similar ion diffusivities[6] and similar level of stability at 37°C, Hunter and Goldberg were able to examine the contribution of binding BSP to collagen on the ability of BSP to promote mineralization.[14] Placing modified BSP without the collagen binding domain in both collagen and agarose produced the same effect, while unmodified BSP (with collagen binding domain) showed a greater ability to mineralization in collagen over agarose.

Of the two static systems presented here, from a fabrication standpoint, the Flowing Infinite Reservoir static design is perhaps the easiest to build. A delivery chamber is essentially fastened to either side of a dialysis cassette and a peristaltic pump is attached to each delivery chamber. The ions (calcium or phosphate) flow into each delivery chamber at a rate slow enough to fill the chamber so that there is a continuous solution/membrane interface but fast enough that the solution is not depleted of ions before it is replaced by new solution. These assemblies are small enough that they can be placed in an incubator, which makes it possible to regulate the temperature. The design used by Hunter and Goldberg is a specifically fabricated mold for the gel, made from a machinable plastic that is chemically modified with silanes to assure good gel adhesion to the chamber and then capped at either end with a dialysis membrane before the solution delivery chambers are attached.[48]

Some important points to consider that may affect mineralization studies in this system:

1. The gel is cast between dialysis membranes to insure that the proteins placed in the hydrogel do not diffuse out of the gel.
2. This system has been designed to primarily operate at sub-threshold conditions. The system can be used to determine whether or not an additive promotes HA formation in a hydrogel, but it is difficult to determine whether or not an additive inhibits HA formation.
3. This system can be operated at super-threshold conditions to elucidate the degree of mineralization induced by additives. Under these conditions, however, it would be difficult to determine whether or not those additives are responsible for triggering the mineralization event.

1.2.2 Dynamic Systems

Dynamic double-diffusion systems (see Figure 1.1b and Table 1.1), such as those used by Boskey [4, 12, 13, 17, 33-38] and Mandel,[9, 49-55] have long sample path lengths L and reservoirs that act as sources of reactants for the hydrogel.[17] In dynamic systems, the path length L of the hydrogel is sufficiently large that steady state is not reached within the time frame t of the experiment. Concentration gradients of the reactants within the hydrogel are dynamic (flux of reactants in and out of the hydrogel is not constant) and the concentrations of reactants in the hydrogel are less than the initial concentrations in the reservoirs. Since the flux of material is itself variable, the governing law for the movement of material is Fick's 2nd Law (the derivative of Fick's 1st Law (Eq. 1.2) with respect to x), where the flux j is itself changing at a given point x during t_1 to t_2 (Fig. 1.1b and Eq. 1.3).

$$j_{i(1)} = -D_i \frac{\partial c_{i(1)}}{\partial x} \neq j_{i(2)}$$

$$j_{i(2)} = -D_i \frac{\partial c_{i(2)}}{\partial x} \neq j_{i(1)}$$

$$j_{i(1)} - j_{i(2)} = \frac{\partial c_{i(1)}}{\partial x} - \frac{\partial c_{i(2)}}{\partial x} = \Delta x \frac{\partial c_i}{\partial t} \qquad \text{(Eq. 1.3)}$$

$$\Delta x \frac{\partial c_i}{\partial t} = \frac{\partial j_i}{\partial x} = \frac{\partial}{\partial x} \; D \; \frac{\partial c_i}{\partial x}$$

$$\frac{\partial c_i}{\partial t} = D_i \quad \frac{\partial^2 c_i}{\partial x^2}$$

A dynamic DDS operates across the supersaturation threshold window (from sub-threshold to super-threshold) because the value of the ion product at a particular position *x* evolves over the course of the experiment. In both static and dynamic systems, precipitation events in the gel are used as 'self-checks' to assure that the system is working properly (both static and dynamic systems). Since the precipitation event in a dynamic DDS cannot be set to 'on' or 'off' at the start of the experiment, like a steady state (static) system, the ability to predict or even program the timing of such an event in a dynamic DDS is important. When and where these precipitation events appear within the hydrogel can be programmed into the design of the system (using both the initial conditions and the boundary conditions).

1.2.2.1 Thin Film Source Dynamic DDS

The Thin Film Source dynamic DDS, [9, 49-55] Mandel is the easiest dynamic design to fabricate (Fig. 1.4) and was adapted from a classical method for growing crystals for crystallography.[8, 56-59]

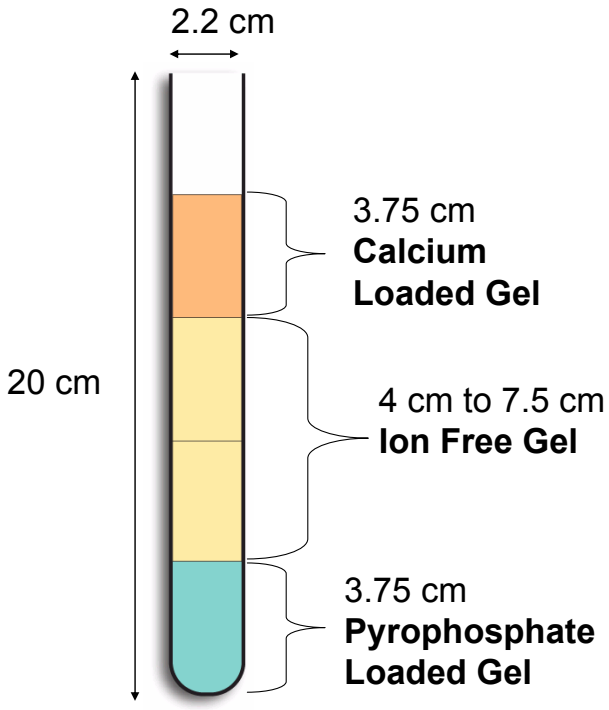

Figure 1.4 The Thin Film Source DDS was used to examine the evolution of calcium pyrophosphate growth given various changes in mineralization conditions such as path length, pH (6-8), and starting concentrations. Experiments were run in test tubes 22mm x 200mm, with four layers of gel (275 Bloom gelatin 3-15% w/v), ~15mL in volume (unless otherwise specified). One layer at either end serves as thin film sources for the ions of (calcium and pyrophosphate, 0.001-0.1M) in the experiment with two ion-free layers of gel in the middle dictating the path length. [9, 49-55]

Layers of gel with and without ions are cast into a laboratory test-tube. The layers at either end serve as thin film sources for the ions with an ion-free layer in the middle dictating the path length. This design allows for modular changes to the system, where sections of gel can be added or substituted with various ions, molecules, or even different pH values. Once set, the system is left to drift towards equilibrium. The precipitation reactions take place over the course of several days to months. With this type of dynamic DDS, Mandel was able to produce a map of various polymorphs of calcium pyrophosphate as a function of both time and position within the hydrogel.

Some important points that should be considered when using this type of system:

1. The system originally used gelatin as the principle hydrogel, but the

uncomplicated design allows for the substitution of various kinds of hydrogels.

2. This type of experiment uses thin layers of ion-doped gelatin acting as "thin-film" finite reservoir sources, and as a result, the value of c_0 in those thin films diminishes over time, thus reducing the rate of ion diffusion over time, and leading to long experimental times (weeks to months).
3. The fundamental design of the system allows it to be setup and left alone, without the need to monitor reservoirs, pumps, etc.
4. The original system was designed to operate between 5-25°C but these experiments could be done at higher temperatures if a gel other than gelatin was used.

1.2.2.2 Circulating Semi-Infinite Reservoir Dynamic DDS

The Circulating Semi-Infinite Reservoir dynamic DDS [7, 12, 13, 17, 33-38] is designed to investigate the role of small amounts of non-collagenous proteins on the initiation of mineralization as well as their effect on seeded crystal growth in mineralization within a gelatin hydrogel (Fig. 1.5). The system has also been carefully designed and tested to predictably and reproducibly grow HA crystals, rather than any of

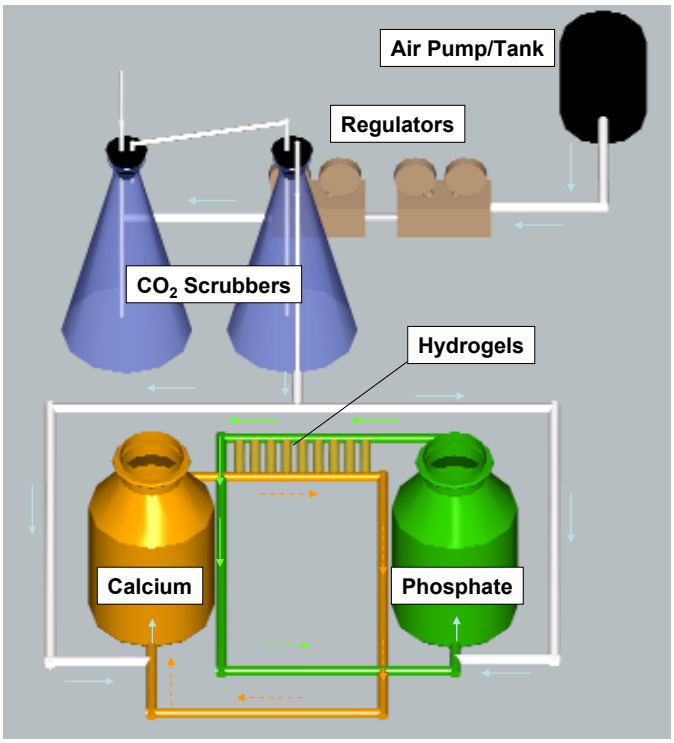

Figure 1.5 The Circulating Semi-Infinite Reservoir DDS, is used to study the effect of biomacromolecules sandwiched in a 10 w/v % gelatin hydrogel on the nucleation and growth of hydroxyapatite. 3 mL of a 10% w/v 275 Bloom Type A gelatin hydrogel in a pH 7.4 Tris buffer is cast into a 6 cm long pipette tube set between two 3-4 L reservoirs of constant volume. Each 3-4 L reservoir is circulated and degassed using either dry, CO_2 scrubbed air or compressed nitrogen, to maintain a constant concentration of 100 mM calcium and 100 mM phosphate. Each reservoir and ion circuit are of sufficient volume that they can be modeled as semi-infinite sources in the time frame of the 5 day experiment. The circuit tubing is constructed of vinyl tubing with polypropylene connectors. The connection of the gel tubes to the circuit are made with thin walled vinyl tubing that is pre-stretched to provide a snug connection with the larger diameter gel filled diffusion tube. [12, 13, 17, 33-38]

the other calcium phosphate phases often encountered in such systems. In this system the hydrogel matrix not only serves as a mineralizing environment, but also as a means to regulate ion delivery via diffusion, with the mineralization space making up only 5% of the total volume of the gel. Taking advantage of the ability to target the location of mineralization, this system has been used to examine the role of various biomacromolecules such as: lipids, matrix vesicles,[7, 13, 34, 35] proteoglycans,[38] collagen fibrils,[17] OPN,[12, 13] and other noncollagenous proteins.[12, 33, 36]

Of all the systems presented in this paper, this one is the most complicated from the standpoint of both engineering and fabrication. Essentially the design of the Circulating Semi-Infinite Reservoir dynamic DDS can be viewed as multiple Flowing Infinite Reservoir static DDS stacked in parallel, with longer gels and a circulating, rather than flow-through, reservoir configuration. Two large vessels, 3-4 L (glass bottles with hose barbs), are constantly circulated with compressed air or an air pump piped into the fluid circuit, with the bubbles taking the shortest path to flow into the reservoirs and venting out through the vessels. The movement of each discrete air-bubble packet pulls fluid along a short path and draws the solution through the circuit into the reservoir vessels creating a turbulent, semi-infinite reservoir system, while at the same time scrubbing CO_2 out of the solution. The original system was designed to hold 18 gels for a single set of experiments connected to the reservoirs through a circuit of flexible tubing. The casting of the gels, is perhaps the most user-friendly part of the design. The gelatin solution is loaded into tubes cut from plastic pipettes which provide built in graduation marks that aide in the mapping of both ion and mineral gradients. The tubes are filled with one end capped by a small plastic disc and parafilm. Once the gels are cast, the parafilm caps are removed from the tubes and the tubes can be placed on the diffusion system. The layered gel strategy as used by Mandel, described in Fig. 1.4 is employed to make gels loaded with proteins at specified locations for mineralization.

Some important points that should be considered when using this type of system:

1. As is expected with a dynamic DDS the onset of the mineralization process is longer than a static system, with mineralization starting around 3 days and considered “complete” (the mineral band is opaque and clearly visible) after 5 days.

2. The system uses gelatin as the principle hydrogel and that carries with it the same issues as the system used by Mandel.
3. Unlike the layered system as used by Mandel, the large circulating reservoirs provide a nearly infinite (on the time scale of the experiment), inexhaustible source of ions.
4. Even though relatively large amounts of mineral are produced compared to static systems, the mineral density per volume of gel is still low (~3% dry weight after 5 days).

1.2.3 Types of Hydrogels

The key component to each of the DDSs presented here is a hydrogel. Knowing the chemical and physical properties each type of hydrogel yields insight into how and why a particular hydrogel is chosen to be paired with a particular DDS. A number of synthetic and natural polymers can be made into hydrogels,[60] but three types of gels have been primarily used for the study of calcium phosphates: gelatin, [7, 12, 17, 20, 29, 33-38] agarose, [7, 18, 20, 31]and collagen.[7, 14, 18, 20, 31]

1.2.3.1 Gelatin

Gelatin hydrogels are protein-based gels made of blends of various purified lots of denatured collagen. Due to large batch-to-batch variations in purity and properties, it is recommended that a single batch of gelatin be used for all studies.[61] Acid-purified gelatins (Type A) have isoelectric points of pH 6.5-9, whereas alkaline-purified gelatins (Type B) have isoelectric points of pH 4.8-6.[62] As such, it is important to consider the type of gelatin and the pH at which it is used. In addition to the purification method, there is also variation in gelatin derived from different organisms and locations from which it is

harvested from within those organisms. A “best practices” option when choosing a gelatin, is to use a gelatin type and manufacture known to be of a certain level of “cleanliness.”[49, 50, 52] Another way to obtain high-quality gelatin is to prepare it in-lab from collagen sources.[62] A few additional points about gelatin that may contribute to its use in a DDS are:

1. The minimum concentration of gelatin to create a hydrogel is about ~5 w/v %.
2. The maximum temperature at which gelatin will remain as a hydrogel is about ~27°C.
3. Consistent and repetitive heating and cooling of gelatin solutions can lead to an increase in the local ordering within the hydrogel[62] that may influence the crystallization results.
4. Gelatin is hydrophobic and has a tendency to be both adhesive and cohesive leading to a gel that adheres well to the vessel in which it is contained.
5. Gelatin hydrogels, below their gelling temperature, tend to swell in water.

1.2.3.2 Agarose

Agarose hydrogels are polysaccharide-based gels purified from seaweed. Different types of agarose can be segregated by purity, strength, chemical modification,[63] and melting temperature. Both the thermal stability and gel strength are closely tied to the relative entanglement of polymer chains within the hydrogel and the hydrogen bonding between those chains. With increasing gel strength the maximum melting temperature also increases, although the thermal hysteresis of different types of

agarose (between melting and setting temperature) can vary widely and should be checked before purchase and use. A few important points about agarose that may contribute to its use in a DDS are:

1. The minimum concentration of agarose to create a hydrogel is about 0.1 w/v %.
2. The hydrophilicity and strong self-hydrogen bonding character of agarose often makes it difficult for agarose to strongly adhere to the inside of a container.
3. With decreasing gel strength, agarose bonds less with itself and is therefore more "sticky" in character.
4. Agarose can have a tendency to be brittle and therefore certain levels of mechanical stress (when handling) can lead to permanent cracks or fracture of the gel.
5. Agarose hydrogels, below their gelling temperature (varies depending on the type of agarose, can be as low as 25 °C and as high as 70 °C), tend to shrink in water.

1.2.3.3 Collagen

Collagen hydrogels are protein-based gels that take advantage of collagen's tendency to self-assemble. Typical collagen gels are based on collagen type-I, purified from rat tail tendons,[29] but the sources and types of collagen used can vary based upon the user's preferences. A collagen gel is formed by raising the pH of an acidified collagen solution to a value of around 7, this change in pH allows for collagen fibril formation and subsequent self-assembly. Collagen gels have the advantage over gelatin gels in that they

are stable at 37°C and "cleaner." A few important points about collagen gels that may contribute to its use in a DDS are:

1. The minimum concentration of collagen to create a hydrogel is about 0.1 w/v%.
2. Upon setting, collagen gels have a tendency to shrink.
3. Collagen can be expensive if purchasing already prepared solutions. If you purify your own collagen, the preparation can be more involved compared to using gelatin or agarose.

In addition to the theoretical considerations for designing and operating a DDS (later discussed in Section 1.3), the practical aspects, such as the choice of hydrogel can also have important consequences. Understanding both the chemical and the physical properties of each of these gels will help you decide which kind of hydrogel is appropriate for your DDS and your mineralization study.

1.2.3.4 The effect of the physical properties of the hydrogel

The shrinking or swelling of the hydrogel matrix changes the boundary conditions (t_0 and x_0) of the sample/experiment, and therefore changes the effective/calculated diffusivity of the solute (Fig. 1.6). It is important to understand that this phenomenon has both a thermodynamic and kinetic component. Thermodynamics dictate the enthalpy of mixing between the hydrogel and the diffusing solvent, and the kinetics of the system describes the diffusion of both the solvent and solutes into the hydrogel.

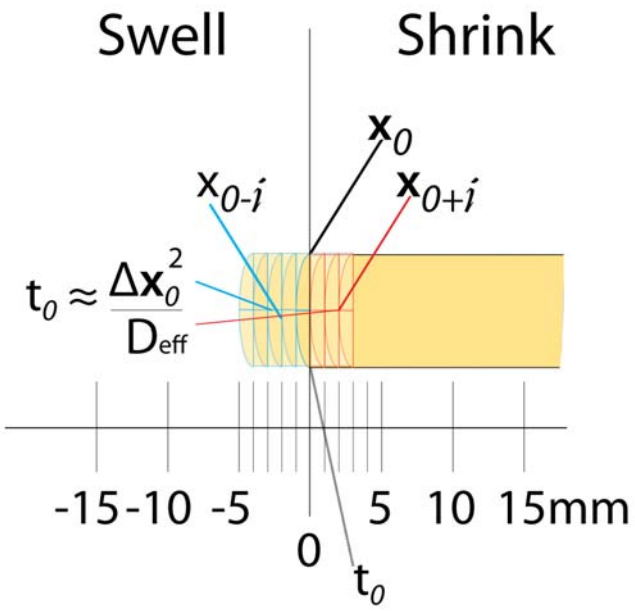

Figure 1.6 The swelling and shrinking of the gel/soultion interface has an effect on the boundary conditons of the system. With changes in *x* the calculated effective values of *t* and *D* can also change.

Thermodynamic concepts for describing solvent/polymer interactions (the χ parameter) can be applied to the solvent/hydrogel interaction. With increasing χ there is a resulting increase in the amount of solvent (water) in the volume fraction of the hydrogel (swelling). With decreasing χ there is a resulting decrease in the amount of solvent (water) in the volume fraction of the hydrogel (shrinking). In thermosetting gels such as gelatin and agarose, the polymer-solvent relation has a baseline qualitative χ parameter that can be termed either good, poor, or theta.[64]

- A "good" solvent will swell a polymer/hydrogel network, physically increasing the size of the network, making $x_0 < 0$.
- A "poor" solvent will shrink a polymer network, physically decreasing the size of the network, making $x_0 > 0$.
- A "theta" solvent will neither swell nor shrink a polymer network therefore

the value of $x_0 = 0$.

For example, gelatin, which has strong polymer-water interactions, swells in water below its gel temperature, whereas agarose, which has strong polymer-polymer interactions, shrinks in water below its gel temperature. As a result gels cast into diffusion tubes without an interface barrier, such as a dialysis membrane, [11, 18, 19, 30, 45] will have at least one (if it is a single diffusion tube) unconfined end that will swell or shrink. If the interface between gel and solution swells or shrinks it will change the overall path-length of the tube L and by default the location of the starting point x_0 (Fig. 1.6).

The kinetics of solvent and solute diffusion in the hydrogels can also effect t_o and x_o. Diffusion of solvents in many polymers can not be described based on the concentration-dependent form of Fick's Law with constant boundary conditions.[22] For example structural changes due to solvent-based swelling or shrinking are strongly time dependent in glassy polymers. On the other hand, rubbery polymers can respond quickly to environmental changes such as temperature and solvent. Hydrogels are different than both rubbery and glassy polymers. One key difference as compared to glassy polymers is that the open network of the hydrogel does not need to change to allow diffusion. However, a change in the hydrogel structure does change the values of x and t in the diffusion equation (Fig. 1.6). Another difference is that since hydrogels are networks of polymers that are structured by water, the diffusion of water is decreased due to hydrogen-bonding interactions with both itself and the polymer.[23] The relative strengths of polymer-polymer and polymer-water interactions play a large role in determining the physical properties of the gel,[23] in particular the degree of swelling/shrinking in water and the ionic diffusion rates. A solute diffusing through a hydrogel on the other hand, has limited interaction with the polymer component due to

the dispersive nature of the network, as a result swelling or shrinking in a radially confined hydrogel (such as in a tube) has an effect on the value of *x* and *t*, but little, to no, effect on the diffusion of the solute itself within the tube. In situations where solute diffusion is intimately tied to the diffusion of the solvent in which they reside, factors that effect solvent diffusion will have an effect on solute diffusivity. For example the diffusivity of calcium chloride has been reported to vary between hydrogels.[30]

1.2.4 The conditions of infinite and semi-infinite

In mathematics, an infinite object or sample has no beginning and no end; it extends from -∞ to ∞.[22] An ion diffusing through an infinite sample would start from a point source located at some position *x* within the sample and then (in the case of a one dimensional sample) diffuse in two directions, -∞ and ∞. [22-24, 32] A semi-infinite object has a beginning, x_0, but no end. An ion diffusing through a semi-infinite sample would start at some start point x_0 and (in the case of a one dimensional sample) continue to diffuse towards ∞.[22-24, 32]

Practically, however, an object is never truly infinite or semi-infinite. The point when or where an ion ceases to continue to infinity needs to be defined. According to Shewmon,[24] a sample has an infinite end if:

$$L > \sim 4.6\ (Dt)^{1/2} \text{ (actual value for the coefficient 4.6-4.8)} \quad \text{(Eq. 1.4)}$$

As a solute diffuses through a material, if the experiment is ended before the solute reaches the end, or it diffuses past the end into oblivion (lost),[24] or high dilution (0.1% c_0), then the sample (in this case the gel) is defined as having an infinite end. If the solute reaches the end of the material and is reflected back into the sample, then

concentration will build up over time (in which case a trigonometric series solution is required).

1.3 Evaluation and Design Strategies

Given the diversity of systems to choose from, here we present a set of evaluation and design strategies for the reliable and reproducible use of hydrogel-based DDSs for specific crystallization studies. The first course of action is the evaluation and/or modification of an already established DDS. If necessary, a second course of action is the *de novo* design or redesign of a DDS. Once constructed, the system can then be tested using three types of experiments to probe the effect the design has on the theoretically and empirically defined boundary conditions.

To begin the selection of a DDS for a particular type of study, the first step is to identify the main goals for the study at hand. Based upon these goals and the target questions of the study, the appropriate type of DDS (e.g., static versus dynamic) can be chosen (Table 2-1). In the evaluation of an already established DDS, the origin of the solution to the diffusion equation must first be understood. In order to obtain a solution, the first step is to determine what kind of diffusion system it is (static or dynamic) based

Table 1-2: Differences between static and dynamic diffusion systems allow the decision of what kind of DDS to use based on the targeted application.

Desired Conditions	Static DDS	Dynamic DDS
Study mineralization within a hydrogel or ECM-like environment	*	*
Quantity of mineral is important.		*
Resolution of the reaction space is important (gradients of concentration and mineral).		*
Small number of tunable variables.	*	
Large number of tunable variables.		*
Questions That Need to be Answered		
Will it mineralize? (Yes/No) (Qualitative)	*	
How much will it mineralize? (Quantitative)		*

on the path length *L* of the gel, the time frame of the experiment, and applications for which the system has been used (Tables 1-1 and 2-1). The next step is to determine what boundary conditions and variables are dependent or independent of the system design. Finally, the corresponding solution to the diffusion equation to which those variables apply can be determined. This solution can be directly obtained by solving Fick's Laws from first principles or by simply looking up an established solution in the literature,[22-24, 32] Based on the solution to the appropriate diffusion equation, the key boundary conditions and variables are determined and accounted for in the design of the DDS.

1.3.1 Solving the diffusion equation

We have described two types of diffusion systems, static and dynamic. To really understand what is going on in these systems, and to design a system of our own, we need to solve the diffusion equation. The variables that determine the corresponding solution to the diffusion equation are identified by examining: the components of the DDS design, the type of experiments run on the DDS, as well as the data collected from

those experiments. As an example of this process, we constructed Tables 1-3 and 1-4 for the Circulating Semi-Infinite Reservoir Design, as used by Boskey. [7, 12, 13, 17, 33-38] Similar tables could be constructed for the other systems presented, and we recommend going through such a process when designing and/or evaluating a DDS for studying biomineralization.

Table 1-3: Correlations between conditions/variables in diffusion theory and real-world engineering considerations and components of double diffusion systems.

Conditions/Variable that Satisfy the Chosen Solution Diffusion Equation $c(x,t) = c_0 erfc\ \frac{x}{2\sqrt{Dt}}$	**Examples of Real World Design Elements of the DDS**
Concentration $c = c_0$ for location $x = 0$ and independent of time t, or all $t > 0$	Keeping the reservoirs at a constant semi-infinite volume (by changing/replenishing frequently), and constantly circulating, which keeps the surface concentration at the fluid/hydrogel interface constant.
Concentration $c = 0$ for location $x > 0$ at time $t = 0$	The hydrogels are made free of the diffusing ions and all gels are placed in contact with the ion solutions at the same time.
The sample path length L is semi-infinite	The hydrogel sample is made to a length long enough such that it is considered semi-infinite throughout course of the experiment for all time t.
The diffusivity D of the ions involved in the experiment are assumed to be constant (independent of: c, x, t)	The diffusivity of the ions are measured as a state function (after the experiment is over), it is therefore assumed that any and all contributing factors to the diffusivity are normalized by this singular measurement.

Table 1-4: Example of an evaluation of the double diffusion system (DDS) used by Boskey [17] where various aspects of the DDS are assigned to their respective impacts/meaning in diffusion theory.

Aspects of the DDS	**What those Aspects Mean**
Used to examine the role of small amounts of Non-collagenous proteins in the ECM.	A hydrogel environment is required.
Designed to measure both whether or not a mineral promotes or inhibits mineralization, and to what degree.	Dynamic DDS is required.
The sample length is 6 cm. The experiment lasts 5 days. The slowest ion (phosphate) diffusion rate is 3.9×10^{-6} cm^2/s. The fastest ion (calcium) diffusion rate is 6.0x10-6^{-6} cm^2/s.	Using Eq. 1, Steady State Condition (L^2/D_{min} = 107 Days) >> Length of the Experiment (5 Days) Therefore, the system is **Dynamic.**
Diffusion occurs in one dimension. Gels are made free of ions ($c = 0$ for $x > 0$ at $t = 0$). Reservoirs are kept at 3-4 L and circulated with N_2 ($c = c_0$ for $x = 0$ for all $t > 0$). Sample length of 6 cm is **not** semi-infinite (6 cm < ~4.6 $(D_{max}t)^{1/2}$). D is assumed constant.	The theoretical solution to the diffusion equation is: $c(x,t) = \frac{4c_0}{\pi}\sin(\pi\frac{x}{L})e^{-\pi^2 Dt/L^2}$ for: t << L^2/(25D) Ref [32] The actual data from experiments as reported by Boskey et. al. reveals that the solution to the diffusion equation is: $c(x,t) = \frac{1}{2}c_0 erfc\ \frac{x}{2\sqrt{Dt}}$ Ref [17]

Finding a solution to the diffusion equation relies on knowing the initial conditions of the experiment and the boundary conditions under which the experiment is conducted. As an example, here is a solution (Eq. 1.5) that can be applied to the Circulating Semi-Infinite Reservoir Design, where the concentration of ions in the hydrogel sample is zero at the start of the experiment, the diffusivity of ions through the

hydrogel is constant, the source (reservoir) of ions is semi-infinite and the hydrogel sample into which the ions are diffusing is also semi-infinite (Tables 1-3 and 1-4). Since it is a dynamic system, we start with Fick's 2nd Law (Eq. 1.3). For a complete description of how to solve such a problem, it is best to consult one of several textbooks available on diffusion.[21-24, 32] Based upon the boundary conditions for the given problem, a solution based on an error-function is obtained (Eq. 1.5).

$$\frac{\partial c_i}{\partial t} = D_i \quad \frac{\partial^2 c_i}{\partial x^2} \rightarrow \; c(x,t) = \frac{c_0}{\sqrt{\pi D t}} e^{\frac{-x^2}{4Dt}} \rightarrow \; \int_0^\infty c(x,t) = c_0$$

$$if \qquad u = \frac{x}{2\sqrt{Dt}} \rightarrow \; c(x,t) = \frac{2c_0}{\sqrt{\pi}} \int e^{-u^2} du$$

$$\boxed{c(x,t) = c_0 erfc \;\; \frac{x}{2\sqrt{Dt}}} \qquad \text{(Eq. 1.5)}$$

To make use of this equation, the boundary conditions, which provide the foundation for this solution, need to be reflected in the design of the DDS (Table 1-3). For example, the solution presented here only applies to the diffusion in one dimension. To fabricate a system that can be simplified to a one-dimensional problem, the gels must be confined in plastic tubes and their connection to the system designed to restrict the diffusion for both ionic species to one dimension.

The value of diffusivity *D* is not truly an independent variable. The movement of ions is strongly dependent on the interaction of those ions with their environment, the type of hydrogel,[6]as well as the overall charge and the nature of impurities in the hydrogel. Precise measurement of the diffusivity and the effect of these variables is

difficult to measure and for the purposes of this work need not be considered. As a result the variables that contribute to the diffusivity eventually average out over the course of the experiment and can be (for the purpose of this work) assumed to be part of the "overall diffusivity" of the species in this system.

When determining or considering values of ion diffusivities, it is important to consider the counter-ion of the element that is diffusing and the temperature of the system. Different salts move at different rates according to the following relation:

$$D_{salt} = \frac{(z_+ + |z-|)D_+ D-}{z_+ D_+ + |z-| D-} \quad \text{(Eq. 1.6)}$$

Where D_+ is the diffusivity of the cation and D_- is the diffusivity of the anion, $z+$ is the charge of the cation and $z-$ is the charge of the anion. Therefore the diffusivity of a calcium "ion" is not necessarily universal to all calcium salts $CaCl_2 \neq CaCOOH \neq CaNO_3$, etc. Temperature also effects the speed of diffusion (+2-3% per °C from a value at 25 °C).[65] These differences in diffusivity can affect the reaction rate, supersaturation thresholds, and the stoichiometry of the resulting product. As such, counter-ions and temperature were not varied in the experiments shown in section 1.3.2.

Though it is clear that the DDS, as originally designed by Boskey, is a dynamic system and the fundamental design implies an semi-infinite reservoir system (Table 1-4), the experimental data presented a solution to the diffusion equation that is unique to a point source of infinite concentration, diffusing in one dimension, from within an infinite sample.[17] The discrepancy between the mathematically derived equation and the experimental results may arise from a poor circulation rate in the reservoirs, small reservoir volume, lack of reservoir replenishment or some additional unknown. Whatever

the cause, Boskey's demonstration of an experimentally driven solution to the diffusion equation is an example of how operational discrepancies with respect to the theoretical design can be compensated for using empirical data. This discrepancy, as well as others, is accommodated for and resolved by careful testing and re-evaluation of this particular design of a DDS. The boundary conditions for our reconstruction of this Circulating Semi-Infinite Reservoir Design and the strategies taken for that design are in Table 1-3.

1.3.2 Design and Evaluation of a Model System.

As our model system we have chosen to optimize the design of a Circulating Semi-Infinite Reservoir dynamic DDS similar to the design shown in Fig. 1.5. Our initial interest in optimizing a DDS arose because we were interested in studying HA mineralization in the presence of surfaces and gradients of small-molecule mineralization inhibitors. Beginning with the DDS shown in Fig. 1.5, we discovered two characteristics that were challenging for our objectives: first, the timing of the mineral band formation was difficult to predict (varied amongst experiments and from tube to tube) and, second, the precise positioning of the precipitation events varied by as much as 1 mm from the center of the 6 cm tube in either direction. Neither of these challenges had posed a problem for the original applications, since they required precipitation to occur within a protein-laced, 0.2 cm thick band in the center of the tube, during the course of the 5 day experiment. In addition, thick (0.3 cm – 0.67 cm wide) sections of gel, which were large enough to accommodate any slight positional variances in the mineral band, were analyzed for ion concentrations and mineral formation. In our desired applications, however, we needed to have mineral bands appear in more precisely defined locations and at more reproducible times from experiment to experiment.

To address these concerns, we made several key modifications to the system

shown in Fig. 1.5 as seen in Fig. 1.7, including the addition of peristaltic pumps to circulate the fluids and stir plates to continuously mix the reservoirs (Fig. 1.7). We also modified how the gelatin diffusion tubes were prepared and changed the angle of the circuit tubing connected to the reservoir to aid in the removal air bubbles from the system and maintain a constant gel/solution interface. We then designed three experiments to validate the chosen boundary conditions and fundamental assumptions we had with regard to our construction of the DDS (Tables 1-3 and 1-4).

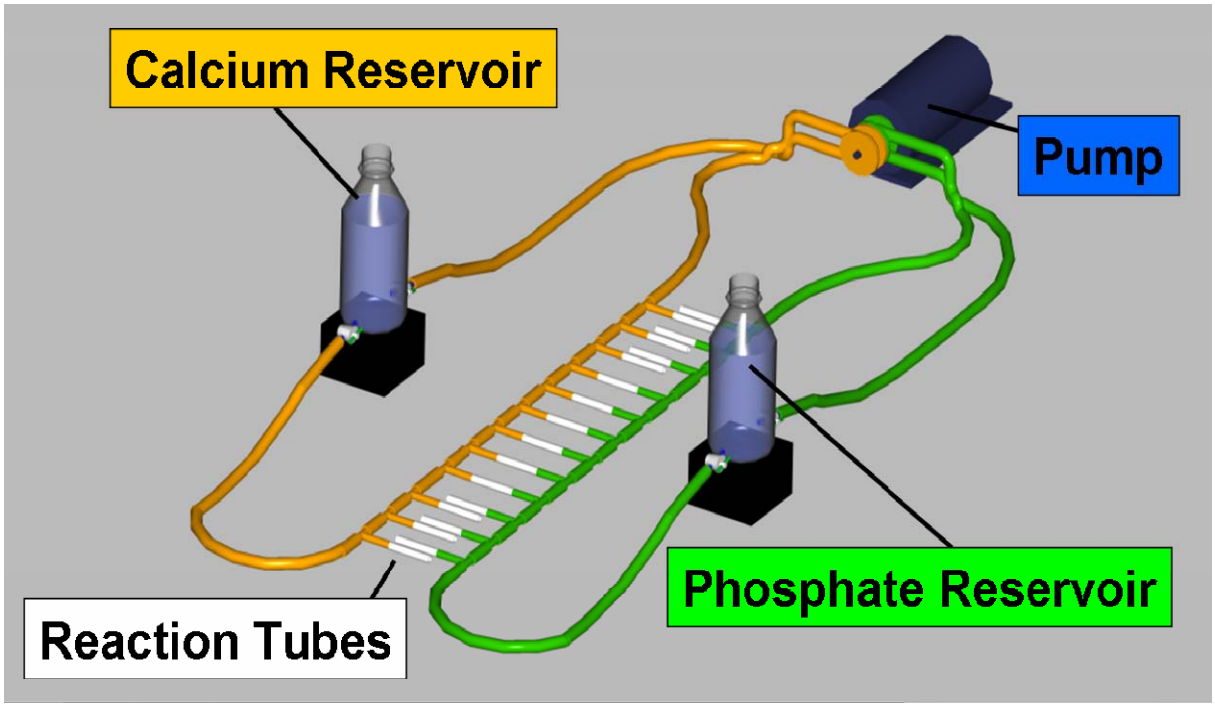

Figure 1.7 Optimized construction of the Circulating Semi-Infinite Reservoir Design (as seen in Fig. 5). To create and maintain turbulent mixing, the air pump/tank and CO_2 scrubbers are replaced with a peristaltic pump for each reservoir circuit (42 mL/min) and stir plates (350 rpm) placed under each reservoir. The reservoirs are constructed from 1 L media bottles modified with stopcocks attached at a 10 degree angle.

1.3.2.1 Experiment I: Effect of boundary conditions $\Delta c_0=0$, $\Delta x_0=0$, and $\Delta t_0=0$, on the kinetics of mineral precipitation.

In order to use Eq. 1.5, three fundamental boundary conditions must be maintained in all of the experiments. In a practical sense the values of c_0, x_0 and t_0 can not change, or: $\Delta c_0 = 0$, $\Delta x_0 = 0$, and $\Delta t_0 = 0$. As such, the variables c_0, x_0, and t_0 (as defined in Fig. 1.1), must be tightly controlled using engineered safeguards to insure reproducibility of the experiments.

The first boundary condition, $\Delta x_0 = 0$, demands that the dimensions of the gel sample do not change (through either swelling or shrinking) throughout the course of the experiment(s). The basic assumption is that the value of x_i and the values of x_0 & L at the boundaries are constant: $x_0(t) = 0$, $x_L(t)=L$. However, if x_0 changes, the functions $x_0(t)$ and $x_i(t)$ would have to be considered (these are cases where $x_0(t) \neq 0$ and $x_i(t) \neq$ constant).

The second boundary condition, $\Delta t_0 = 0$, demands that the starting time for diffusion must always be the same for every experiment. To consider all experiments normalized to the same start point, the reactant solution must make contact with the surface of each hydrogel in the experiment at the same time. In our system (Fig. 1.7), the start time t_0 of the experiment is controlled by using valves on the reservoirs, and a pump to introduce the reservoir fluid to each of the diffusion tubes at the same time or on a sufficiently short time scale. The "short" time scale required is found by applying the steady state condition (Eq. 1.1) to the thickness of the gel edge at the interface layer. For this condition, we consider a gel edge to be 0.075 cm and a short time scale to be less than 15 minutes. In our system, new fluid from the reservoir is circulated by a peristaltic pump through the ~150 mL circuit in less than 3.5 minutes, making the lag time between

the start of the pump and the connection of fluid to the ends of the hydrogel less than 5 minutes. New fluid from the circuit makes contact with the gel within 15 minutes. The movement of fluid through the system was monitored in an independent test using the circulation of colored dye. The 1 Hz oscillating flow of 42 mL/min is fast enough to equalize the system but slow enough to not dislodge the gel from the reaction tubes.

The third boundary condition, $\Delta c_0 = 0$, demands that there is no change in concentration of the reactants both at the solution/gel interface and in the source reservoir (the semi-infinite source condition). A constant value of c_0 at the solution/gel interface can be achieved by using either a single tube per large reservoir or by circulating the contents of the reservoir through a circuit of tubes at a rate faster than the concentration at the interface can be depleted by 0.1% of c_0.[24] In our system with multiple tubes, the use of peristaltic pumps and stir plates under each reservoir helps to maintain the value of c_0 at the solution/gel interface. The challenge of achieving a semi-infinite source is similar to the challenge of meeting the semi-infinite sample condition (see Section 1.3.2.2). A reservoir must be created such that, in either theory or practice, it can be considered semi-infinite. Two ways to achieve this condition are: use a reservoir sufficiently large in comparison to the sample specimen or change the solution in the reservoir frequently enough that there is negligible change in concentration over time.

In practice, the boundary conditions are not as straightforward as described above since values of certain boundary conditions are interdependent. For instance, the value of t_0 can change with the value of x_0 and c_0. Since the value of t_0 is defined as the point in time at which the concentration c_0 crosses the point x_0, if either c_0 or x_0 changes (or is different from tube to tube) then the value of t_0 will also change (assuming a constant diffusivity, D) (Fig. 1.6). If the solution/gel interface changes due to swelling or

shrinking of the gel, x_0 will change, leading to an effective change in t_0. Such structural changes of the hydrogel were not accounted for in the original design and use of the Circulating Semi-infinite Reservoir dynamic DDS. These structural changes may contribute to the observed discrepancies in the timing and the location of the precipitation bands, and may also contribute to deviations from the theoretical solution to the diffusion equation. For these reasons, we further examined the factors that lead to changes in x_0 and developed an approach to mitigate any structural changes that might be occurring in the gelatin tubes.

The thermodynamics that dictate changes in the hydrogel network, at the solution/gel interface, need to be correlated with the kinetics that dictate the movement of ions and water through the free volume of the hydrogel. To make this correlation, we use the same diffusion classifications (Cases, outlined below) used when considering structural changes in the diffusion of solutes and solvents in glassy polymers.[21] These Cases clearly describe the various scenarios where the movement of a solvent/polymer interface is entangled with the diffusion of solutes through a polymer. In all Cases, we clearly explain the similarities and differences between structure changes glassy polymers and hydrogels.

Case I: *The rate of diffusion is much slower than the rate of the structural changes.* In the case for solute diffusion in glassy polymers this condition gives rise to a Fickian solution, since the polymer structure changes before the solutes even begin to diffuse, the diffusivity of the solute becomes the rate limiting step. In the case of a dispersive hydrogel network, however, the structural changes do not necessarily accommodate nor hinder diffusion, they in fact change the effective path length L of the gel. D_{eff} can still be considered constant, but the value of x_0 and/or t_0 will change

depending on which variable is chosen to remain constant. One way to look at this case is to assume that changes in the structure will change the way x_0 or t_0 is determined, (for instance t_0 will be a function of x_0 which may change before all the tubes on the system can be started within the required "short" time scale), since in our use of the DDS, D is considered invariant, only x and t would be variable.

Case II: *The rate of the structural change is very slow compared to the rate of diffusion.* In solute diffusion in glassy polymers, this condition gives rise to non-Fickian diffusion, because the rate limiting step is the change in the polymer structure (the movement of the border between structurally changed and unchanged polymer). Simply put, the solutes need to wait for the polymer structure to change before they can move. For the case of a hydrogel, the network would neither swell nor shrink within the time frame of the experiment (making diffusion in a hydrogel Fickian), so this case would be an ideal situation for a DDS where $\Delta x_0 = 0$ and $\Delta t_0 = 0$.

Case III: *The rate of diffusion is roughly equal to the rate of structural change.* Again in this case, the diffusion through glassy polymers is non-Fickian. In this case both the diffusion rate and the rate of structural change are important and must be considered. In a hydrogel if t_0 is held constant, both D_{eff} and x_0 will vary with time, but if D_{eff} is considered constant then only x_0 will vary with time. This case is not a concern for t_0 since $\Delta t_0 = 0$.

For the evaluation of a DDS, since the swelling of the hydrogel network and the movement of ions are not monitored in real-time throughout the course of the experiment, it is difficult to determine which class of diffusion (either Case I or Case III, Section 3.2.1) is taking place when the case is not explicitly Case II. We chose, therefore, to create a 'theta' condition, which (for the most part) eliminates structural changes in the

gel over the course of the experiment. To create a 'theta' situation and provide a Case II scenario there are a number of paths that could be taken (many have been explored but are not presented here). In the end, we adopted a "pre-hydration" strategy in which the gel/solution interface is pre-hydrated to the point where the gel ceases to shrink or swell anymore. For the gelatin tubes, the swelled ends of the hydrogel are then cut flush to the diffusion tubes before starting the experiment.

We then demonstrated the effects of controlling x_0, t_0, c_0, from a phenomenological point of view, by observing the time and location of the precipitation event in the system (Experiment I). We tested four different experimental conditions, with varying boundary conditions: a non-circulating system with non-hydrated gels (Condition A), a non-circulating system with hydrated gel (Condition B), a circulating system with non-hydrated gels (Condition C) and a circulating system with hydrated gels (Condition D). The time at which the precipitation event could first be observed by eye in the gel tube was recorded for all 12 double-diffusion tubes (Fig. 1.8).

In examining the data from Experiment I, we can see how changing the conditions that affect the boundary conditions affect the timing and error in the timing of the mineral precipitation event in the gel (Fig. 1.8). In the optimized system (Condition D) where c_0 was maintained by circulating the reservoirs and the values of t_0 and x_0 were maintained by pre-hydrating (swelling) the gels, the precipitate appears after 71.42 hours, with no timing error variation amongst all 12 tubes. In contrast, in the un-optimized system (Condition A) where the reservoirs were not circulated and the gels were not pre-hydrated, precipitation is observed more than 24 hours after Condition D, with a large variation (up to 4 hours) among the 12 tubes.

This experiment highlights how critical the experimental conditions (and the

resulting boundary conditions) are for determining the timing and reproducibility of the precipitation reaction. Circulation of the reservoir circuits (maintaining c_0) has the largest impact on when the precipitation occurs, whereas the pre-hydration of the gel (defining t_o and x_o) strongly effects the reproducibility in the timing of the precipitation event.

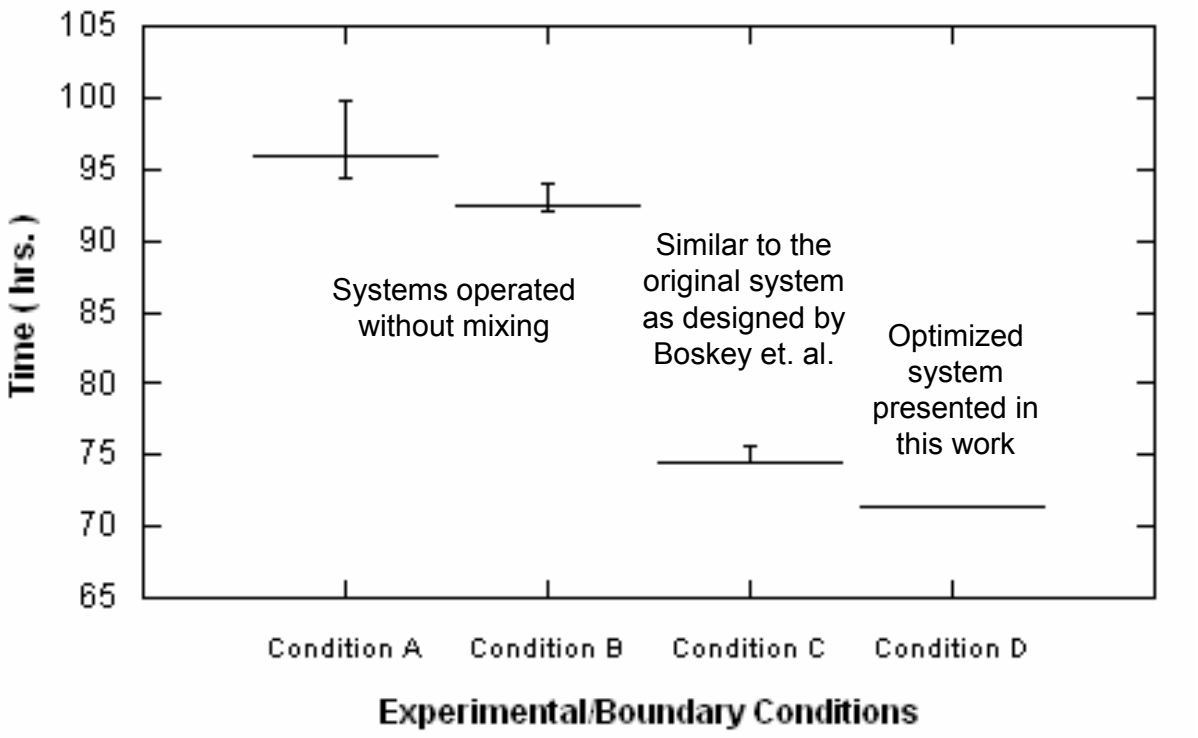

Figure 1.8 Timing in the onset of precipitation bands from the start of the experiment, in four different DDSs, Condition A: No reservoir circulation, no pre-hydration of the hydrogel; Condition B: Reservoir circulation, no pre-hydration of the hydrogel; Condition C: Reservoir circulation, no pre-hydration of the hydrogel; Condition D: Reservoir circulation, pre-hydration of the hydrogel. All systems used 225 Bloom Type-A gelatin 10% w/v. The mode of the precipitation events for each condition is plotted with a horizontal line, with the error bars representing the maximum and minimum timing of precipitation in the tubes (12 each) under each condition.

1.3.2.2 Experiment II:

A key boundary condition for the Circulating Semi-infinite Reservoir dynamic DDS is the semi-infinite sample condition ($\lim x_{i \to L} = \infty$), and the semi-infinite reservoir condition, which is required for Eq. 1.5 to be applicable. The sample must be long enough in order to be considered semi-infinite for the time scale of the experiment.

In order to quantitatively assess the validity of the assumed boundary conditions, an appropriate experiment to address each boundary condition must be performed. As an example, we designed an experiment using the semi-infinite sample length and semi-infinite reservoir size as our assessable boundary conditions. Since an evaluation of these two conditions must be performed when working with a new or different hydrogel, we evaluated these conditions using 225 Bloom Type-A gelatin (10 w/v % in Tris buffer pH 7.4).

1.3.2.2.1 Experiment IIa: Evaluating the boundary conditions of "semi-infinite sample length"

For hydrogel-based DDSs the semi-infinite sample condition is a function of the diffusivity of an ion through a particular hydrogel, therefore each hydrogel (by type, concentration, strength, etc.) has a different semi-infinite sample condition. Using Eq. 1.4 and $D = 6.0 \times 10^{-6}$ cm^2/s from the literature (the diffusivity of calcium in 10 w/v % 275 bloom gelatin in Tris buffer pH 7.4),[17] it was found that a sample length greater than 7.4 cm would be required for a 5 day experiment to achieve the semi-infinite sample condition in this system. The semi-infinite condition can also be achieved using a sufficiently large enough sink tank (opposing reservoir) that would dilute the concentration of reagents to <0.1% of c_0, in a 12 tube system with a 6 cm sample length

(3 mL tube), theoretically such a dilution can be achieved if the sink tank is 25 mL in volume (or continuously flushed away).

In cases when a condition does not have an infinite end, as calculated by theory, it could be considered "quasi-infinite" if the error in measuring the concentration is such that there is no statistical difference between a result using a theoretically valid semi-infinite source versus a result using a theoretically invalid semi-infinite source. More simply put, if in theory it is not semi-infinite, but in practice there is no difference, then we will define it as quasi-infinite.

To confirm that the sample lengths are truly semi-infinite, an experiment was run using all Single Diffusion (SD) tubes, capped at one end, in the double diffusion system and employing the "best practices" boundary conditions (Condition D) identified in Experiment I. We tested both 6 cm tubes [17] (theoretically not semi-infinite, i.e. < 7.4 cm) and 8 cm tubes (theoretically semi-infinite) for 5 days. After 5 days, the sample was removed from the system and the concentrations of ions along the length of the tube were determined and used to calculate diffusivities. In order to properly assess the validity of the semi-infinite boundary conditions, the measured concentration values were then compared with theoretically predicted values.

The evaluation of the semi-infinite boundary conditions of the DSS hinges upon the measured concentration of ions in the hydrogel. More broadly, the concentration analysis of ions in a hydrogel yields insight into: the threshold conditions, the map of ions across the specimen, the diffusivities of ionic species, and the validity of the boundary conditions. Concentration analysis of the mineralized product yields both the stoichiometry (ion ratios in the product) and the amount of material created. The concentration of ions in the hydrogel can be determined multiple ways. [5, 9, 17, 18, 20]

Here we use Inductively Coupled Plasma-Atomic Emission Spectrometry (ICP-AES), to determine the concentrations of both calcium and phosphate. The concentration data gathered from Experiment II was used to calculate the diffusivities of calcium and phosphate ions in 10 w/v% 225 Bloom Type-A gelatin gels (Table 1-5).

Table 1-5: The calculated diffusivities, calculated concentrations, and measured concentrations of ions used to validate the semi-infinite sample boundary condition for a 10 w/v% 225 Bloom Gelatin Type A.

Reservoir[a] Tube Length	**$c_0/4$ (μM)**	**Diffusivity[b] (x 10^{-6} cm^2/s)**	**Measured conc. at end section (μM)**	**Calculated conc. at end section using *D* (μM)[b]**	**Calculated concentration at *x*=*L* (μM)[b]**
Ca^{2+} **6 cm**	25340	5.81 ± 0.17	407 ± 51	1,160 ± 118	750 ± 85
Ca^{2+} **8 cm**	25340	6.27 ± 0.21	93 ± 17	100 ± 19	60 ± 12
PO_4^{3-} **6 cm**	29360	3.91 ± 0.41	251 ± 41	241 ± 130	129 ± 75
PO_4^{3-} **8 cm**	29360	4.03 ± 0.48	55 ± 14[c]	5 ± 2	2 ± 3

[a] The reservoirs contained either a calcium chloride solution (c_0 Ca^{2+} = 101.34 mM) or an ammonium phosphate monobasic solution (c_0 PO_4^{3-} = 117.45 mM).
[b] The diffusivities were calculated from the concentration of ions found in three sections of each diffusion tube (sets of 6), and then used to calculated the concentrations in the end sections of each tube, as well as the value of c at $x = L$.
[c] The error in measurement is on the order of the value measured, demonstrating the detection limit of the ICP-AES for this ion at this concentration.

Diffusivities can be determined by a number of ways. The first method is one of brute force (for lack of a better term), where the value of an ion's concentration about a given point is taken in *multiple* slices along the path length of *multiple* samples of *varying* lengths, at *multiple* times.[17] From *all* this data, the applicable solution to the diffusion equation, which is unique to the boundary conditions of the experiment, such as the equation used for our system (Eq. 1.5), is used to solve for *D* at all points (along) given points *x* and *t.* Commonly, a fit-line based on the governing solution to the diffusion equation for a particular DDS is applied to the data and solved for *D.*[17]

There is another, easier method for calculating diffusivities that requires less time and without the need for high-end multivariable modeling programs (e.g., Matlab® or Mathematica®). This method involves using the estimation of the diffusion penetration

distance from a point source where the concentration has fallen to 25% of the concentration at x_0 (x= 0). This estimation, which is $x = 1.6\sqrt{Dt}$, is unique to a diffusion equation where the error-function is the solution and the value of *c* is such that the solution of *erf*(x) is ¾, or *erfc*(x) = ¼ and is unique to a semi-infinite point source.[32] In our solution to the diffusion equation, our concentration target is $c = c_0/4$. Similar approximations exist for other solutions to the diffusion equation.[32] This estimation simplifies the calculation of diffusion coefficients down to an algebraic fit. This straightforward method only requires one to:

- Determine the concentration of three sections/slices (at the very least),
- Plot those concentrations against the distance of each slice from the source,
- Apply an exponential fit line and solve for *x* in such situations when for example $c = 25$ mM (in the case where $c_0 = 100$ mM).

The location of those three slices is dependent on the type and length of gel used, in cases where there is not an intuitive sense (or literature reference) of where the targeted *c* value might exist, it is a best practice to examine the concentration along the entire path-length of at least one gel to find three regions on or about where the targeted *c* value may lie. Using the three concentrations and three corresponding *x* values, a fit line is applied to find *x* where $c=c_0/4$. Once *x* is found for $c = c_0/4$ that value is plugged into $x = 1.6\sqrt{Dt}$ at a constant time *t*. In general, for an experiment, the average from a set of 3-6 tube should be then taken and reported.

The concentration measurements taken in Experiment IIa show that both theoretically semi-infinite (8 cm) samples and theoretically finite (6 cm) samples yield statistically similar (but not within error) diffusivities for each calcium and phosphate species (Table 1.5). The calculated diffusivities were used to subsequently extrapolate the

values of ion concentrations (using Eq. 1.5) at the end of their respective tubes and the center of the 6.67 mm wide end-slice (Table 1-5). These calculated values were then compared to measured values of ions within that end slice (Fig. 1.9) to confirm the validity of using the semi-infinite-based-estimation ($x = 1.6\sqrt{Dt}$), for calculating the diffusivities). As a final comparison the target value of c = 0.1% of c_0 at $x = L$ (for each ion) serves as a benchmark; if the measured values lie under this benchmark then the sample clearly satisfies the semi-infinite sample condition.

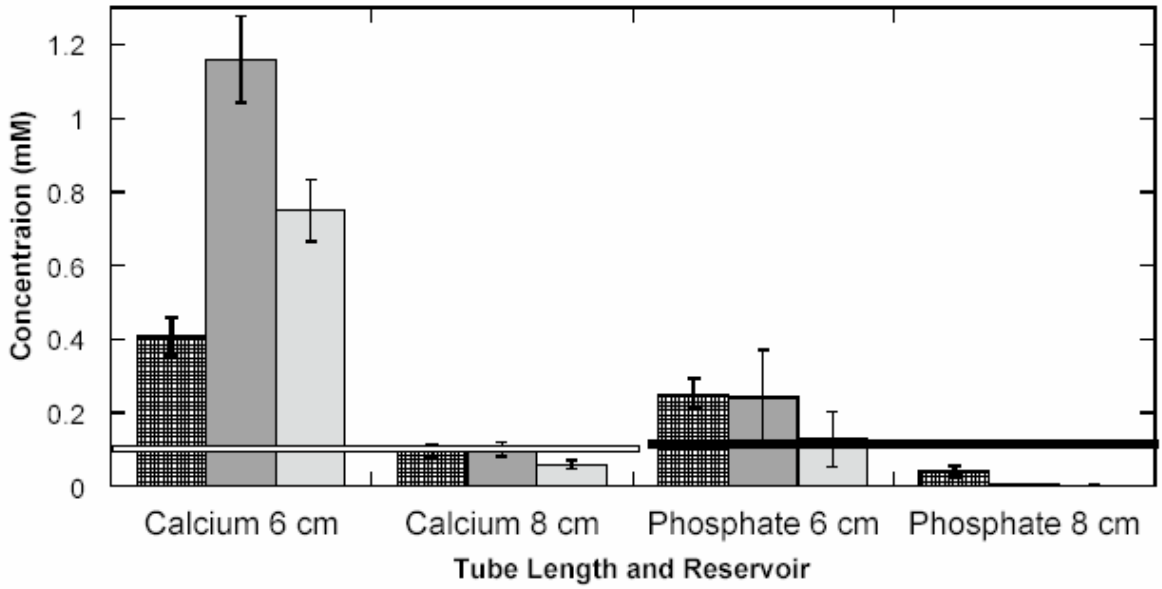

Figure 1.9 Plot of the measured ( )and calculated ( ) values of calcium and phosphate concentration in the end sections of two types of diffusion tubes (6 cm and 8 cm) compared to the calculated value of c at $x = L$ ( ) and the targeted theoretical value of 0.1% of c_0 shown as lines. (calcium, phosphate). When the measured and calculated values are within error of each other, then the data are self-consistent and the assumed condition is considered valid (8 cm calcium and phosphate). When the measured value is equal to or less than the targeted value line, but the calculated value for c at $x = L$ is greater than the targeted value line, the condition is considered quasi-infinite (not seen here). When both the calculated value for c at $x = L$ and the measured value at the end section are equal to or less than the targeted value line, then the condition can be considered semi-infinite (ex., calcium and phosphate 8 cm).

Though the calculated diffusivities are statistically similar, the data shows that the

calculated value of the calcium concentration (the fastest ion for which the semi-infinite condition was originally calculated) in the 6 cm tube does not accurately predict the concentration of ions at the end of the 6 cm SD tubes (Table 1-5). The calculated diffusivities for calcium in the 6 cm tubes are therefore incorrect (not even considered "quasi-infinite") because both the measured values and calculated values for a given location *x* are not consistent. In the 8 cm tubes for calcium, however, there is no statistical difference between the calculated calcium concentration and the measured calcium concentration. Therefore the calculated diffusivities for calcium in the 8 cm tubes are correct, and the 8 cm tube can be considered semi-infinite for calcium. In contrast, when considering the ion concentration for phosphate, where a 6 cm tube is within the theoretical semi-infinite condition for that ion in 10 w/v % 225 Bloom Type-A gelatin,. Therefore the calculated diffusivities for phosphate in both the 6 cm and 8 cm tubes are correct and both a 6 cm tube and an 8 cm tube can be considered semi-infinite for phosphate.

A question not investigated was whether or not, statistically, it makes any difference having a SD tube capped or connected to a sink reservoir. Since the space on the bench top occupied by the 8 cm SD tubes was not an issue, we found that the semi-infinite condition could be satisfied by this extension, and there was no need to explore the use or efficacy of a sink reservoir. For some users, there may be situations (i.e. certain kinds of diffusion tubes were capped ends are not an option) where they want to explore the option of having a sink reservoir.

In conclusion, 8 cm tubes must be used for this type of gelatin, when examining the single diffusion of calcium or phosphate ions over the course of a 5 day period to obtain accurate concentration profiles. Based on ion diffusivities in this hydrogel, we can

demonstrate if a 6 cm tube used in the case of double diffusion is semi-infinite up until the point of precipitation. After this point, any diffusion equation breaks down and the semi-infinite condition no longer matters. Using our calculated diffusivity for calcium from Table 5 ($D_{Ca} = 6.27\text{x}10^{-6}\text{cm}^2/\text{s}$), a 6 cm path length *L,* and Eq. 4, we solved for *t* and found that the moment when the semi-infinite condition breaks down is 75.37 hours. The data from Experiment I show that precipitation can happen as early as 71.42 hours. So even though an 8 cm tube is required for all SD tubes, a 6 cm tube is long enough to use for DD tubes, since the semi-infinite condition is still valid up until the time of precipitation.

1.3.2.2.2 Experiment IIb: Evaluating the boundary conditions of "semi-infinite reservoir"

To probe the semi-infinite source condition ($c > 99.9\%$ of c_0 for all time t) for the 1 liter reservoirs, sample concentrations of the reservoirs were taken at 0, 3, and 5 day time points, from the calcium and phosphate reservoirs in a DDS running only SD tubes (12 tubes per reservoir). Analyzing only reservoirs from an all SD system assured no change in the effective concentration of the reservoir as a result of cross-contamination from the opposing reservoir while using DD tubes, over the course of the 5 day experiment. The theoretical calculations for the reservoir semi-infinite condition are based on the total flux of material during the time frame of the experiment, from the source reservoir into the gel, and from the gel into the sink reservoir, using values and conditions from the literature.[17] Based on these calculations the source reservoir would need to be over 2 liters for the course of a 5 day experiment in order to be considered semi-infinite (for details of the calculation, see supporting information, section 1.5.5), and the 1 liter reservoir ceases to be considered semi-infinite after 2.5 days (60 hours). If

however there is no statistical difference between the measured concentration values and the calculated concentration values at a given time *t*, presented here we can consider these source reservoirs as "quasi-infinite" sources.

Concentration analysis of the diluted (100:1) reservoir samples revealed two important results. First, the error of measurement for the ICP-AES instrument changes depending on the standards used for calibration, which are dependent on the target concentration one seeks to analyze. In our measurements of the reservoir samples we found that the error for a ~40 ppm calcium concentration is 0.1-0.4 ppm (0.25-1 mM calcium), while for a ~36 ppm phosphorus concentration it is 0.06-0.25 ppm (0.2-0.8 mM phosphorus). Second, the concentration of reagents in the reservoirs did not effectively change from day zero to day three, while concentration analysis of the reservoirs on day 5 showed a ~2% drop in concentration in each reservoir. The instrument does not have the resolution to determine at what point the value of the reservoir concentrations *c* drop below the semi-infinite reservoir condition. The measured reservoir concentrations after 3 days are the same as c_0 on day 0, even though the theoretical semi-infinite condition for a 1 liter reservoir ceases after 60 hours. In conclusion, the reservoirs can be considered quasi-infinite for the time frame of the experiment. In practice, to avoid violating the quasi-infinite reservoir condition, 1 liter reservoirs should be changed just prior to the 3 day time point to maintain the effective c_0 concentration.

1.3.2.3 Experiment III: Empirically measuring the effect of changing x_0, t_0, c_0, on the measured ion product.

The final experiment correlates changes in the measured concentrations of ions, that result from changes in x_0, t_0, and c_0, to differences in the phenomenological precipitation events seen in Experiment I. This experiment not only examines the

concentration of ions, but also the resulting ion product for calcium and phosphate, for each system at a given time, to demonstrate the differences between two different experimental conditions. As already discussed, controlling $\Delta x_0 = 0$, $\Delta t_0 = 0$, $\Delta c_0 = 0$ is essential for maintaining the boundary conditions of the system. Changes in these boundary conditions result in only small changes in the value of *D* for a given ion, as well as slight differences in the measured concentrations for those ions. Upon initial examination, these small changes and slight differences suggest that changes in the boundary conditions have little to no effect on the system as whole. These small differences, however, add up to significant changes in the value of the ion product in the system, at a given location *x* for a given time *t* (Fig. 1.1b), thereby affecting precipitation events.

Precipitation in a hydrogel is the foundation for studies that use a DDS, therefore the consideration of the threshold for such an event is important. Observing, controlling, and understanding the precipitation event is essential in order for work being done with a hydrogel-based DDS to be practical. The onset of precipitation signifies that a reaction has taken place. If the concentration values required to reach the supersaturation threshold can be accurately predicted, then the time and location of the precipitation event can also be accurately predicted. A possible pitfall when considering the use of the precipitation event in mathematically modeling the system, is that "Phenomenological-In" becomes "Phenomenological-Out" with no understanding of how and why. This experiment helps us to determine the how and why, by tying small variations in concentration gradients to the observed timing of the precipitation event.

In cases of static DDSs operating at sub-threshold conditions, a precipitation event signifies that the gel or whatever is in the gel is promoting mineralization.[18]

Ideally, control gels in such a static DDS will not mineralize over the course of the experiment, if they do mineralize then an error was made in either preparing the gels or the solutions.[48] In this way, precipitation events can be used as a self-check of the experiment. In a dynamic DDS, the timing and shape of the precipitation event can yield insight into the effect that the gel or proteins in the gel are having on the formation of mineral, for instance, an early appearance of precipitate (relative to the control) can indicate a mineralization promoter, where as a delay in precipitation can indicate an inhibitor.[17]

As precipitation occurs, a strictly diffusion-based model of any system by the diffusion equations breaks down due to crystal growth, local changes in the chemical potential, and local ion fluxes. As a result the calculation and modeling of the system becomes increasingly difficult once precipitation occurs. [17, 66-73] Based on our current observations and mathematical limitations in modeling the system, once precipitation has occurred, the study of the system becomes phenomenological.[17]

The empirical formula for HA is $Ca_5 (PO_4)_3OH$ and therefore the supersaturation for the formation of a precipitate in solution is dependent on a 9^{th} order reaction ($[Ca]^5[PO4]^3[OH]$). In a hydrogel, the supersaturation threshold is reduced to a two component reaction of A + B = C where the supersaturation is the ion product [A]x[B], and the reaction is reduced to 2^{nd} order, AB mM^2, regardless of the true order of the reaction. [74] empirical value of this threshold is unique to the type of hydrogel used, the phase of the crystal being grown (ratio of ions, etc.), and the ions being used. A list of supersaturation threshold values for hydroxyapatite found in the literature (for a variety of hydrogels and conditions) has been compiled in Table 1-6.

Table 1-6: Measured values for the supersaturation threshold from various diffusion systems examining a variety of hydrogels, in differing concentrations and temperature conditions

Gel Type	Temperature	Ion Product [A]x[B]	Reference
10 w/v % Collagen[a]	37°C	13 $mM^2 < c^2 < 14.4\ mM^2$	[20]
0.5 w/v % Agar[a]	37°C	13.69 $mM^2 < c^2 < 15.2\ mM^2$	[20]
1.0 w/v % Agar[a]	37°C	14.8 $mM^2 < c^2 < 20.7\ mM^2$	[20]
5.0 w/v % Agar[a]	37°C	9.5 $mM^2 < c^2 < 19.3\ mM^2$	[20]
5.0 w/v % Gelatin [a]	25°C	16.8 $mM^2 < c^2 < 24\ mM^2$	[20]
10 w/v % Gelatin[a]	25°C	15.2 $mM^2 < c^2 < 25\ mM^2$	[7]
10 w/v % Type A 275 Bloom Gelatin	20-25°C	[†]37 mM^2 36.85 $mM^2 < c^2 < 41.5\ mM^2$	[6, 17]
5 w/v % Type A 275 Bloom Gelatin	24°C	32 $mM^2 < c^2 < 50\ mM^2$	[6]
0.2 w/v % Collagen	24°C	32 $mM^2 < c^2 < 50\ mM^2$	[6]
1 w/v % Agarose	37°C	32 $mM^2 < c^2 < 50\ mM^2$	[6]
2 w/v % Agarose	37°C	56.25 mM^2	[6]
10 w/v % Type A 225 Bloom gelatin [b]	20°C	[†]29.45 mM^2 18.92 $mM^2 < c^2 < 37.82\ mM^2$	This work

[†]Calculated from determined diffusivities and recorded precipitation time
[a]Precipitates in the gels were analyzed only after free ions were first removed from the gel.

[b]Original work presented in this Highlight (using average values from Experiment II and Experiment III)

For all of Experiment III, dynamic DDSs were run with varying boundary conditions with either exclusive DD tubes or a combination of DD and SD tubes. The two extremes from Experiment I, conditions A and D, were used. First, an all DD system was run under Condition D to establish the supersaturation threshold window for this gel (10 w/v % 225 Bloom Type-A gelatin) in this system (Table 1-6). Once we established the point in time at which precipitation occurred, this time point was used as a marker for the next experiment. In a comparison of the two conditions, two systems were run looking at

each condition (Conditions A and D), 6 DD tubes were run, 3 for Condition A, 3 for Condition D, and 12 SD tubes were also run, 6 for calcium (Conditions A and D), 6 for phosphate (Conditions A and D). The two systems were stopped 2 hrs. ± 0.1 hrs. before precipitation was expected to occur for Condition D.

As a whole, the data from Experiment III show how the values of the ion product, used to measure supersaturation, change when x_0, t_0, and c_0 are changing for a given time t and a given location x due to changes in the experimental conditions. These experiments reveal the necessity of maintaining boundary conditions as a means to control the quantitative value of the ion product and the timing of precipitation in a DDS.

The first part of Experiment III established a supersaturation window for the optimized system (Condition D). An all DD system was run with 9 DD tubes (triplicates for each time point). Each set of three tubes was place on the DD system at different time points (one hour apart from each other). When the first set of three showed signs of precipitation, all nine were taken off to determine the value of supersaturation at the time of precipitation and at time points up to two hours before precipitation was seen. Upon removal at 71.43 hours, only the first set of tubes showed signs of precipitation, the other two sets of tubes were clear. After removal from the system, the tubes were placed in the refrigerator for 45 mins to firm-up the gelatin before handling and cutting. After 45 minutes the two remaining sets of tubes began to show signs of precipitation but fainter than the first set of tubes (Fig. 1.10). The gels were cut and the center sections analyzed for ion content.

In the second part of Experiment III, both DD and SD tubes were run, a total of 12 tubes for each condition A & D, and the two systems were stopped at 69.36 hours (2 hrs. ± 0.1 hrs. before precipitation was expected to occur for Condition D). The measured

values of the ion product in all DD tubes is higher than would be expected based upon the recorded values of calcium and phosphate from the SD tubes (Fig. 1.11). This difference is most likely due to the formation of mineral product, not visible to the naked eye, in the diffusion tube. Comparing the calculated ion product for Condition A to Condition D

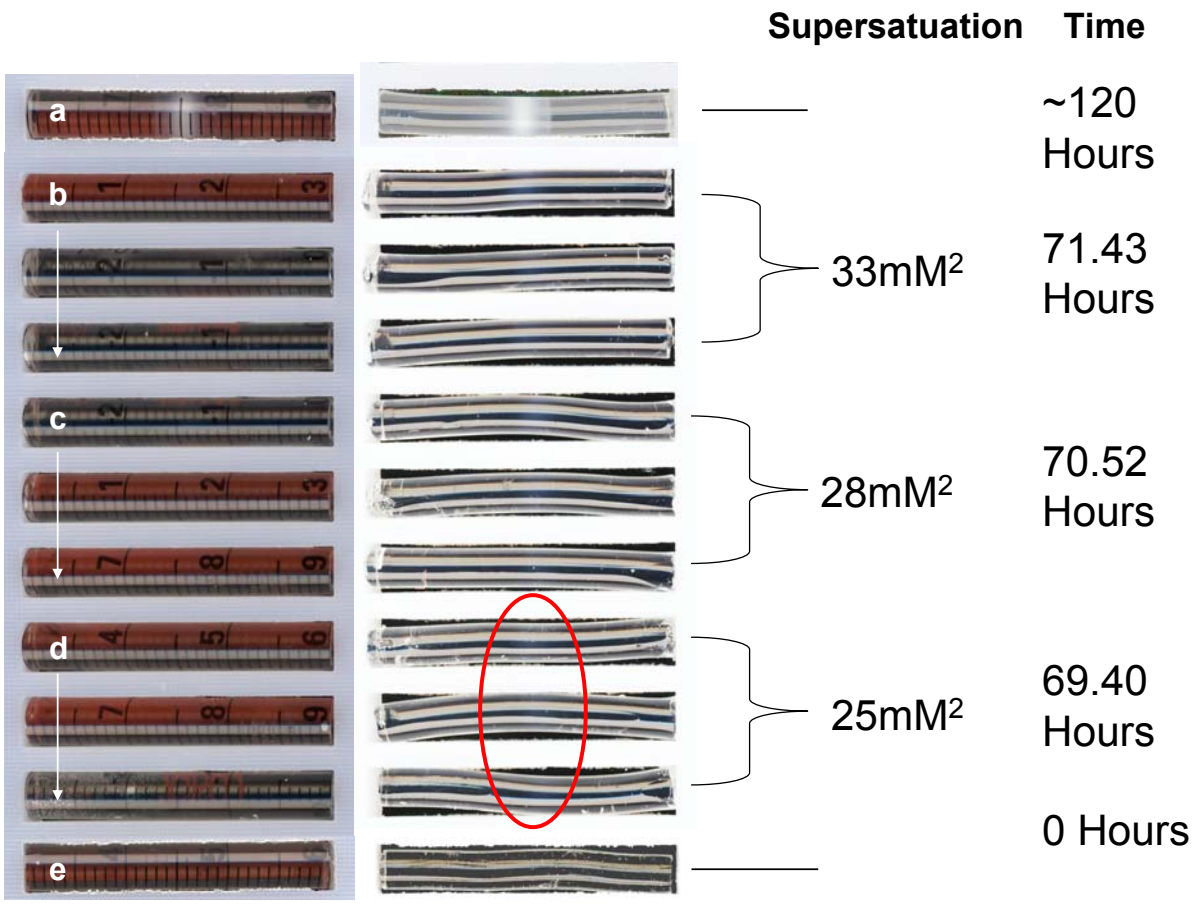

Figure 1.10 Scans of diffusion gels, cast from 10 w/v % 225 Bloom Type-A gelatin, from a Circulating Semi-infinite Reservoir DDS. (a) Mineralized control gel with a dense mineral band formed after 5 days, (b) gels with the initial precipitation band seen at 71.43 hours, (c) gels removed ~1 hour before precipitation was seen and then left to sit for 45 mins after being removed from the system, (d) gels removed ~2 hours before precipitation was seen (the faintest bands are circled for easy spotting) and then left to sit for 45 mins after being removed from the system, (e) blank gel as cast and not placed on a DDS.

reveals why the timing of band precipitation is so different between the two types of systems (Fig. 1.12).

On average, the measured ion product of Condition A at 69.36 hours with no visible precipitation, was well below the minimum measured supersaturation-threshold value (19 mM^2) required for precipitation to be seen within the same timeframe in the

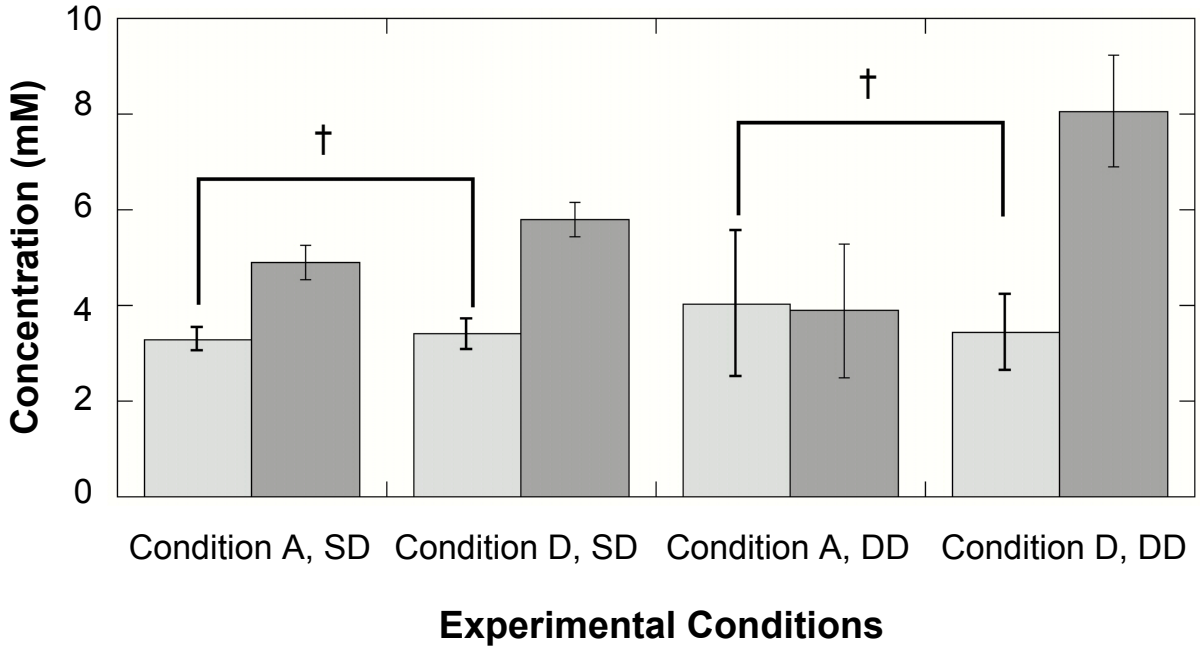

Figure 1.11 Measured calcium ( ) and phosphate ( ) values for the optimized (condition A) and un-optimized (condition D) in the circulating semi-infinite reservoir design after 69.36 hours (2 ± 0.1 hours before precipitation was expected). Values for calcium and phosphate from the SD tubes in both conditions were statistically similar. The main difference between the two conditions is the measured calcium concentrations for the DD tubes in each case. († the values for phosphate are within error of each other)

optimized system (Condition D). Even with the wide variation in the statistical error of the measured ion product of Condition A, precipitation was not seen in any of these tubes. In contrast, the measured ion product for Condition D at 69.36 hours, just hours before visible precipitation, was well within the previously measured supersaturation-threshold window (Table 1-6), with the statistical error of the experiment lying above the lowest supersaturation value of that window.

In conclusion, even though the measured concentration values for phosphate, for

both Condition A and Condition D are within error of each other for the SD tubes, and the measured values for calcium are similar to each other in the SD tubes (Fig. 1.12), the differences in the ion product for each condition clearly shows the importance of maintaining the boundary conditions of x_0, c_0, and t_0, in the performance of a hydrogel-based DDS. These differences in the value of the measured ion product translate to the

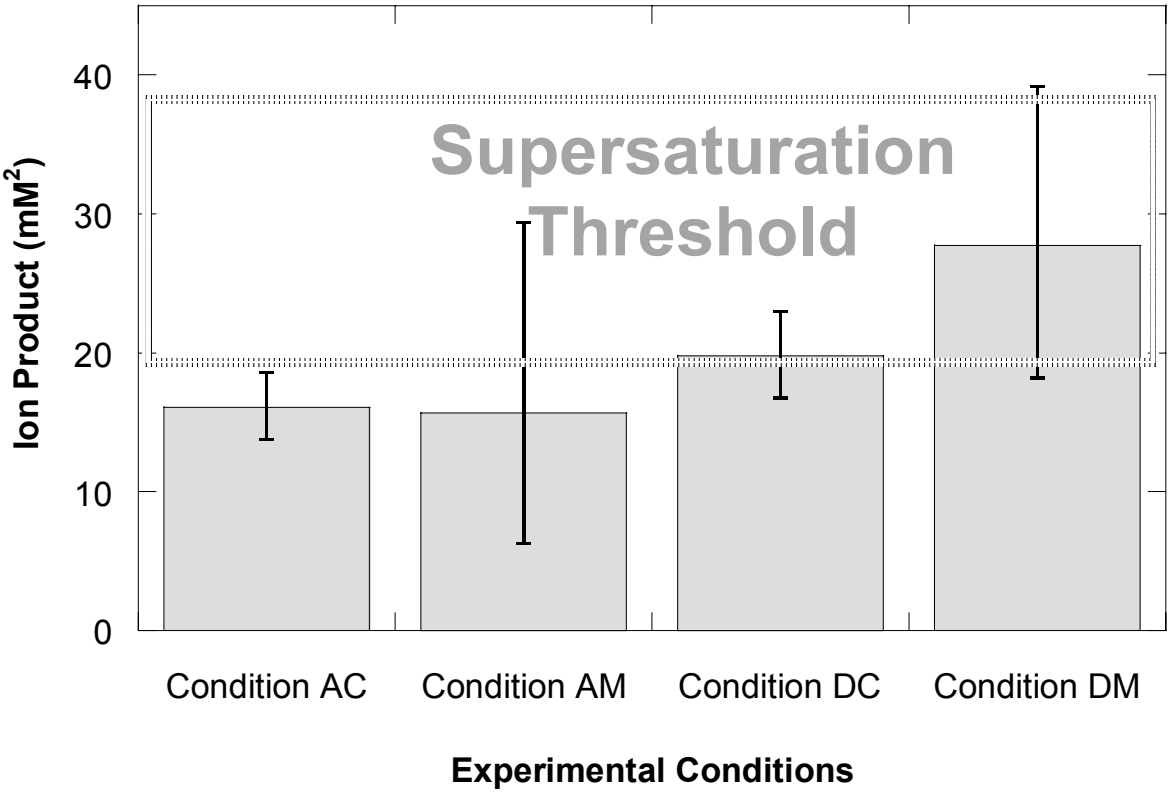

Figure 1.12 Values of ion products about location x = 3 cm. Shown are the average values of the ion product as calculated (Condition AC and DC) from concentrations in SD tubes and the values of the ion product as measured (Condition AM and DM) directly from DD tubes. The error bars represent the maximum and minimum possible (based on the standard deviation of the concentration values measured) values of the ion product. The average values for both the calculated and measured ion products for Condition D are within the supersaturation threshold window while only the maximum possible value for the ion product for Condition AM, falls within the supersaturation threshold.

differences and variability in timing of the precipitation events seen earlier in Experiment I. In short, as the boundary conditions change/vary, so too do the conditions and timing of the mineral precipitation, which is strongly dependent on the concentration and ratio of

ions at a given location in the hydrogel tube.

1.4 Conclusion

We have presented a survey of several established hydrogel-based DDSs that have been used to study the formation of calcium phosphate minerals as they relate to biomineralization. We have highlighted four distinct and unique systems, their application, the methods and reasons for their construction. In addition we have presented a protocol that can be used to either evaluate and/or construct and design a system for a specified application in studies of biomineralization. By exploring both the mathematical aspects regarding the governing diffusion equations, as well as the practical engineering and fabrication aspects, we hope to have made this class of diffusion systems more accessible. When designing a new DDS, one must keep in mind, the simpler the design, the less that can go wrong, but the less control you have over the system. The more controls you design into a DDS, the more complicated the design becomes, but the greater the chances for one small thing to make everything go wrong. In principle, for designing a DDS, the questions that must be asked and answered include: What are the intended boundary conditions? And how can they be maintained with high fidelity? Through this "Highlight" we hope we have provided the reader with the necessary tools to ask and answer these questions.

In our explorations of the DDS, we have developed a detailed understanding of the operation of a DDS in the context of diffusion theory. By closely examining the underlying design criteria for all of these hydrogel-based DDSs, we have rediscovered what a powerful tool hydrogel-based double-diffusion can be for studying crystal growth and nucleation. We can now explore interesting questions in biomineralization such as:

What is the role of substrates in mineralization within an ECM-like matrix?[15] What are the effects regulating gradients of inhibitors on mineral formation within an ECM-like environment?[15] What are the effects of various types of hydrogels on both the crystal morphology and degree of mineralization in an environment where the rate of diffusion is the same?[15] And what is the role of calcium and phosphate as destabilizing agents on biological amorphous calcium phosphate to promote mineralization?[15] We hope that by sharing the insights we have found, new doors will be opened by those seeking to model mineralization within an extracellular matrix microenvironment; bringing even more exciting results to the field of biomineralization.

1.5 Supplemental Materials:

The supplemental materials describe:

- A review of the general design of a Circulating Semi-Infinite Reservoir DDS (Section 1.5.1)
- A guide for the construction of a Circulating Semi-Infinite Reservoir DDS (Section 1.5.2)
- The material and methods for the paper (Section 1.5.3)
- A general protocol for using a Circulating Semi-Infinite Reservoir DDS (Section 1.5.4)
- The calculations for the semi-infinite reservoir condition for a Circulating Semi-Infinite Reservoir DDS (Section 1.5.5)
- Notes and considerations when using a Circulating Semi-Infinite Reservoir DDS (Section 1.5.6)

1.5.1 Design of the Circulating Semi-Infinite Reservoir System:

Essentially the design of the Circulating Semi-Infinite Reservoir system can be viewed as multiple Flowing Infinite Reservoir Designed Static DDS stacked in parallel, with longer gels and a circulated, rather than flow-through, reservoir configuration. Two large vessels, 1 L (glass bottles with hose barbs and stopcocks), are constantly circulated with a peristaltic pump creating a turbulent, infinite reservoir. The system is designed to hold 18 gels for a single set of experiments connected to the reservoirs through a circuit of tubes. The circuit tubing is constructed of vinyl tubing with polypropylene connectors. The various segments of the circuit are connected together through a series of quick disconnects that make disassembly, troubleshooting, repair and cleaning of the system easy. The connection of the gel tubes to the circuit are made with thin walled vinyl tubing that is pre-stretched to accommodate the gel tubes with a snug connection.

The start time t_0 of the experiment is controlled by placing gel-filled diffusion tubes on a dry system at the start of the experiment, the use of valves on the reservoir, and a pump to introduce the reservoir fluid to each of the diffusion tubes at the same time or with a sufficiently short time scale. The "short" time scale required is found by applying the steady state condition of $\tau >> L^2/D$ to the thickness of the gel edge at the interface layer. If we assume that the thickness of the gel edge is only 500 μm (0.05 cm) and we use the value of calcium diffusivity (the faster of the two diffusivities) found in literature $6.0 \times 10^{-6} cm^2/s$, the most amount of allowable time lag between fluid contact from the first tube to the last tube would be 6.9 minutes. If we assume that the thickness of the gel edge is as large as 1 mm (0.1 cm) then the most amount of time lag between fluid contact from the first tube to the last tube would be 27.75 minutes.

The use of peristaltic pumps and stir plates under each reservoir helps to maintain

the value of c_0 at the solution/gel interface. In this system fluid is circulated through the system at a rate of 42 mL/min through a circuit that is less than 150 mL in volume. New fluid from the reservoir completes a circuit in less than 3.5 minutes, making the lag time between the start of the pump and the connection of fluid to the ends of the hydrogel less than 5 minutes. New fluid from the circuit makes contact with the gel within 15 minutes. The movement of fluid through the system was monitored in an independent test using the circulation of colored dye. The 1 Hz oscillating flow of 42 mL/min is fast enough to equalize the system but slow enough to not dislodge the gel from the reaction tubes.

1.5.2 Construction and Assembly of a Circulating Semi-Infinite Reservoir System

The Circulating Semi-Infinite Reservoir DDS is assembled from a series of tygon (vinyl) tubing, polypropylene connectors, modified media bottles with stopcocks and a peristaltic pump with dual pump heads, head dedicated to each reservoir circuit. As can be seen in the diagram of Fig. S1, the: list of materials (ordered from Fisher Scientific) need for the construction of one reservoir circuit is:

- 1 x 16”, ¼” OD silicone, L/S-15 Masterflex pump tubing
- 5/8” OD, 3/8” ID poly-vinyl (PVC) tubing
    - 1 x 9”
    - 2 x 7”
    - 1 x 5.5”
    - 2 x 5”
    - 1 x 3”
    - 11 x 2”
- 1 x 20”, ½” OD, 3/8” ID PVC tubing
- 12 x 1¼”, 7/16” OD, 5/16” ID PVC tubing

- 13 x poly-propylene 3/8” tubing tees
- 5 sets of quick-disconnects for up to 3/8” ID tubing
- 1 set of quick-disconnects for up to ¼” ID tubing
- 1 pinch clamp for ½” OD tubing

All sizes ID and OD (in inches) are made such that connections are snug fits without the need for hose or cinch clamps. To aid in the assembly of the tubing network the ends of the PVC tubing are dipped in a beaker of acetone to temporarily swell the tubing and then immediately fitted over the polypropylene connectors. The 5/16” ID thin walled tubing (D) used for connecting the hydrogel tubes to the reservoir circuits; once cut, are plugged with #000 rubber stoppers (at either end) and placed in an oven at 70°C for 30-60min. Every 10 min or so the stoppers in the tubing are pushed deeper into the tubing, stretching the ends of the pre-cut tubes. Once pre-stretched, the tube ends are dipped into acetone to temporarily swell the tubing and then immediately placed on the ports of the reservoir circuit. Only the PVC tubing connections to the quick disconnects are secured with hose clamps and the disconnects are locked together using zip ties, to assure there is no accidental disconnecting of the tubing during handling and operation.

The reservoirs are assembled from commercially available media bottles modified by a glass blower with stopcocks attached to the base of the reservoir at a 10 degree angle. Assembly proceeds a shown Fig. 1.14-1.20

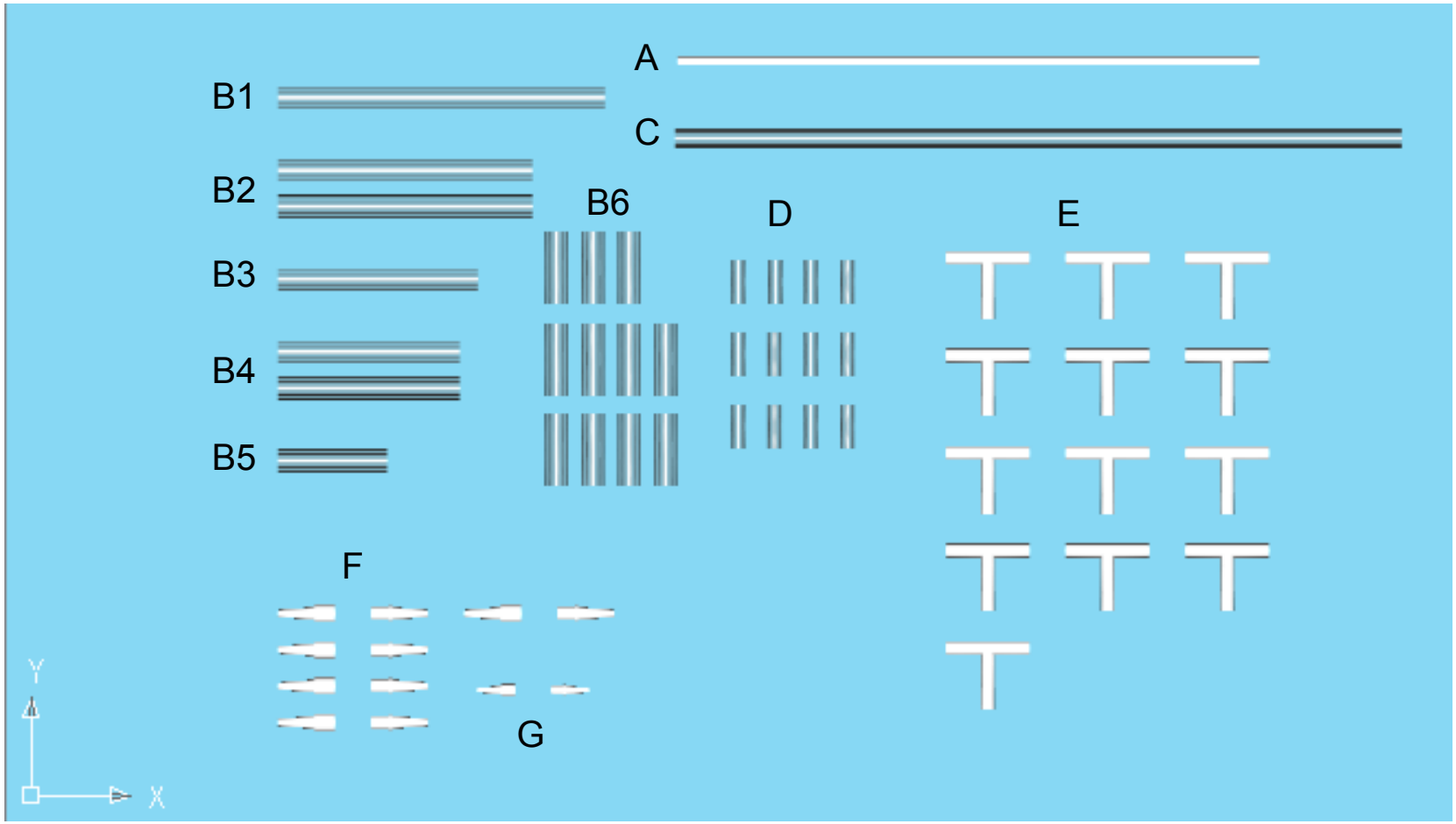

Figure 1.13 Materials needed for the construction of a Circulation Semi-Infinite Reservoir DDS: (A) 1 x 16", ¼" OD silicone, L/S-15 Masterflex pump tubing, (B) 5/8" OD, 3/8" ID poly-vinyl (PVC) tubing, (B1) 1 x 9", (B2)2 x 7", (B3)1 x 5.5", (B4) 2 x 5", (B5)1 x 3", (B6)11 x 2", (C) 1 x 20", ½" OD, 3/8" ID PVC tubing, (D) 12 x 1¼", 7/16" OD, 5/16" ID PVC tubing, (E) 13 x poly-propylene 3/8" tubing tees, (F) 5 sets of quick-disconnects for up to 3/8" ID tubing, (G) 1 set of quick-disconnects for up to ¼" ID tubing , (H) 1 pinch clamp for ½" OD tubing.

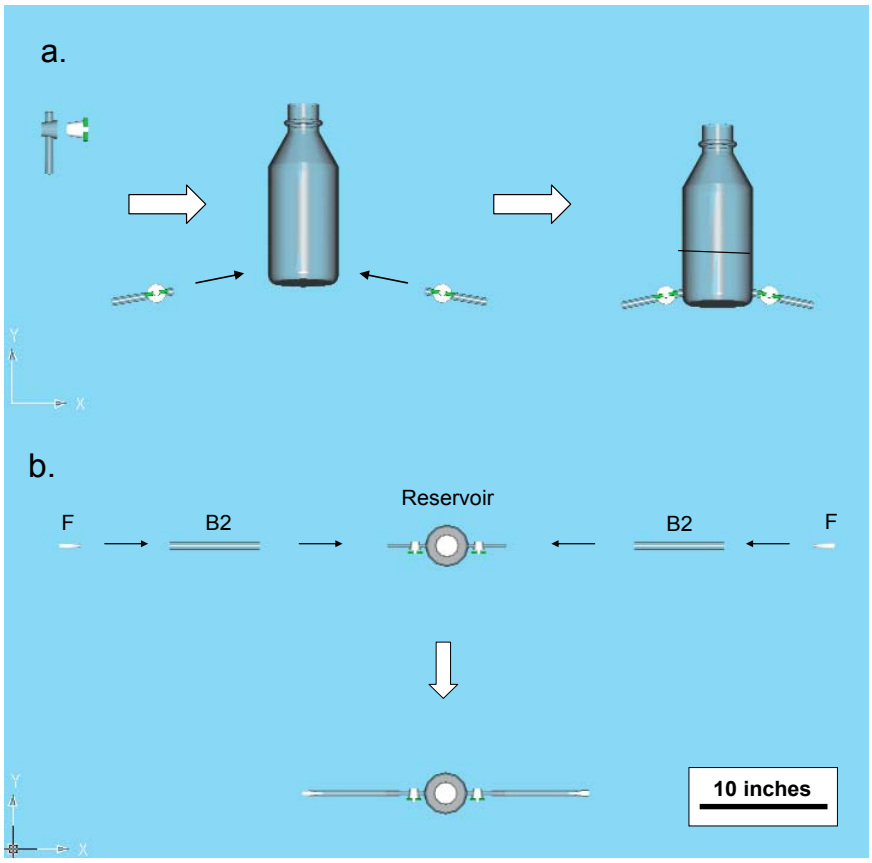

Figure 1.14 Reservoir Assembly. (a.) Stopcocks are attached at a 10 degree angle to the bottom of commercially available media bottles, (b.) PVC tubing is attached with polypropylene disconnects.

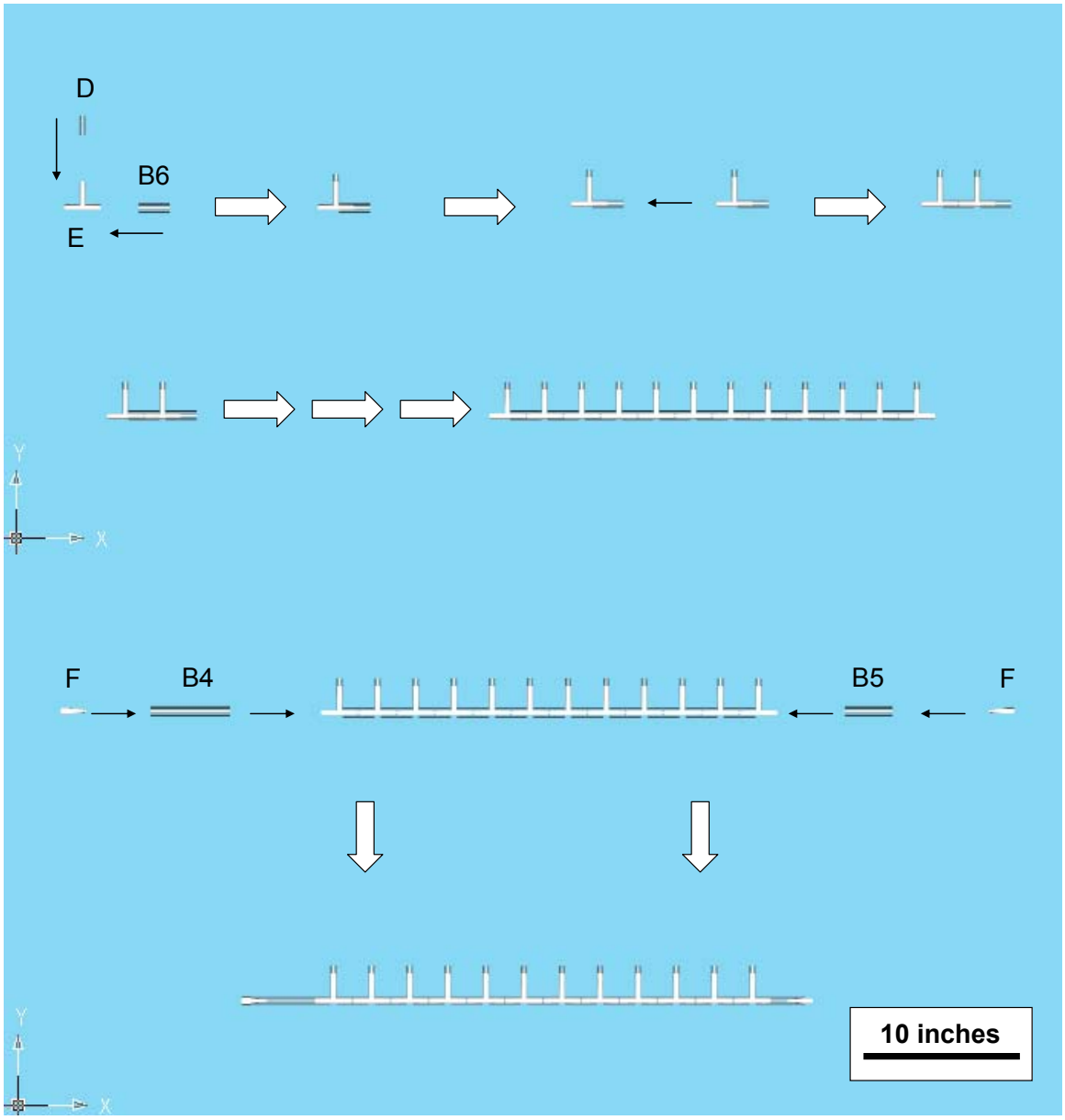

Figure 1.15 Diffusion manifold assemble constructed from PVC tubing, poly-propylene tubing tees, and quick disconnects. Once assembled, gel filled diffusion tubes can be attached to the diffusion manifold before being connected to the DDS.

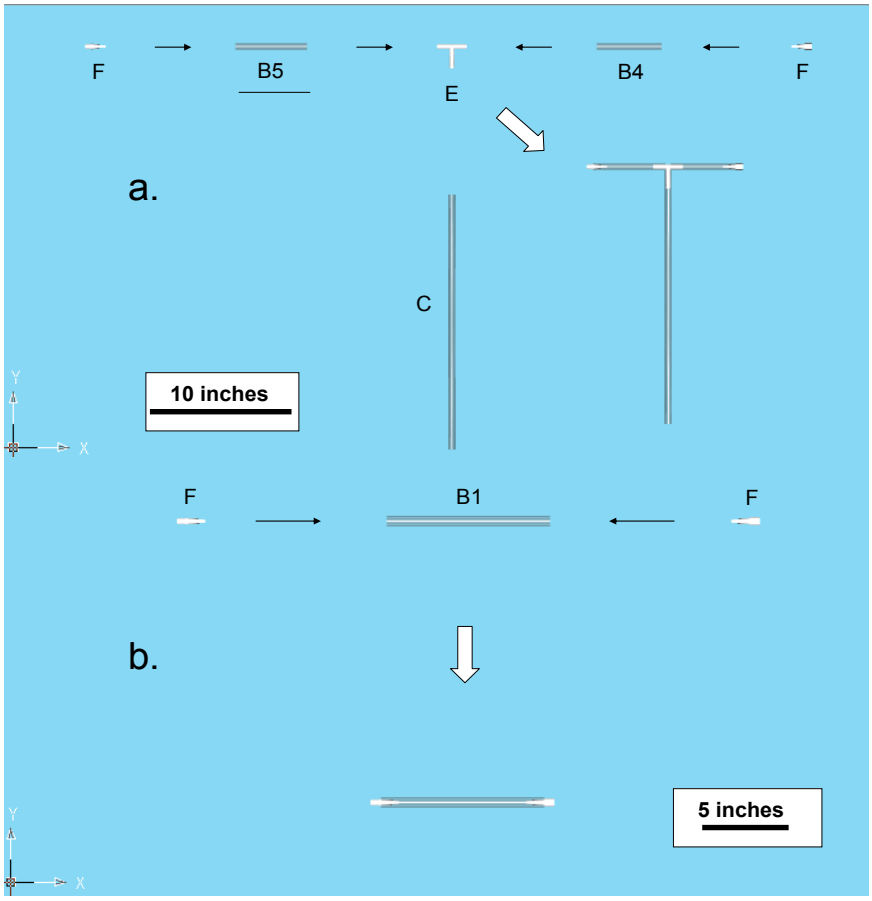

Figure 1.16 Drain tube assembly (a.) constructed from PVC tubing, poly-propylene tubing tees, and quick disconnects. Once assembled a hose pinch clamp (H from Figure S1) can be attached to the long drain tube to act as a valve. The drain tube can also be used to connect to an air pump to circulate the reservoirs in lieu of using a peristaltic pump. Extension tube (b.) constructed from PVC tubing, and quick disconnects, connects the reservoir to the pump assembly.

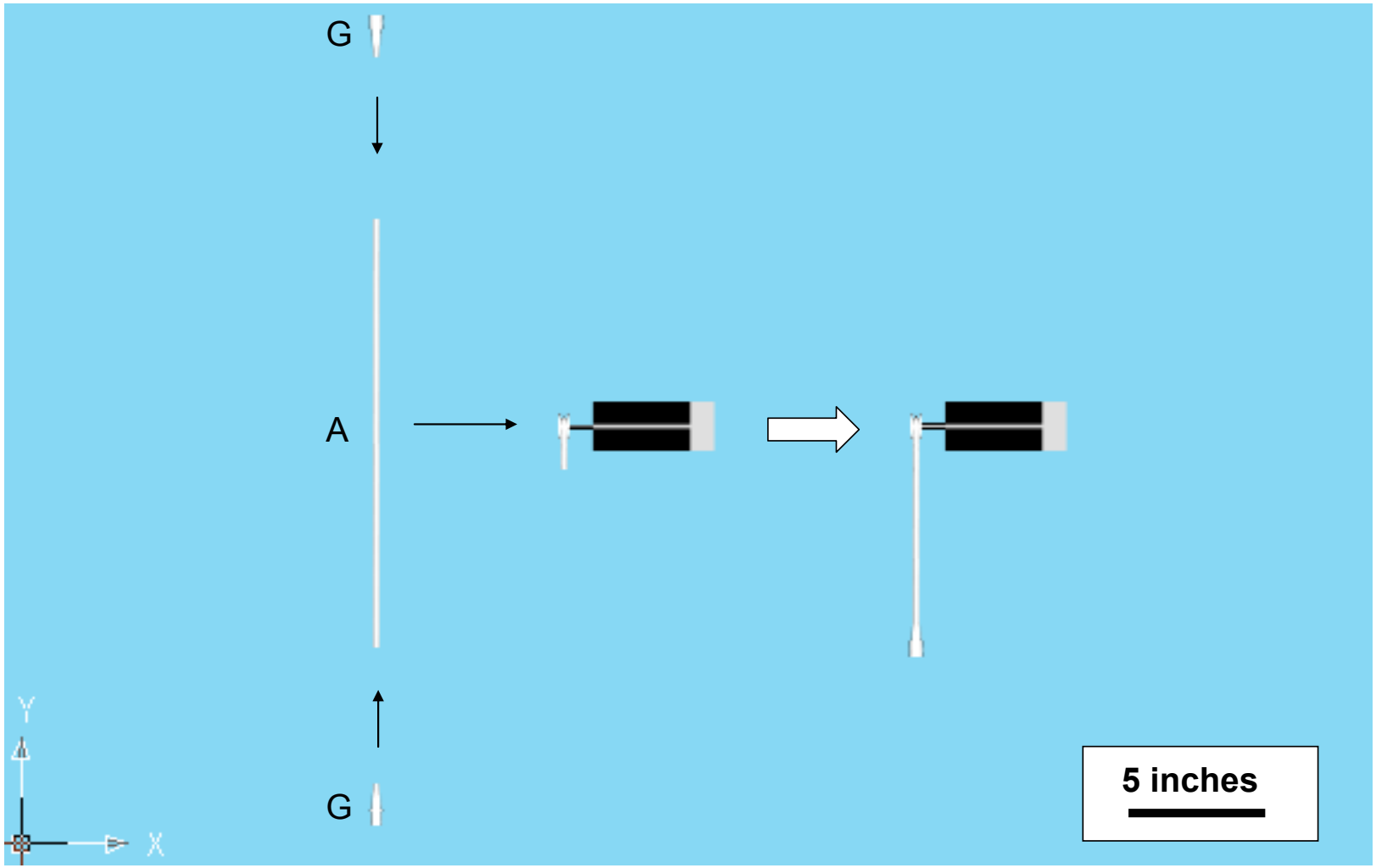

Figure 1.17 Pump assembly, constructed from a peristaltic pump, silicone tubing and quick disconnects. Once assembled the pump can be attached to the DDS to circulate the reservoir. If the peristaltic pump needs to be bypassed for maintenance or substituted by an air pump, the peristaltic pump can be disconnected from the DDS and the corresponding quick connects on the DDS can be connected together to preserve the reservoir circuit.

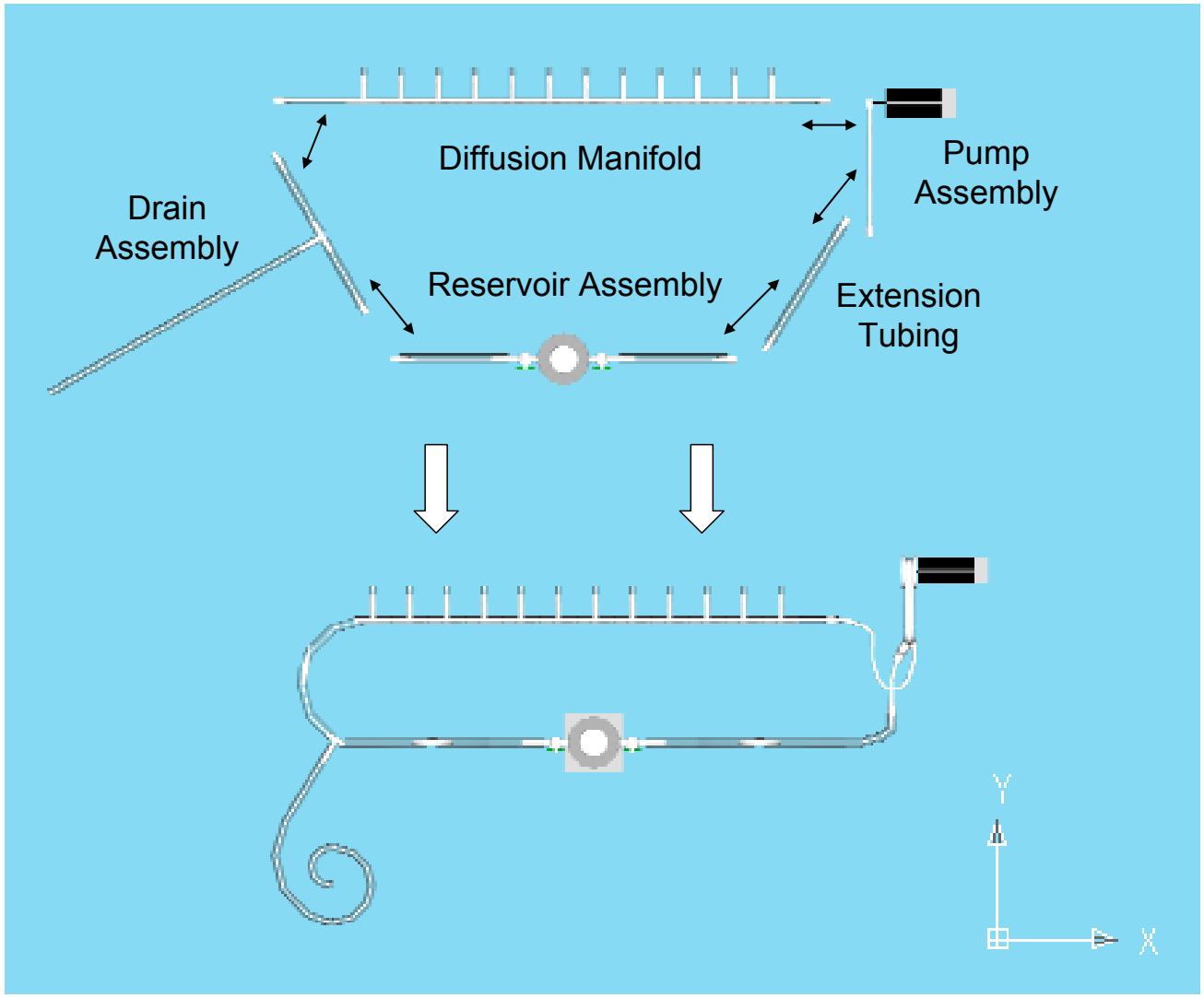

Figure 1.18 DDS reservoir circuit is assembled from the various system components using quick disconnects.

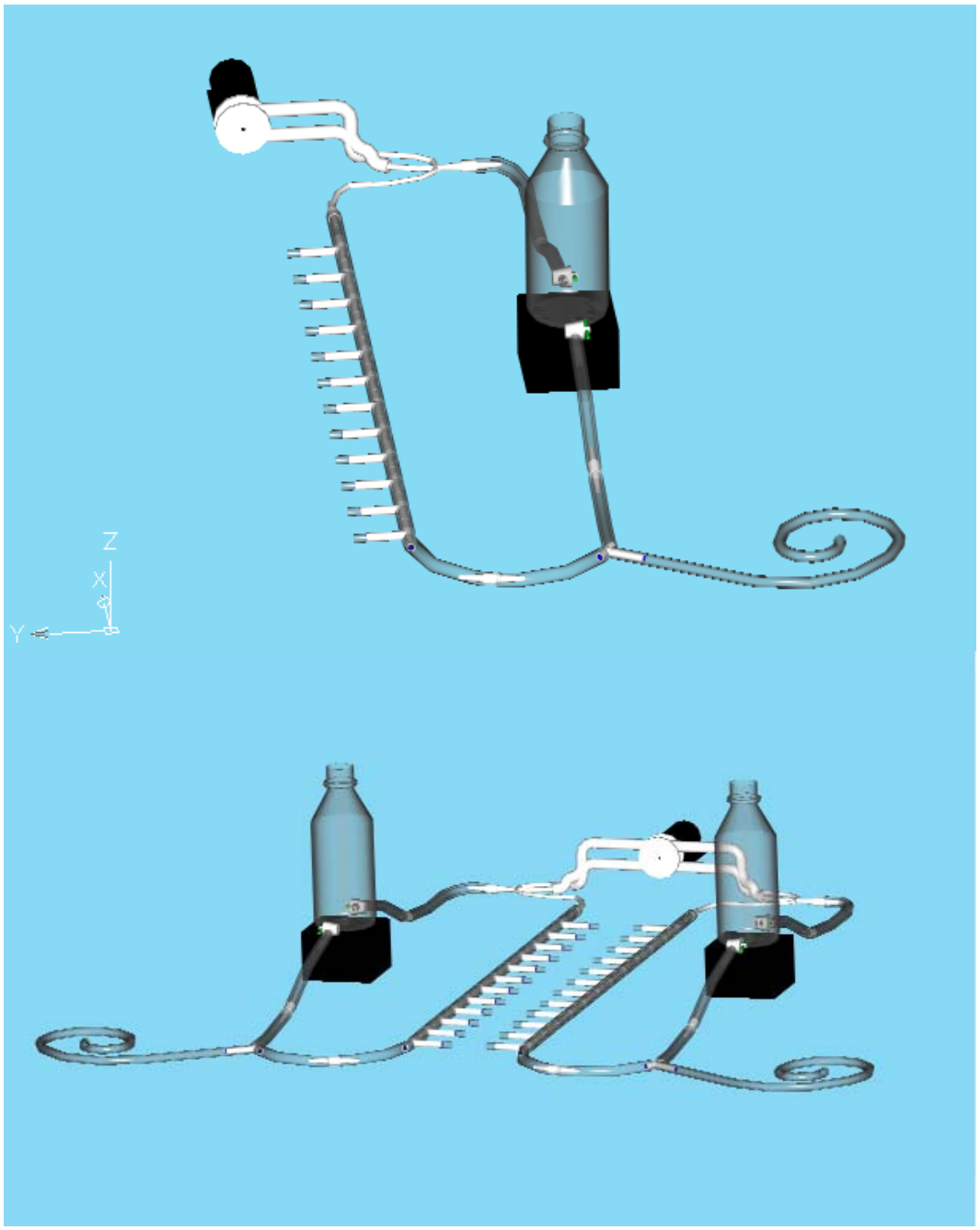

Figure 1.19 Once assembled with a stir plate under each reservoir, two reservoir circuits make a complete DDS.

1.5.3 Materials and Methods:

1.5.3.1 Solutions:

A 150 mM Tris Buffer stock solution is prepared with 0.5% sodium azide (Fisher), used to prepare gelatin solutions and as a hydrating solution for diffusion gels.100 mM Calcium Chloride Dihydrate +99% (Sigma-Aldrich) in 150 mM Tris Buffer (pH 7.4) with 0.5% sodium azide is used as the calcium source, the phosphate source is 115 mM Ammonium Phosphate Monobasic (Sigma-Aldrich) in 150 mM Tris Buffer (pH 7.4) with 0.5% sodium azide.

1.5.3.2 Gelatin Gels:

Gelatin 10 w/v % in Tris Buffer pH 7.4, is prepared with gelatin powder, 225 Bloom Type-A (MP-Biomedicals), in pre-prepared Tris buffer with 0.5% sodium azide.

1.5.3.3 Experiment I:

Dynamic DDSs were run with varying boundary conditions, all 12 tubes in the system are DD (double diffusion) tubes. The experimental conditions used were: a non-circulating system with non-hydrated gels (Condition A), a non-circulating system with hydrated gel (Condition B), a circulating system with non-hydrated gels (Condition C) and a circulating system with hydrated gels (Condition D). The time of the initial precipitation event was recorded in all of the experiments for all tubes.

Condition A was made by filling 12, 6 cm diffusion tubes with 10 w/v % 225 Bloom Type-A gelatin in Tris buffer pH 7.4. The gels were left to set at 20 °C for 30-45 minutes. Once the gel was firm, the plastic caps used when filling the tubes were

removed and the gel was cut flush to the diffusion tube using a razor blade. Tubes were then placed on the DDS, and once the bubbles in the reservoir circuits were removed using the peristaltic pump, the system was disconnected from the pump and run for 5 days.

Condition B was made by filling 12, 6 cm diffusion tubes with 10 w/v % 225 Bloom Type-A gelatin in Tris buffer pH 7.4. The gels were left to set for 30-45 minutes. Once the gel was firm the plastic caps used when filling the tubes were removed and the tubes were placed in 15 mL centrifuge tubes and pre-filled (to avoid the trapping of air bubbles) with ~6 mL of Tris buffer pH 7.4 (so the entier tube is submersed). Tubes were then placed in a water bath at 25°C for 2 days. After pre-hydration the tubes were removed and the gels cut flush to the diffusion tube using a razor blade, then placed on the DDS, and once the bubbles in the reservoir circuits were removed using the peristaltic pump, the system was disconnected from the pump and run for 5 days

Condition C was made by filling 12, 6 cm diffusion tubes with 10 w/v % 225 Bloom Type-A gelatin in Tris buffer pH 7.4. The gels were left to set for 30-45 minutes. Once the gel was firm the plastic caps used when filling the tubes were removed and the gel was cut flush to the diffusion tube using a razor blade. Tubes were then placed on the DDS with a circulating peristaltic pump and run for 5 days.

Condition D was made by filling 12, 6 cm diffusion tubes with 10 w/v % 225 Bloom Type-A gelatin in Tris buffer pH 7.4. The gels were left to set for 30-45 minutes. Once the gel was firm the plastic caps used when filling the tubes were removed and the tubes were placed in 15 mL centrifuge tubes and pre-filled (to avoid the trapping of air bubbles) with ~6 mL of Tris buffer pH 7.4 (so the eniter tube is submersed).Tubes were then placed in a water bath at 25°C for 2 days. After pre-hydration the tubes were

removed and the gels cut flush to the diffusion tube using a razor blade, then placed on the DDS with a circulating peristaltic pump and run for 5 days.

To monitor the timing for precipitation events in each system, a DDS with each condition was run once and the precipitation in the gels was checked every 6-12 hrs. until precipitation was first seen in any tube. Once a rough time frame for the onset of precipitation was determined, a second DDS with each condition was run and monitored (starting 12 hrs. before the rough time frame for each condition was established) every 15 minutes until every diffusion tube had precipitation. Time when precipitation occurred in each tube was recorded for each tube.

1.5.3.4 Experiment II:

For this experiment, we used the "best practices" boundary conditions (Condition D) from Experiment I. Both 6 cm single diffusion (SD) tubes and 8 cm SD tubes were tested for 5 days. In evaluating the semi-infinite condition for the reservoirs as ion sources, each reservoir was sampled every-other day of the experiment (total time of 5 days).

1.5.3.4.1 Tubes

A DDS was run with, 6 cm SD tubes and 6, 8 cm SD tubes for each reservoir circuit, for a total of 12 tubes per circuit and 24 tubes for the whole DDS. The system was setup by filling each diffusion tube with 10 w/v % 225 Bloom Type-A gelatin in Tris buffer pH 7.4. The gels were left to set for 30-45 minutes. Once the gel was firm the tubes were removed and the tubes were placed in 15 mL centrifuge tubes and pre-filled with ~6 mL of Tris buffer pH 7.4 (so the entire tube is submersed). Tubes were then placed in a water bath at 25°C for 2 days. After pre-hydration the tubes were removed

and the gels cut flush to the diffusion tube using a razor blade, then placed on the DDS, with a circulating peristaltic pump and run for 5 days.

After 5 days the DDS was stopped, the exact time run was recorded and the tubes removed from the system. The gel tubes were then placed in the refrigerator for 30-45 min to harden the gels. Once firm, the gels were removed from the diffusion tubes by cracking the diffusion tubes with a pair of pliers and peeling away the shattered plastic. The gels were then cut into even 0.67 cm sections using a custom designed gel cutter. The last sections of each gel was taken, as well as the three sections located at x = 1.995 cm, 2.665cm and 3.335 cm, from the diffusing ion source. The gel slices located at x = 1.995 cm, 2.665cm and 3.335 cm, were placed in 10 mL of 0.8 M nitric acid, for a total dilution of 31:1. The end slices were placed in 5 mL of 0.8 M nitric acid, for a total dilution of 15.5:1. The slices in nitric acid were sealed in 15 mL centrifuge tubes and place in the oven at 70°C for two days to hydrolyze the gels. Once hydrolyzed the solutions were then run through an axially viewed ICP trace analyzer emission spectrometer (model ICAP 61E trace analyzer, Thermo Electron, Waltham, MA). The transfer optics had been replaced with a short depth of field transfer optics to reduce matrix effects.

The resulting concentration from each solution was reported in ppm for Ca and P. To convert the concentration in ppm to mM each value was multiplied by the corresponding dilution factor and then divided by the molecular weight of each element. The average concentration value for a location *x* was determined across each set of 6 tubes for each tube length and diffusing ion.

Diffusivities of ions through each tube were determined using the estimation $x = 1.6\sqrt{Dt}$, of the diffusion penetration distance from a point source where the

concentration has fallen to 25% of the concentration at x = 0. Each concentration value for the three sections at x = 1.995 cm, 2.665cm and 3.335 cm, from the diffusing ion source were plotted against the distance of the middle of each slice from the source. An exponential fit line was applied to the points and x was solved for $c = c_0/4$.

Once x was found for $c = c_0/4$ that value was plugged into $x = 1.6\sqrt{Dt}$ at a constant time t (recorded at the end of the experiment).

These diffusivities were used to subsequently calculate the values of ion concentrations (using Eq 5.) at the end of their respective tubes and the center of the 6.67 mm wide end-slice. These calculated values were then compared to measured values of ions within that end slice.

1.5.3.4.2 Reservoirs

To probe the semi-infinite volume condition (c > 99.9% of c_0) for the 1 liter reservoirs, sample concentrations of the reservoirs were taken at zero, three and five day time points, from the calcium and phosphate reservoirs in a DDS running only SD tubes (12 tubes per reservoir). Each reservoir sample (0.1 mL) was diluted to 10 mL in 0.8 M nitric acid. The solutions were then run through an axially viewed ICP trace analyzer emission spectrometer (model ICAP 61E trace analyzer, Thermo Electron, Waltham Ma). The transfer optics had been replaced with a short Depth of field transfer optics to reduce matrix effects.

The resulting concentration from each solution was reported in ppm for each element Ca and P. To convert the concentration in ppm to mM each value was multiplied by the corresponding dilution factor and then divided by the molecular weight of each element.

1.5.3.5 Experiment III:

1.5.3.5.1 Baseline Experiment

Dynamic DDSs were run with varying boundary conditions with either all DD tubes or a combination of DD and SD tubes. The two extremes from Experiment I, conditions A and D, were used. An all DD system was run under Condition D to establish the supersaturation threshold window for this gel (10 w/v % 225 Bloom Type-A gelatin) in this system.

Three sets of 3, 6 cm diffusion tubes were filled with 10 w/v % 225 Bloom Type-A gelatin in Tris buffer pH 7.4. The gels were left to set for 30-45 minutes. Once the gel was firm the plastic caps used when filling the tubes were removed and the tubes were placed in 15 mL centrifuge tubes and pre-filled with ~6 mL of Tris buffer pH 7.4 (so the entire tube is submersed). Tubes were then placed in a water bath at 25°C for 2 days. After pre-hydration the tubes were removed and the gels cut flush to the diffusion tube using a razor blade. Each set of three tubes were placed on the DDS one hour apart, with a circulating peristaltic pump and run until precipitation was seen in the first set of tubes. Based on the data from Experiment I the system was monitored every 15 min starting 6 hrs. before precipitation was expected to occur. Once precipitation occurred, the DDS was stopped and the tubes removed. Once removed only the first set of tubes (71.43 hours) showed signs of precipitation, the other two remaining sets of tubes were clear. After removal from the system the tubes were placed in the refrigerator for 45 mins to firm-up before handling and cutting. After 45 minute the two remaining sets of tubes began to show signs of precipitation but fainter than the first set of tubes. The gels were then scanned on a flatbed scanner (Canon 4440F). After imaging, the gels were removed from the diffusion tubes by cracking the diffusion tubes with a pair of pliers and peeling

away the shattered plastic. The gels were then cut into even 0.67 cm sections using a custom designed gel cutter. The middle section (center of the section at x = 3.0 cm, which contained the precipitate) of each gel was placed in 10 mL of 0.8 M nitric acid, for a total dilution of 31:1.

The solutions were then run through an axially viewed ICP trace analyzer emission spectrometer (model ICAP 61E trace analyzer, Thermo Electron, Waltham Ma). The transfer optics had been replaced with a short Depth of field transfer optics to reduce matrix effects. The resulting concentration from each solution was reported in ppm for each element Ca and P. To convert the concentration in ppm to mM each value was multiplied by the corresponding dilution factor and then divided by the molecular weight of each element. The average concentration value for each ion was determined across each set of 3 tubes for each middle section. The average concentration values of calcium and phosphate for each middle section for each set of tubes were then multiplied together to give a supersaturation value for each time point. The minimum possible supersaturation value was found by taking the lowest value, by standard deviation, for calcium and phosphate concentrations in the earliest time point (69.40 hrs.) and multiplying them together. The maximum possible supersaturation value was found by taking the highest value, by standard deviation, for calcium and phosphate concentrations in the latest time point (71.43 hrs.) and multiplying them together.

1.5.3.5.2 Ion product for Condition A and Condition D

Once the point in time at which precipitation occurred was established (71.43 hrs.), this time point was used as a marker for the next experiment. Two systems were run looking at each condition (Conditions A and D from Experiment I), 6 DD tubes were run, 3 for Condition A, 3 for Condition D, and 12 SD tubes were also run, 6 for calcium

(Conditions A and D), 6 for phosphate (Conditions A and D). The two systems were stopped 2 hrs. ± 0.1 hrs. before precipitation was expected to occur for Condition D.

Condition A tubes were made by filling 3, 6 cm DD tubes and 6, 8 cm SD tubes with 10 w/v % 225 Bloom Type-A gelatin in Tris buffer pH 7.4. The gels were left to set for 30-45 minutes. Once the gel was firm the plastic caps used when filling the tubes were removed from 3 DD tubes (left on the 6 SD tubes) and cut flush to the diffusion tube using a razor blade. Tubes were then placed on the DDS, and once the bubbles in the reservoir circuits were removed using the peristaltic pump, the system was disconnected from the pump and run until 69.36 hrs.

Condition D tubes were prepared two days before the Condition A tubes; by filling 3, 6 cm DD tubes and 6, 8cm SD tubes with 10 w/v % 225 Bloom Type-A gelatin in Tris buffer pH 7.4. The gels were left to set for 30-45 minutes. Once the gel was firm the plastic caps used when filling the tubes were removed from 3 DD tubes (left on the 6 SD tubes) and the tubes were placed in 15mL centrifuge tubes and pre-filled with ~6 mL of Tris buffer pH 7.4 (so the entire tube is submersed). Tubes were then placed in a water bath at 25°C for 2 days. After pre-hydration the tubes were removed and the gels cut flush to the diffusion tube using a razor blade, then placed on the DDS with a circulating peristaltic pump and run until 69.36 hrs.

Once the experiments were complete, the tubes were removed from the system and placed in the refrigerator for 45 mins to firm-up the gelatin before handling and cutting. The gels were removed from the diffusion tubes by cracking the diffusion tubes with a pair of pliers and peeling away the shattered plastic. The gels were then cut into even 0.67 cm sections using a specially designed gel cutter. The three sections of each gel located at x = 1.995 cm, 2.665cm and 3.335 cm, from the diffusing ion source were

selected and placed in 10 mL of 0.8 M nitric acid, for a total dilution of 31:1. The slices in nitric acid were sealed in 15 mL centrifuge tubes and place in the oven at 70°C for two days to hydrolyze the gels. Once hydrolyzed the solutions were then run through an axially viewed ICP trace analyzer emission spectrometer (model ICAP 61E trace analyzer, Thermo Electron, Waltham Ma). The transfer optics had been replaced with a short Depth of field transfer optics to reduce matrix effects.

The resulting concentration from each solution was reported in ppm for each element Ca and P. To convert the concentration in ppm to mM each value was multiplied by the corresponding dilution factor and then divided by the molecular weight of each element. The average concentration value for a location *x* was determined across each set of 9 tubes for each tube length and diffusing ion. The ion product for each set of conditions A & D was found by multiplying together the average concentration of calcium and phosphate from the middle sections of each set of DD tubes. The maximum and minimum possible ion product values were found by taking the highest and lowest values, by standard deviation, for calcium and phosphate concentrations in the middle sections and multiplying them together. Calculated ion products were found by using the ion concentrations found at x = 3.0 cm for the SD tubes for each condition. The error values were found by taking the highest and lowest values, by standard deviation, for calcium and phosphate concentrations in the middle sections and multiplying them together.

1.5.4 Protocols:

1.5.4.1 Solution Preparation:

0.15 mM Tris Buffer Solution in a 1 Liter solution:

19.83 g Tris HCl (Sigma),

2.91 g Tris Base (Sigma),

0.4 g Sodium Azide (Fisher),

In 1 liter of DI H_2O.

Dissolve the powders in 75% of total volume and adjust the pH to 7.4 with either 1 M HCl or 1 M NaOH, then fill to the full volume.

100 mM Calcium Chloride Solution:

29.4 g $CaCl_2 \cdot H_2O$, (Sigma-Aldrich)

39.7 g Tris HCl,

5.82 g Tris Base,

0.8 g Sodum Azide.

In 2 liters of DI H_2O.

Dissolve the powders in 75% of total volume and adjust the pH to 7.4 with either 1 M HCl or 1 M NaOH, then fill to the full volume.

115 mM Ammonium Phosphate Monobasic:

[1]26.4 g $NH_4H_2PO_4$, (Sigma-Aldrich)

39.7 g Tris HCl,

5.82 g Tris Base,

0.8 g Sodum Azide,

In 2 liters of DI H_2O.

Dissolve the powders in 75% of total volume and adjust the pH to 7.4 with either 1 M

[1] for 100mM Phosphate, use same mass with $(NH_4)_2HPO_4$ (Ammonium Phosphate Dibasic)

HCl or 1 M NaOH, then fill to the full volume.

1.5.4.2 Gelatin Preparation:

10 w/v % volume solution:

Add 22 g of gelatin powder to 220 mL of 0.15 M Tris Buffer solution.

Heat to 55°C in a hot water bath while stirring.

Once dissolved, adjust the pH to 7.4 with either 1 M HCl or 1 M NaOH. Once the solution has been made it can be immediately used or stored in the refrigerator (good policy to store the gelatin no more than 3 weeks).

1.5.4.3 Tube Preparation and Filling:

Tubes are prepared from disposable polystyrene serological pipettes (10 mL pippets, 3/8" OD, 5/16" ID) cut to length with a hotwire cutter, washed with soap and water, rinsed with DI H_2O, and dried in the oven at 70°C. Tubes are capped with polypropylene caps punched from the pre-cleaned lids of food containers using a 9-10 mm cork borer, and sealed with parafilm.

Remove the gelatin from the refrigerator and heat in a water bath between 40-50°C. Any higher temperature and the solution can develop bubbles.

Tubes are capped and filled in such a way that the highest number on the pipette will be closet to the calcium source or furthest from the phosphate source. (This convention makes it easy to identify which ends of the tube have been in contact with which ion solution).

Tubes are filled slowly using plastic transfer pipettes and by dispensing the solution along the inside edge of the tube.

In addition there is a labeling convention for setting up a system to study both

single and double diffusion (an 18 tube system)

Position of the Tube	**Calcium Single Diffusion**	**Double Diffusion**	**Phosphate Single Diffusion**
Sample	A,C,E	G,I,K	N,P,R
Control	M,O,Q	H,J,L	B,D,F

For an all double diffusion system (a 12 tube system) the labeling convention follows a simple 1-12 numbering system. While an all single diffusion system (a 24 tube system) uses the 1-12 numbering convention with a C or P letter (for either calcium or phosphate) so that the labeling appears something like this 3C or 5P.

Once the tubes are filled, they are overfilled so that the meniscus of the gelatin provides a mushroom-cap-like appearance as the gel protrudes out of the tube. The tubes can either be set on the counter or placed in the refrigerator to cure the gel.

Once cured, the caps on the tubes are either removed (for double diffusion tubes) or left on (for single diffusion tubes) and the tubes are placed in 15mL centrifuge tubes and pre-filled with ~6 mL of Tris buffer pH 7.4 (so the entire tube is submersed).

Tubes can be left at lab temperature (20°C) for 3 days or room temperature (25°C) for 2 days. A temperature controlled bath can be used to maintain these temperatures

1.5.4.4 Setting up the Diffusion System:

If the diffusion system is dry, the sample tubes can be place on the system before the fluid is added. Fill the reservoirs with their respective solutions. Open the reservoir valves (make sure that the drain valve is closed), turn on the peristaltic-pump, turn up the

setting to level number 3 (42 mL/min). IF the pump is turned on before the valves to the reservoirs are opened then pressure will build in the system and the weakest point in the system will likely rupture.

As the pump moves fluid through the tubes any bubbles will be displaced by the fluid. Removing the air bubbles can be assisted by raising and lowering the tubing assembly to help guide the air pockets out through the reservoir. Once the air has been displaced from one half of the tubing (for each side, calcium/phosphate), turn the pump to '0', switch the direction on the pump, turn the pump back up to '3' and remove the air from the second half of the tubing.

Once the air has been removed from all the junctions between the tubes and the manifold, the system is considered "started".

If the diffusion system is filled with DI H_2O, drain the system as completely as you can. Fill the reservoirs with 300-400 mL (~30% reservoir volume) of the reagent solution. Circulate the reagent solutions through the system, removing the bubbles completely. Allow the solutions to circulate for 15-30 mins before emptying the circuits and then add the sample tubes to the system and refill the system with the target reagents.

1.5.4.5 Changing and Re-filling the Reservoirs During an Experiment

If it has been determined that in order to maintain the semi-infinite condition for an experiment that the reservoirs need to be changed, then the following describes how to change the reservoirs without disturbing the experiment.

- A few hours before the infinite condition is violated, open the valve of the drain tube while the pump is running and the stir plates are stirring.
- Let the level of the reservoir drop to just above the drain of the reservoir so no air bubble get into the system.

- Refill the reservoir to 100-150mL above the normal operating fill line of the reservoir and let the system run/circulate for at least 15-30min.
- After the system has circulate, drain the reservoir to the normal operating fill line and leave running until the next time the reservoir has to be changed.

1.5.4.6 Stopping an Experiment

To stop the DDS:

- Turn off the pump
- Close the valves on the reservoirs
- Open the drain tubes and drain the fluid in contact with the gel tubes
- If the diffusion manifold (gel tube assembly) can not be removed from the system, raise and lower the tubing to direct the fluid towards the drain and out of the tubing. If the diffusion manifold can be removed from the system, disconnect the assembly and drain the assembly into a sink, bucket or proper disposal vessel.
- Once fluid is no longer in contact with the gel tubes the system is considered “stopped”

1.5.4.7 Analysis of the Tubes:

Once gel-filled tubes have been removed from the DDS they are placed in a refrigerator (30-45min) depending on the initial temperature of the gels, to firm up the gels for handling.

1.5.4.7.1 Image scanning

Once set, the gels can be placed on an image scanner, either side-by-side or in a custom designed rack. For best results, scanning the gels without the lid down provides a black background for high contrast. To scan bare gels without their plastic tubes, the plastic tubes can be removed by cracking the polystyrene tube using a pair of pliers. The soft gels absorb the force while the plastic simply cracks and can be peeled away. The bare gels can then be placed on the scanner and scanned.

1.5.4.7.2 Concentration Analysis

1.5.4.7.2.1 Removal of Gels from Tubes:

To remove the gels from the plastic tubes, the polystyrene tube can be cracked open using a pair of pliers. The soft gels absorb the force while the plastic simple cracks and can be peeled away. Once made bare, the gels are cut into even slices. Slicing the gel can be accomplished by either careful measurement and use of a razor blade, or they can be cut using a specialized tool designed to cut every slice to the same length all at one time. Our lab uses such a tool where commercially obtained circular razor blades are spaced so each slice is equal to 0.667 cm or 1/9 the total length of a 6 cm long gel (1/12 the total length of a 8 cm long gel). At 0.667cm each gel has a volume of 0.333 mL.

1.5.4.7.2.2 Total ion concentration

These gel slices are then placed in a 15 mL centrifuge tube, filled with 10 mL of 0.8M Nitric Acid (for a total of 1:31 dilution), the tubes are sealed and set in the oven at 70°C for two days. The hydrolyzed samples are then run through an axially viewed ICP trace analyzer emission

spectrometer (model ICAP 61E trace analyzer, Thermo Electron, Waltham Ma),. The transfer optics had been replaced with a short Depth of field transfer optics to reduce matrix effects.

1.5.4.7.2.3 Mineral concentration

Gel slices are placed in 15 mL centrifuge tubes, filled with ~10 mL of 0.15M NH_4OH, and placed on a rocking table for 15 min. The solution is decanted and changed 2 more times. After the final decanting, the gels are pat dry and are then placed in a 15 mL centrifuge tube, filled with 10 mL of 0.8M Nitric Acid (for a total of 1:31 dilution), the tubes are sealed and set in the oven at 70°C for two days. The hydrolyzed samples are then run through an ICP-AES.

1.5.5 Calculating the Semi-Infinite Condition for Reservoirs.

Using a Circulating Semi-Infinite Reservoir dynamic DDS as the basis for our calculations and the reported literature values for: the fastest moving ion ($D_{Ca} = 6.0x10^{-6}$ cm^2/s),[17] the timing (5 days) and the length of the diffusion tube (6 cm) [17], the semi-infinite sink and source condition for a reservoir was determined. To determine the total amount of material leaving a source reservoir and entering a sink reservoir the total flux of material at each point (in and out of the diffusion tube) must be determined. Essentially the calculation is based on the second derivative of Fick's first law (first derivative of Fick's second law). Rather than find the integral of an erfc function at two points along a tube for 432000 seconds, we chose instead to construct a Matlab® script processed the necessary calculations in a loop.

For the semi-infinite sink condition, the total flux of material *V* out of the

diffusion tube is calculated from the first point *y*, 6.0 cm (end of the tube) to the second point *z*, 6.1 cm (1 mm into the sink reservoir). The total time of the system *t* is 432000 seconds (5 days), and the concentration *f* of ion at the first point *y* and the concentration *s* at the second point *z* are calculated using the solution to the diffusion equation for each second, and the diffusivity *D* found in literature for calcium in a 10 w/v % 275 Bloom Type-A gelatin. The instantaneous flux for each time point *j* is calculated by Fick's first law (Eq.1.1). This calculation is made by finding the difference in concentration between the two points (*y* and *z*) and dividing by the distance between the two points, converting the volume in liters to cm^3 and multiplying this value by the diffusivity *D* of the system.

$$j_1 = D_1 \frac{\partial c_1}{\partial x} \quad \text{(Eq.1.1)}$$

This calculation yields a solution for *j* in $mmol*cm^{-2}*s^{-1}$. Each value found for *j* at each time point is then successively added to each other for all time *t*, producing at total flux of material *V* per unit area (cm^2).

The total amount of material *E* (in mmol) per tube, is calculated by multiplying the total amount of total flux of material *V* per unit area by the cross-section of the diffusion tube. The total amount of material entering the sink reservoir *T* is found by multiplying the value for total amount of material *E* leaving each tube by the total number of tubes. The value of *T* is then multiplied by 10 to find to target volume *N* (in liters) for a reservoir that will satisfy the infinite condition of c = 0.1% of c_0.

1.5.5.1 Matlab script for calculating the semi-infinite condition for a sink reservoir:

```
V = 0;                  % Total flux of material per unit area
D = 6.0*10^-6;          % Diffusion constant
y  = 6.0;               % Start point in cm
z = 6.1;                % Final point in cm
```

```
for t = 0:1:432000;                 % Time in seconds
f = 100*erfc((y/2*sqrt(D*t)));      % Concentration at the first point y in mM
s = 100*erfc((z/2*sqrt(D*t)));      % Concentration at the second point z in mM
k = (f-s)/0.1;
j = (D*k)/1000;                     % The instantaneous flux
V = V+j;                            % Total flux of material per unit area
end
E = V*((0.35^2))*pi                 % Result: the total amount of material per tube in mmol
T = E*12                            % Result: the total amount of material entering the sink reservoir
n = E*10                            % Result: target volume per tube (in liters)
N = T*10                            % Result: target volume (in liters)
```

In order to calculate the semi-infinite condition for the source reservoir, the same technique is applied as finding the condition for a sink reservoir except the total flux of material is calculated from the first point $y = 0.01$ cm to the second point $z = 6.0$ cm (the entire length of the gel diffusion tube).

1.5.5.2 Matlab script for calculating the semi-infinite condition for a source reservoir:

```
V = 0;                              % Total flux of material per unit area
D = 6.0*10^-6;                      % Diffusion constant
y  = 0.001;                         % Start point in cm
z = 6;                              % Final point in cm
for t = 0:1:432000;                 % Time in seconds
f = 100*erfc((y/2*sqrt(D*t)));      % Concentration at the first point y in mM
s = 100*erfc((z/2*sqrt(D*t)));      % Concentration at the second point z in mM
k = (f-s)/0.1;
j = (D*k)/1000;                     % The instantaneous flux
```

```
V = V+j;                    % Total flux of material per unit area
end
E = V*((0.35^2))*pi         % Result: the total amount of material per tube in mmol
T = E*12                    % Result: the total amount of material leaving the source reservoir
n = E*10                    % Result: target volume per tube (in liters)
N = T*10                    % Result: target volume (in liters)
```

1.5.6 Additional Notes and Considerations

1.5.6.1 Bubbling vs. Pumps

The main differences between the system described here and a system that uses bubbling air (CO_2 scrubbed or plain nitrogen) are: control, precision, and accuracy of the flow rate not only between the two types of systems but even when comparing two reservoir circuits on the same system. By design, each reservoir circuit needs to be circulated. Turbulent mixing for the reservoir itself, in the bubbling system, is achieved by the passing of bubbles through the reservoirs from the bottom of the reservoir all the way to the top. Turbulent mixing of the reservoir in the pump system is achieved by placing a stir-plate under the reservoir. Contrary to many misconceptions the systems using an air-pump/air-tank ARE NOT under pressure. The reservoirs are open to the atmosphere so the bubbles introduced can rise to the surface; which allows fluid to be drawn into the reservoir circulating the system, and degassing the solutions. Often the idea that the system is under pressure is a concern, especially when the CO_2 scrubbers become over-pressured and rupture. The rupturing of the CO_2 scrubbers is because those components of the system are sealed and therefore ARE under pressure. Localized pressure build up is a concern for both systems but it must be understood where the

pressure is, and how it develops. The concern of pressure in the pump-driven system arises when the valves to the reservoirs are close and the pump can not circulate the solution and instead builds the pressure in the circuit leading the system to rupture at what ever the weakest point may be (often the corks, in a system without DD tubes, or SD tubes attached to the system).

Using a manometer placed on the system, attached to a diffusion tube port, the differences in the circulation between the two types of system can quantified. On a system using a peristaltic pump circulating a 150 mL circuit at a rate of 42 mL/min, the liquid column oscillates evenly at a rate of 1 Hz, fluctuating ±0.5 cm around a level that is even with the fluid level in the reservoirs. Oscillation rates higher than 1 Hz using the peristaltic pump can dislodge gels from the tubes in the system. On a system circulated by compressed air where the bubbling rate, controlled by pressure regulators, is dialed in to about 1 Hz with and air pocket formed between the air tube and the reservoir, the oscillations on the manometer were erratic with fluctuations that are uneven and range from as little as 0.5 cm to as large 3 or 4 cm around a level that is the same height as the fluid level of the reservoirs. These inconsistencies and variations between these two systems are largely because the sizes of the bubbles eluted in the bubbling system are not made uniform; bubbles break apart and fuse together creating variable rates and variable oscillations in the circulation of the system. The sometimes violently, erratic, fluctuations can help to explain the reason why increasing the rate of bubble elution can rip apart the gels in the diffusion tubes. A good practice to create a more consistent oscillation is dial down the bubble rate (using an individual regulator for each reservoir circuit) so that individual “discrete” bubble packets form in the fluid tube as air is introduce from the air tube, this technique minimizes the erratic nature of air-bubble based circulation.

1.5.6.2 Bubbles

Aside from the bubbles that are introduced into the compressed-air based system, and only travel a short distance in the circuit before eluting through the reservoirs, there are other bubbles to consider in the diffusion system. Bubbles can form in the reservoir circuit as air in the tubing is displaced as fluid is introduced to the circuit. Bubbles can also form when air is introduced to the system, when the gel filled diffusion tubes are inserted into a circuit already filled with fluid or if there is a small, slow leak in the tubing. The presence of bubbles in the reservoir circuit can drift to the gel/fluid interface and hinder diffusion by removing fluid from the interface. These bubbles can be removed by letting the system circulate while raising and lowering the tubing, guiding the bubbles to the reservoir and out of the system. Occasional taping and bumping will dislodge stubborn bubbles so that they glide along the tube. If there are especially stubborn bubbles that can not be easily dislodged, but they are downstream from the diffusion tube manifold then leave them alone, it is better to leave bubbles which do no harm, than potentially damage the system trying to remove them.

Bubbles can also form in the gels cast in the diffusion tubes. Bubbles in the gel can cause a number of problems. Diffusion through an air bubble is often not possible since there is no place for the air to be displaced, the fluid/ions will diffuse around this air-pocket increasing the effective path length of the ions travel in the system. Air bubbles at the gel/tube interface can affect the adhesion of the gel to the tube and can serve as a defect where fluid can bypass the gel and affect the rate of reaction. Once bubbles form in the gel or along the diffusion tube the sample should be scrapped. To prevent bubbles from forming, gel solutions should be used just above ($\sim {}^{+}10°C$) their gelling temperature. Temperatures consistently higher than the gelling temperature of a

hydrogel can cause bubbles to form in solution. Casting the gel in the tubes should be done slowly. Quickly pipetting the gel solution into the tube can cause bubbles to form as the solution is agitated. Pipetting the gel solution along the wall of the tube prevents air from getting trapped and allows the tube to fill along the tub/air interface and from the bottom up, slowing displacing the air as it rises in the tube. If bubbles do form as the gel is being cast, but while the solution is still molten, the bubbles can be removed by taping the tube so that they rise to the top where they can be removed with a pipette.

1.5.6.3 Reservoir Height

The pressure of the fluid in the DDS is the result of the height of the fluid in the reservoirs. The pressure of fluid on a hydrogel does not affect the rate fluid flow through the hydrogel. There is no flow in a hydrogel, the movement of material is strictly based on diffusion. An SD tube filled with a hydrogel (which has good adhesion to the tube in which it is cast) can be placed on a reservoir and left uncapped and the fluid will not flow through the tube, the only risk in that case is that the gel begins to dry out, shrinks, and the fluid leaks around the gel. A case where a pressure differential may be a problem is when there is poor adhesion between the gel and the tube. When a gel does not adhere to the tube or the pressure applied is greater than the adhesive force keeping the gel in the tube then the gel will be pushed from the tube and fluid can flow along the gel/tube interface. The fluid level of each reservoir however, should be kept at the same height, but not for any possible difference in pressure. Maintaining the same fluid level between reservoirs assures that the same volume of fluid is used for each experiment.

CHAPTER 2

2 A comparison of the formation of hydroxyapaptite in gelatin, collagen, and agarose hydrogels: specific & generic "gel-effects"

In hydrogel-based in vitro models for biomineralization, an important feature is the hydrogel. Here we explore the effects of the hydrogel microenvironement on mineralization, using the innovative design of a layered gel construction. Based on our understanding of diffusion in double diffusion systems, and the control offered by a circulation semi- infinite reservoir dynamic DDS, we are able to compensate for any role changes in diffusion may have in evaluating mineralization in different hydrogels.

2.1 Introduction

Previous studies using hydrogel-based single diffusion systems (SDS) have demonstrated that the use of different types of hydrogels results in differing levels of mineral content when comparing such gels to each other.[6]The accepted rational to explain this phenomenon has been that the rate of diffusion for the ionic species in each gel corresponded to the relative mineral content in each hydrogel. The faster ions move into and through a hydrogel, the higher the resulting mineral content. Studies using hydrogel-based DDSs demonstrate that a sufficiently small target area for mineralization coupled with a long hydrogel path length in which ions diffuse can eliminate potential problems due to changes/differences in the diffusion constant by biomacromolecules at the targeted site for mineralization.[12, 13, 17, 33-38]

Using the innovative capability of a dynamic DDS to separate the diffusing

medium from the mineralizing medium, together with a layered hydrogel construction we compare the formation of HA in gelatin, agarose and collagen hydrogels while eliminating the issue of differing diffusion constants found in each type of hydrogel. For the purpose of this work we will refer to gels formed from non-fibrillar based denatured collagen as gelatin gels, and we will refer to gels formed from fibrillar based unmodified collagen as collagen gels.

We examine the effect of three types of hydrogels (10 w/v % gelatin, 2 w/v % agarose, and 0.2 w/v % collagen), on the formation of HA, in a system where the diffusion constants (D, measured as cm^2/s) are normalized. In this work we report similar findings presented in the literature[6] with regard to relative mineral content in three types of hydrogels, however our data suggests that increased diffusivity of ionic species may not be the only cause for increased mineral content.

2.2 Background

There are important and significant differences in how crystals form in both solution [2, 3] and hydrogels.[7, 10-13, 17-19, 28-31, 33-40, 42-46, 75-78] Changing the crystallizing microenvironment from a solution to a hydrogel has a noticeable effect on the degree of mineralization by additives [12, 13, 17, 18, 28-31, 33-38]and the morphologies of the resulting crystal aggregates. [10, 11, 19, 39, 40, 42-46, 79-82] Further changing the chemistry of the hydrogel microenvironment leads to a change in the resulting crystal morphology, [79, 80] while changes in the type of hydrogel can effect the relative mineralization effect of additives such as bone sialoprotein (BSP) in those hydrogels.[18, 31] To understand the effects additives and changes to hydrogels have on crystal formation, the individual contribution of particular hydrogel environments must be considered. The first and seemingly only work to establish this

baseline for HA formation was performed by Hunter in 1986.[6] In that work, Hunter demonstrated that there is a difference in the degree of mineral content of calcium phosphate depending on the hydrogel microenvironment. The conclusion of that study was that the difference in mineralization observed in these hydrogels is attributed to the differences in the relative diffusivity constants for ions (specifically calcium) in the respective hydrogel.

The effect of differing diffusivity constants is to cause change in the rate at which ions are delivered to the site of mineralization. This rate can be translated into two different effects on mineralization: a) the timing of the reaction for a set amount of mineral produced or b) the overall quantity of mineral produced for a fixed length of time. The timing of the reaction can be viewed as proportional to the diffusivity by 1/D. The data from the literature[6] suggests that agarose and collagen mineralize 54% and 64% respectively, faster than gelatin. By extension, the amount of mineral that can be produced in a given amount time is more than double in both agarose and fibrillar collagen when compared to gelatin. The rate of mineral formation not only has an effect on the overall mineral content, but can have a drastic effect on the morphology of the crystals grown. For example crystals grown at a faster rate will have a more disorganized, amorphous-like character.

There may be multiple reasons for the differences in calcium diffusivity constants and relative mineral content observed in different hydrogels. One reason may be the relative concentrations of the hydrogels. Hunter has shown that with changing gel concentration there was a measured change in the amount of precipitation in the gel; as the relative gel concentration increased, the amount of precipitation in that gel decreased.[6] However, Hunter also demonstrated that concentration was not the only

factor governing the amount of precipitation when comparing two different gels. A 0.4 w/v % collagen gel had a significantly lower amount of precipitation (as measured by ^{45}Ca cpm) than what was measured in a 0.5 w/v % agarose gel.[6] This information suggests that the chemical make-up of the gel may contribute to the observed mineral content. Structure is also a possible consideration since collagen and gelatin (heat denatured collagen) are similar in chemistry but differ in their respective structures.[83] Collagen gels are composed of triple helicies twisted into fibrils and wrapped into bundles to form structured fibers, but the gel itself consists of random aggregates of these fibers ranging from cotton-like strands to coarse interconnected membranes, [84] while agarose gels are composed strands of sugar chains aggregated into fiber bundles and microgel domains.[85, 86]

It may be possible that the underlying structure of the gel may have an effect on the promotion and inhibition of HA formation. Gel-based assays are the best way to evaluate the function of these proteins since gels more accurately represent in vivo conditions than solution based assays.[7] The potential contributions of chemistry and structure by these hydrogels in the formation of HA have been thus far difficult to examine due to unavoidable fact that mineralization within a homogeneous gel has been largely dictated by diffusivity constants of ions within those gels.[6] By removing the effective differences in ion diffusivity between each hydrogel, any remaining differences between HA nucleation and growth within these gels would be the result of gel concentration, structure and chemical make-up.

2.3 Experimental Design

A layered hydrogel design was constructed where the majority of the hydrogel (diffusing medium) is composed of gelatin and less than 10 % of the construct is

composed of a target hydrogel to be mineralized. The gel tube is then placed into a circulating semi-infinite reservoir designed dynamic DDS (Fig.1.7). Using this design, it was calculated that the volume/path-length of the target hydrogel is relatively small compared to the total gel and the effects of diffusivity through the target gel are made negligible. The effect of these target gels on the size, shape, and crystalinity of HA were examined using powder X-ray diffraction (pXRD), Fourier transform infrared spectroscopy with a attenuated total reflectance (FTIR-ATR), and field emissive scanning electron microscopy (FE-SEM). The data shows that the type of chemistry in each gel does have an effect on the crystal morphology of the HA aggregates which is consistent with the work by Grassman.[79] The combined data from pXRD and FTIR-ATR suggest that the crystallinity and length of the crystals along the c-axis of the HA change with the changing chemistry of the hydrogel microenvironment. Composition of collagen hydrogels and gelatin hydrogels are similar but differ in structure.[83] The structure arrangement inherent in collagen fibers may be responsible for the increase in mineral content in this case. [87-91] Agarose also has a fiber based structure, but the polysaccharide nature of the agarose polymer lends it self to distinctly different chemistry than what is found in the protein based gels. The polysaccharide chemistry of the agarose hydrogel and its affinity for HA may contribute to its tendency to promote mineral formation.[92, 93]

2.4 Results and Discussion

The chemical and physical properties of hydrogels not only affect the relative diffusivity, mineral content, and morphology of crystals grown in them, but these properties also affect how these gels can be handled and used from a practical, experimental point of view. The particular type of DDS used for this work (Fig. 1.7) was

specifically designed to make use of gelatin hydrogels alone. Gelatin hydrogels at 10 w/v % are hydrophobic, adhesive, and swell below their gelling temperature when in contact with water. It is these chemical and physical properties of gelatin around which the design of a circulating semi-infinite reservoir dynamic DDS was originally conceived and constructed.[17] Made of polystyrene tubes cut from serological pipettes the diffusion tubes, which hold the hydrogel samples, perfectly accommodate the hydrophobic, sticky, easily swellable gels. Both agarose and collagen gels have stronger polymer-polymer interactions and weaker polymer-solvent interactions than gelatin, as a result, these gels have more cohesive rather than adhesive tendencies. The chemical and physical properties of collagen and agarose hydrogels make it difficult to set and affix these gels in diffusion tubes designed for this kind of dynamic DDS, they simply do not stick. Because of these issues, it was not practical to measure the individual diffusivity constants of ions in these collagen and agarose hydrogels using this dynamic DDS. Since the empirical quantification of these hydrogel-specific ion diffusivity constants was not possible, we were forced to consider values from the literature.[6] We used literature based values to calculate the effective diffusivity constants of calcium ions, for agarose and collagen hydrogels, in a circulating semi-infinite reservoir dynamic DDS.

To calculate the expected values for calcium, phosphate, and ultimately the mineral content, literature values for ion diffusivities in gelatin, agarose and collagen hydrogels were used. When researching these reported values, it was found that the values for the calcium diffusivity constants in gelatin using an SDS with radioactive tracers (for concentration analysis)[6] did not match the values found in gelatin using a DDS with a flame AA (for concentration analysis).[17] A number of factors may contribute to this discrepancy, among them: the lot # of gelatin used (since the type of

gelatin, 275 Bloom Type-A from Fisher used in this work was the same used by Hunter), the concentration of gelatin, the temperature at which the experiment was performed, and the type of measurement used to determine the diffusivity constant. Whatever the source of this anomaly, the relative differences in ion diffusivity between the various kinds of hydrogels should remain the same. Given this assumption, the relative values of the calcium ion diffusivity constants in a DDS were calculated using measured diffusivity constants for calcium in gelatin from both an SDS [6] and a DDS [17] and using the relative ratio of the two values to extrapolate the values of calcium diffusivity constants for both agarose and collagen hydrogels. The contribution of temperature was not accounted for when making these calculations since the known relation of temperature to diffusivity (+2-3% per °C from a value at 25 °C) [65] begins at 25 °C, and the measured calcium diffusivity constants for gelatin are at 20 °C [17]and 24 °C.[17] By ignoring the effects of temperature, the calculated diffusivity constants for calcium in agarose and collagen, and the resulting calculated ion concentrations for each of these gels tend to be estimated on the high end.

Using the estimated diffusivity constants, the resulting calcium and phosphate concentrations were calculated (Table 2-1). To calculate the ion concentrations the following solution to the diffusion equation was selected

$$c(x,t) = c_0 erfc\ \frac{x}{2\sqrt{Dt}} \quad \text{(Eq. 1.5)}$$

based on both the initial and boundary conditions at which the DDS was operated. The conditions of operation were: concentration of ions in the hydrogel sample were zero at the start of the experiment, diffusivity constants of ions through the hydrogel were constant, source (reservoir) of ions was semi-infinite, hydrogel sample into which the

ions were diffusing was also semi-infinite and ions diffusing in the system traveled in one dimension.

Table 2-1: Expected ion concentrations and hydroxyapatite mineral content after 5 days (432000 s) for agarose and collagen hydrogels as compared to gelatin, based on established literature values. The calculated difference in expected ion concentrations and mineral content are within the expected error of the ICP-AES.

Hydrogel	Reported calcium diffusivity[a] constant in an SDS (10^{-6} cm^2/s)	Expected calcium diffusivity constant for a DDS (10^{-6} cm^2/s)	Expected calcium value at x = 3 cm (mM)	Expected phosphate concentration assuming hydroxyapatite Ca:P = 1.67 (mM)	Expected mineral content hydrogel after 5 days. (µg)	Expected change in mineral content (%)
Gelatin	2.1	6.00[b] ± 0.500	21.10 ± 1.85	12.63 ± 1.1	658.83 ± 54.23	N/A± 8.77
Agarose	3.85	11.00 ± 0.92	21.74 ± 1.88	13.02 ± 1.2	678.93 ± 55.00	+ 3.05 ± 8.64
Collagen	3.28	9.37 ± 0.78	21.59 ± 1.87	12.93 ± 1.2	674.19 ± 54.82	+2.33 ± 8.67

[a]By radioactive tracer[6]
[b]Mesaured by flame AA[17]

To make use of Eq. 1.5 to calculate the potential ion concentrations, both the calcium diffusivity constants unique to each gel as well as the path length along which ions travel within each gel, are taken into account. Using a total hydrogel length of 6 cm and a targeted hydrogel length of 0.6 cm positioned in the center of the diffusion tube, we establish the start and end point for each gel. The first segment of blank, gelatin hydrogel, with a calcium diffusivity constant D_1 starts at $x_0 = 0$ cm and ends at $x_1 = 2.7$ cm, while the targeted hydrogel with a calcium diffusivity constant D_2 starts at x_1 with the site of mineralization at $x_2 = 3$ cm, yielding a path length in the target hydrogel $\Delta x = 0.3$.

$$c(x,t) = c_0 erfc\ \frac{x_1}{2\sqrt{D_1 t}} = c_1$$

$$c(x,t) = c_1 erfc\ \frac{\Delta x}{2\sqrt{D_2 t}} = c_2 \qquad \text{(Eq. 2.1)}$$

$$c(x,t) = (c_0 erfc\ \frac{x_1}{2\sqrt{D_1 t}}) \bullet (erfc \frac{\Delta x}{2\sqrt{D_2 t}})$$

The value of c_0 is taken from the concentration of the ions in the reservoir, while the value of c_1 at the gel/gel interface is calculated from Eq.1, the value of c_2 at x_2 is found using c_1 as the starting concentration (Eq. 2.2), c_2 is assumed to be the average concentration across the 0.3 mL volume that makes up the target hydrogel. The value of calcium concentration = c_2 is then used to find the concentration of phosphate assuming that the mineral product is HA ($Ca:PO_4 = 1.67$). From these calculated values, the overall mineral content for each targeted hydrogel volume (0.3 mL) is estimated as well as the percent difference in mineral content as compared to gelatin (Table 2-1).

These calculations revealed that the potential mineral content in the agarose and collagen gels target gels with this layered hydrogel configuration is within the error of the control gelatin gel. It should also be noted that the calculated average amount of increased mineral content in both the agarose and gelatin gels are within error of measurement by the ICP-AES used in this work to measure ion concentrations in the hydrogels. The difference in diffusivity constants may have an effect on the relative mineral content in a longer 3 cm gel,[6] but given the short path length of the reaction space in this system, the differences in mineral content because of differing diffusivity constants becomes negligible.

Two DDS systems were used, both with three sets of three double diffusion tubes (one set per gel type). Three gel types were tested as the target gels: 10% w/v gelatin, 2% w/v agarose, and 0.2% collagen. The target gels were placed in the center region of each tube, the known region for mineralization in this type of system, each target gel comprising of 0.3 mL of material (total path length of 0.6 cm) was sandwiched in between two layers of gelatin which was used as the primary diffusing medium in each case. Using this layered gel technique the targeted gel was trapped between the two layers of adhesive gelatin, eliminating the previous issue (described earlier) of the hydrogels not sticking to the inside of the diffusion tubes. Both systems were run for 5 days, at which point the target gels for one system were excised, heated and melted away while the mineral was isolated, collected, washed, dried and characterized using FE-SEM, pXRD, and FTIR-ATR. The target gels for the second system were excised at a precise volume (0.333 mL) with a custom gel sectioning tool that cut the gel into nine even slices. Each gel slice was washed repeatedly with 0.15 M NH_4OH to remove free salts and then examined for total calcium and phosphate content using ICP-AES.

The ion concentrations recorded for each set of target gels are plotted in Fig 2.1 and the total mineral content that was measured is tabulated in Table 2-2 The concentration data obtained reflects only the concentration of bound ions in each hydrogel and demonstrate that both the agarose and collagen hydrogels produced more mineral that the gelatin hydrogel, which is consistent with the reports in the literature.[6] However, unlike what was reported in the literature, the amount of mineral in the collagen gels was (within error) equal to the same quantity of mineral found in the agarose gels (which had the largest margin or error).. In this system, where the underlying diffusivity constants were kept constant using a long path length for the

diffusing medium and a short path length for the mineralizing medium, the data suggests that other properties of agarose and collagen may be responsible for the previously observed increase in mineral content.

The morphologies of the crystal aggregates, as examined by FE-SEM (Fig. 2.2), were similar, if not the same for both the collagen and gelatin gels. The aggregates from both the collagen and gelatin gels had floret-like morphologies clustered together. The HA aggregates from the agarose gel had a slightly different morphology than the crystals from the collagen and gelatin gels, with an appearance that could be describe as "melted" version of the floret-like morphology seen in both the gelatin and collagen gels. This "fused" character, where the platelets of HA seem to have little to no distinction from each other within the floret, may suggest an intimate interaction between the morphology of the HA crystals and the polysaccharide polymer as the crystals form.

Table 2-2: Measured ion concentrations and hydroxyapatite mineral content after 5 days (434558 s) for agarose and collagen hydrogels as compared to gelatin. The measured ion concentrations and mineral content show that both agarose and collagen promote mineralization (within error of each other) when compared to gelatin.

Hydrogel at 20°C	Measured calcium concentration (mM)	Measured phosphate concentration (mM)	Mineral content (ug)	Change in mineral content (%)
Gelatin 10 w/v %	19.81 ± 0.672	14.61 ± 0.10	778.99 ± 12.75	N/A ± 1.64
Agarose 2 w/v %	24.92 ± 1.94	17.24 ± 1.09	939.89 ± 64.43	20.64 ± 8.27
Collagen 0.2 w/v %	25.08 ± 0.68	17.49 ± 0.41	951.00 ± 23.70	22.08 ± 3.04

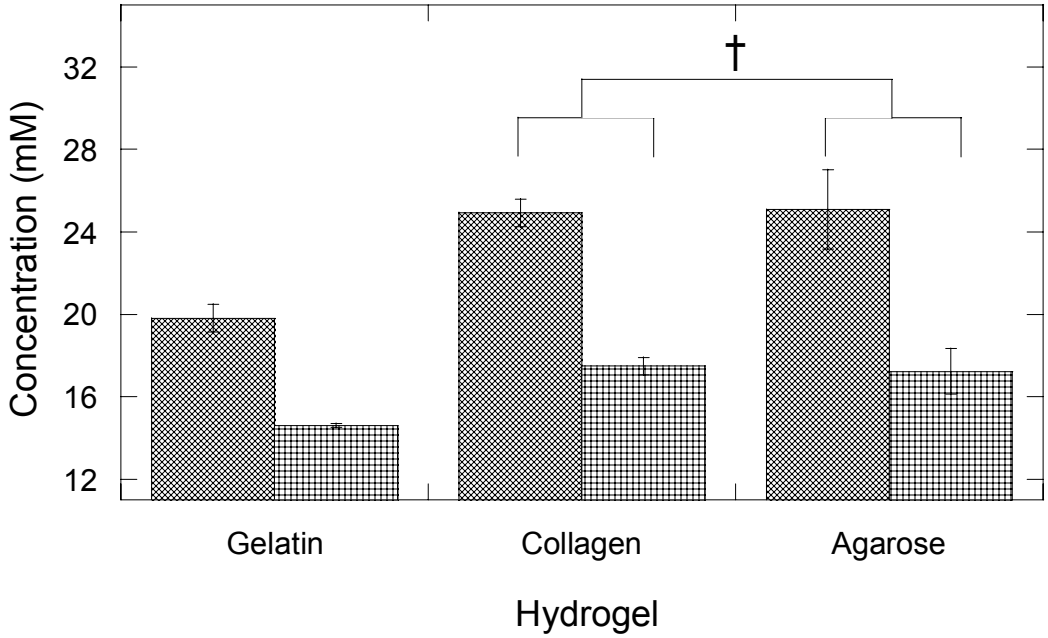

Figure 2.1 Measured calcium (solid bars) and phosphate (hatched bars) values for HA from gelatin, collagen,and agarose hydrogels, after 5 days of being placed on a dynamic DDS. Values for calcium and phosphate (and therefore the overall mineral content) found in the collagen and agarose are within error of each other (†).

The low interaction energy between the crystals and the hydrogel microenvironment leads to an intimate relation between the crystals and the substrate in/upon which they grow. This lower energy of interaction leads to less distinct crystal formations since the character of the crystal morphology is strongly tied to the polymer interface. In contrast, the chemistry of the gelatin and collagen hydrogels likely leads to a higher interaction energy between the crystals and hydrogel microenvironment leading to more distinct HA crystals within the crystal aggregates.

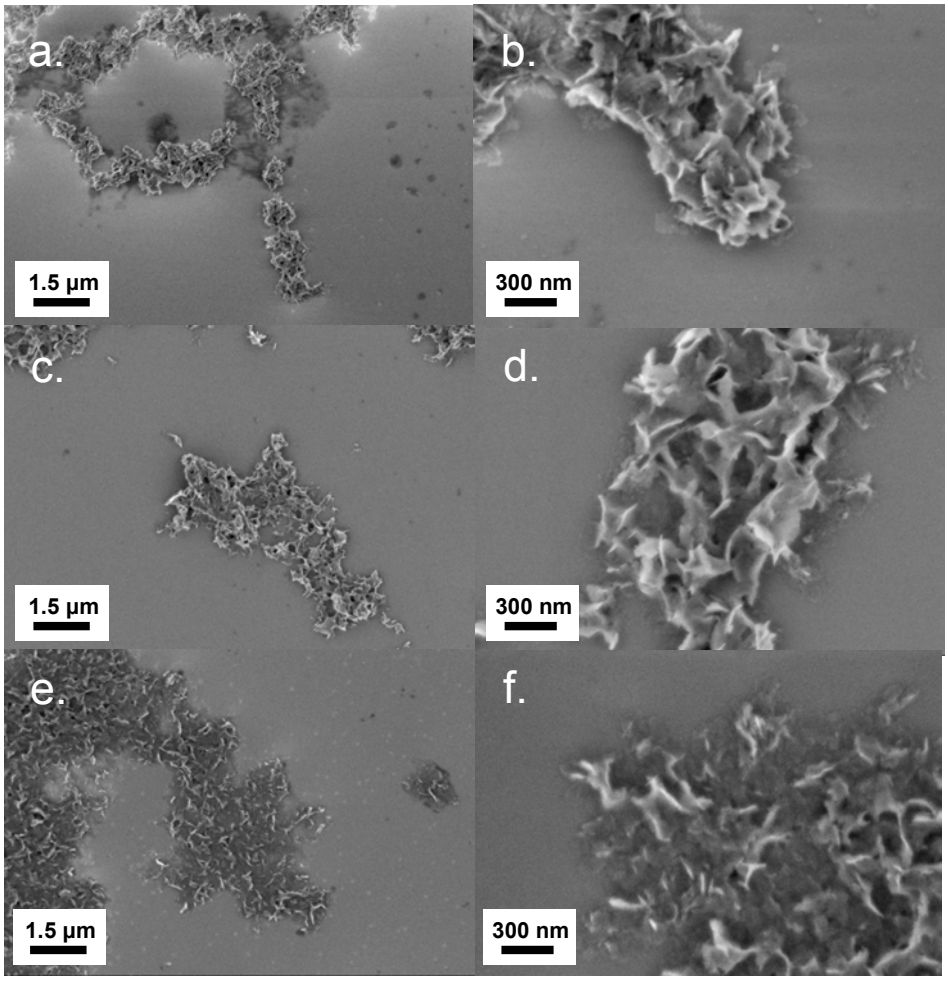

Figure 2.2 FE-SEM images of HA aggregates excised from gelatin (a-b), collagen (c-d), and agarose (e-f) hydrogels, after 5 days.

The crystal aggregates from each hydrogel were examined with pXRD and the phase was confirmed as HA by the presence of the (002) peak and the mixed (211/202) peak (Fig. 2.3). The size of the crystallites along the *c*-axis was determined using Scherrer analysis of the peak at $2\theta \approx 25.85°$, and by comparing the sample spectra to a corundum standard to correct for any instrument broadening. Two different methods of background correction were used (Spline-fit) to account for the poor quality of spectra obtained. The two different forms of correction resulted in two values for the crystallite

size as tabulated in Table 2-3. The HA crystals grown in agarose appear to be slightly larger than the HA crystals grown in either gelatin or collagen.

Table 2-3: Tabulation of the crystallite sizes (by pXRD) and relative crystallinity of HA crystals extracted from a hydrogel after 5 days (434383 s).

Hydrogel	Cryatlite size along the *c*-axis[a] (nm)	Phosphate *v4* Splitting Factor[b]
Gelatin	24	2.97
Collagen	18	2.94
Agarose	26	2.79

[a]Determined by pXRD, Scherrer analysis compared to a corundum standard, using a spline-fit.
[b]Determined by the sum of the ~562 cm^{-1} and ~600 cm^{-1} peak heights divided by the height of the minimum between this doublet.

The crystals aggregates from each hydrogel were examined with FTIR-ATR and again the crystals phase HA was confirmed by the presence of the locations of the phosphate *v1*, *v3*, and *v4* peaks (Fig. 2.4). The relative crystallinity of each HA samples was determined by calculating the splitting factor (SF) of the phosphate *v4* peak[94, 95]. These values were tabulate in Table 2.3. The values of this SF calculation suggests that the relative crystallinity of the HA crystals grown in agarose is less than that of the crystals grown in both gelatin and collagen. This suggestion is confirmed by visual inspection of the HA crystals seen in the data from the FE-SEM.

The data presented here affirms the idea that the increase in mineral content found in the collagen gels is strongly dependent on the hierarchal structure of the collagen fibers and not the chemistry of the hydrogel. Though the structure of the collagen gel may be favorable for the nucleation/creation of mineral, [87-91] the chemistry of the collagen fibers does not a provide a favorable enough interaction to cause change in the resulting crystal morphology as the crystal grows. And subsequently, may be the reason why it is difficult to fully mineralize collagen fibers alone *in vitro*.[87-91, 96, 97] In contrast, the same evidence of changes in crystal morphology, size, crystallinity and mineral content in agarose, suggest that the chemistry of the agarose hydrogel is likely the cause for

increased mineral content in that gel. This data also suggest that favorable interactions between hydroxyapatite and polysaccharides [92, 93] not only promote nucleation but also effect the growth of HA in this hydrogel.

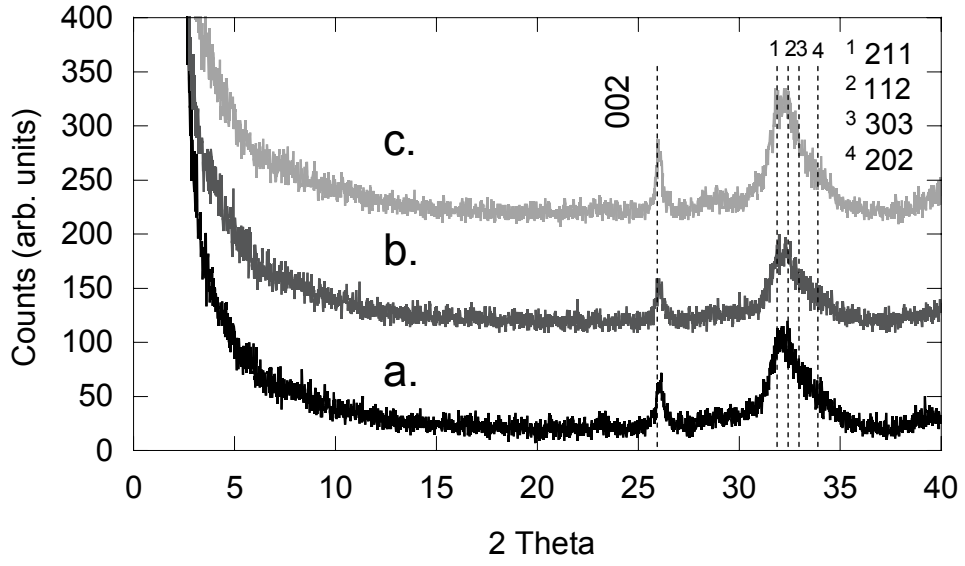

Figure 2.3 Powder XRD spectra of HA crystals from (a) gelatin, (b) collagen, and (c) agarose hydrogels, after 5 days.

2.5 Conclusion

By removing the issue of differing ion diffusivities within the targeted hydrogels, we were able to correlate changes observed in the resulting morphology of hydroxyapaptite crystal aggregates to the structure and chemistries of those gels. It should be considered that when using these types of gels for *in vitro* mineralization models that not only do the diffusivities of the ions within the gels contribute to the overall mineral content but so too do the chemical and physical properties of the those gels. These properties unique to each kind of hydrogel may in fact contribute to the behavior and effectiveness of mineral modifying additives in these gels. It is possible that

soluble proteins associated with crystal growth may obtain some of their structure and function from the gel-environment. Hydrophobic organic matrix associated with some biominerals (e.g., collagen fibers in calcified cartilage, bone, and dentin) provides structure to other, mostly hydrophilic proteins, thus promoting interaction of those proteins with the crystals.

2.6 Material and methods

2.6.1 Gel preparation:

Gelatin: 30g of 275 Bloom Type A Gelatin (Fisher) was mixed with 300 mL Tris Buffer pH 7.4, heated to 50°C in a hot water bath and pH balanced using 2M NaOH until the pH was 7.4.

Agarose: 0.2 g of low melt agarose used for nucleic acid purification (Fisher) was dissolved in 10mL of Tris Buffer pH 7.4, heated to boiling in a microwave (set on low) and pH balanced using 2M NaOH until the pH was 7.4.

Collagen: 2 mL of Collagen Type-I Rat Tail Tendon Solution 3 mg/mL in 0.02M acetic acid (Olaf Pharmaceuticals) was added to 1 mL of Tris Buffer pH 7.4 while stirring. 4 drops of 1M NaOH was gradually added to the vial until the pH was 7.5 (as measured by pH paper).

2.6.2 Filling the diffusion tubes:

24, 3 ml (6cm long) were cut from 10 mL polystyrene serological pipettes using a hotwire cutter. Each graduated tube was capped at the end with the highest number, with a polypropylene disc (8 mm diameter) and sealed with parafilm.

Gelatin tubes were fully filled to the 3 mL mark for a full length of 6cm

Agarose tubes were filled to the 1.35 mL mark (2.7 cm) with gelatin and then

filled with 0.3 mL (0.6 cm) of 2% Agarose in Tris buffer (with a needless syringe) followed by gelatin filled to the top of the tube (6 cm).

Collagen tubes were filled to the 1.25 mL mark with gelatin and then filled with 0.4 mL of 0.2% collagen in Tris buffer (with a syringe) followed by gelatin filled to the top of the tube (6 cm).

2.6.3 Pre-hydration:

Once the gels were set, all tubes were uncapped and place in 15 mL centrifuge tubes filled with 6 mL of Tris buffer at pH 7.4 and left to set at 25°C for 3 days. After hydration both the agarose gel and the collagen gel layers changed slightly. The agarose layer became hazy as it set and the collagen layer (which was cloudy as it was poured) shrank to a thickness of 0.3 mL (6mm), as expected.

2.6.4 Calcium and Phosphate Solutions:

2 liter solutions of Calcium and Phosphate solutions were prepared in 0.15 M Tris buffer, with 39.7g Tris HCl (Sigma), 5.82 g Tris Base (Sigma), 0.4g sodium azide (Fisher), and either 29.4g (calcium chloride dihydrate (Sigma-Aldrich)) or 26.4g (Ammonium phosphate dibasic (Sigma-Aldrich)) to make 100mM solutions in Tris bluffer pH 7.4. Solutions in the DDS reservoirs were changed at 2.5 days to preserve the semi-infinite condition.

2.6.5 System placement:

Tubes were placed of the DDS alternating the tubes from gelatin to agarose to collagen for a total of 9 tubes on the system (each gel in triplicate).

2.6.6 Removal of tubes from the system:

When tubes were removed from the double diffusion system they were placed in the refrigerator for 30-45min to firm up the gels for handling.

2.6.7 Concentration analysis:

The layered gels were sectioned in to 9 nine equal slices and the center section (0.333 mL) containing the mineral and target gel was isolated, and soaked/washed for 45 min in 10 ml of 0.15 M NH_4OH, changing the solution every fifteen minutes. The gels were then pat dry and hydrolyzed in 10 mL of 0.8 M HNO_3 at 70°C for 2 days. Once hydrolyzed the solutions were then run through an axially viewed ICP trace analyzer emission spectrometer (model ICAP 61E trace analyzer, Thermo Electron, Waltham Ma). The transfer optics had been replaced with a short depth of field transfer optics to reduce matrix effects.

2.6.8 Analysis of crystal morphology:

For the composite gels, the gel layers were separated from each other taking advantage of the underlying mechanical differences between the various types of gels. The gels were placed in the freezer for 15 mins, once the gels were sufficiently cooled the difference in thermal expansion between the gels, allowed the gels to be peeled away from each other at the gel/gel interface. The gelatin gels were simply cut with a razor blade. One isolated, each gel section was place in 3 ml of 0.15 M NH_4OH, and pulsed in a microwave (set on high) for 3-5 seconds (to a state just below boiling), causing the gels to fall apart in solution. The solutions were then agitated on a vortex and centrifuged at 16,000 G for 5 min. The supernatants were then decanted-off the resulting pellets. The pellets were then resuspend in 3 mL of 0.15 M NH_4OH and kept in a hot water bath at 50

°C for 5 mins. Before being vortexed and centrifuged again. This washing and centrifuging step was repeat once more. Once washed the pellets were rinse with acetone twice to remove the water and left to dry in air. The resulting HA powders were then analyzed by pXRD (Scintag Theta-Theta Xray Diffractometer), FTIR-ATR (Bruker Optics - Vertex80v) and FE-SEM (LEO 1550).

2.6.8.1 pXRD

For pXRD, the washed and centrifuged mineral samples were powdered with a pestle and mortar and place on zero a background hold (single crystal quartz cut-off-axis) and scanned (in an Scintag Theta-Theta X-ray Diffractometer) between $2\theta = 2°$ to 40°. The size of the crystallites along the *c*-axis was determined using Scherrer analysis of the $2\theta \approx 25.85°$, and by comparing the sample spectra to a corundum standard to correct for any instrument broadening. Two different methods of background correction were used (Spline-fit and Box-fit (with a 1.5 degree width)) to account for the poor quality of spectra obtained.

2.6.8.2 FTIR-ATR

For FTIR-ATR, a background was taken of the chamber under vacuum before the powdered samples (from XRD) were placed on the diamond ATR stage and then scanned (in a Bruker Optics - Vertex80v, vacuum FTIR) at a resolution of 4 cm^{-1} with 32 scans, using a liquid nitrogen cooled detector. The SF of the phosphate *v4* peak was calculated using the established technique [94, 95, 98] as the sum of the ~562 cm^{-1} and ~600 cm^{-1} peak heights divided by the height of the minimum between this doublet.

2.6.8.3 FE-SEM

For FE-SEM, after extraction of the mineral from the hydrogel, but prior to the

final centrifuging and decanting of the acetone wash solution the mineral suspension in acetone was pipetted on to a silicon substrate and left to dry. The samples were place in the FE-SEM without coating and examined at 1 kV and an aperture setting of 7.5 μm.

CHAPTER 3

3 Oxidized porous silicon as substrates for *in vitro* biomineralization

Here we explore the expansion of hydrogel based in vitro models through the introduction of nucleating substrates.

3.1 Introduction

In biomineralization, both crystal nucleation and growth are under tight regulation.[2, 3, 41, 99-106] The components required for biomineralization are: the controlled delivery/deposition of reagents required for crystal growth, a nucleating substrate, a growth medium (hydrogel-like matrix) and growth modifying elements (proteins/hydrogel-like matrix). Using synthetic substitutes of theses components found in biology, *in vitro* models can be created to study the various aspects of biomineralization. There are two major types of *in vitro* models used to study biomineralization phenomena: solution-based [2, 3, 41, 87, 96, 97, 99-103, 106-109] and hydrogel-based.[7, 10, 11, 19, 39, 40, 42-46, 79-82] Solution-based systems can elucidate the underlying chemical and physical driving forces for crystal growth, while hydrogel-based systems most closely mimic the natural crystal growing environment found in biology, making hydrogels the ideal microenvironment for the study of crystal-protein interactions.

One of the most interesting things we found when looking at *in vitro* models for mineralization was that changing the crystal growing environment lead to significant changes in the crystal morphology. [19, 45, 79-82]These changes in the morphology of the crystals were sometimes the result of changing the phase of the particular crystal

grown, [9, 46, 51, 52, 54, 81, 82] but in many cases the crystal phase remained unaffected despite the noticeable change in the appearance of the crystals.[10, 11, 39, 40, 43-45, 75, 76, 79, 80]

Here, we explore the development of our own gel-based *in vitro* model for HA nucleation and growth, using porous silicon (pSi) [102, 103, 110, 111] as the nucleating substrate and a gelatin hydrogel as an extracellular matrix-like environment. Both solution-based and hydrogel-based studies are used to examine how changes in the crystal growth microenvironment affect changes in crystal morphology

Crystal nucleation conditions dictate crystal phase, while crystal grow conditions dictate morphology. [108] As such, we strive to maintain the crystal nucleating conditions such that the targeted crystal phase is HA, by using 0.15 M Tris buffer to maintain pH at 7.4, we use calcium and phosphate concentrations close to stoichiometric conditions, and we use the same type of nucleating substrate (oxidized pSi) in all conditions. In this work we confirm the crystal phase using pXRD, SAED, and GADDs; follow by FE-SEM to examine the resulting crystal morphologies.

3.2 Background

3.2.1 In vitro Models

In biological systems, functionalized surfaces are coupled with extracellular matrices (ECM) and select biomacromolecules to control: crystal nucleation, growth and rate of formation. Solution based *in vitro* models for biomineralization provide a fundamental system for the examination fundamental questions and obtain an understanding of crystal growth in aqueous environments. Solution-based models can be as simple as providing a metastable or highly saturated solution (with respect to crystal

growth) or they can be as complex as a constant composition system where the pH, ion concentrations, and total dissolved solids are carefully monitored and regulated.[2, 3] In either case, the effect and/or role of: pH, ion flow, reagent concentrations, reagent ratios, temperature, and additives both biological and synthetic, introduced into the system, can be elucidated. The utilization of solution-based *in vitro* models provide a basic foundation for understanding the underlying chemical and physical driving forces that contribute to crystal growth in biological systems.

Hydrogel-based *in vitro* models make use of a medium that was traditionally used as a technique by crystallographers to grow large crystals;[8, 53-59, 112-114] to instead simulate a biologically-relevant microenvironment. In the invertebrate system there exists the Addadi-Weiner model [112-114] for the formation of nacre in mollusk shells, highlighting the role of various organic components as nucleating substrates (glycoproteins on chitin), growth media (silk-like hydrogels) and crystal growth modifiers (acidic glycoproteins). [81, 82, 115-117] In contrast the vertebrate system, however, the model for bone formation is not as clear. The organic components of bone are collagen, non-collagenous proteins, and other organic species within the ECM; but the roles of these organic components, in the formation of the inorganic mineral component, are not yet clear. [16, 88, 89, 91] There exists a number of questions in the bone formation model: Is the ECM simply a growth medium or is it a growth modifier as well? Is the collagen substrate a nucleator of HA or simply a substrate upon which preformed mineral is applied? Do the non-collagenous proteins work alone or in concert with the collagen substrate? Are the non-collagenous proteins responsible for mineralization of the collagen, inhibition of pathological mineralization, both, or are these contextually dependent? To answer these and other questions, an *in vitro* model

system that recreates key features of the bone microenvironment is required.

3.2.2 Porous silicon as a platform for crystal growth

The chemistry and techniques to functionalize substrates is well established for a variety of surfaces: self-assembled monolayers (SAMs) of alkanethiols on gold, [106, 118] silanes on silica,[119] or alkenes on silicon.[105] Once functionalized, these surface can be introduced to solution-based *in vitro* models as nucleating substrates. For example, Allara and co-workers have used a quartz microbalance to follow the crystallization of apatite on carboxylate-terminated SAMs on gold. [105] These results, suggest that nucleation first occurs in solution, followed by settling of these crystallites onto the SAM surface, followed by further growth. Other researchers have used SAMs formed using silanes on silicon to induce the nucleation of apatite crystals.[106] Their results suggest that hydroxyl-terminated surfaces are the best type of surface for promoting the growth of apatite crystals. Neither of these reports used any biological macromolecules or other additives to control the growth (and therefore morphology) of the crystals after nucleation. In addition, the effect of the SAMs on crystal morphology were not discussed (or investigated) in depth.

In the work by Canham [102, 103] the "bioactivity" of pSi was demonstrated through the growth of HA on the surface of oxidized pSi in simulated body fluid (SBF) for various lengths of time. The morphology of the crystal aggregates seen on the substrate were spherical in appearance.

3.2.3 The hydrogel environment

Previous studies have utilized hydrogels as analogs for the ECM microenvironment to study the effects of small concentrations of biological

macromolecules, specifically their role in the promotion and inhibition of the formation of HA. [7, 12, 13, 17, 33-38] The circulating semi-infinite reservoir designed dynamic DDS[17] utilizes a gel medium for the growth of biological minerals. Hydrogels suppress convection, making the dominant mechanism of mass transport diffusion,[8] regulating the rate of ion delivery and thus regulating the nucleation and growth of HA. Capitalizing on high concentrations of ions in the source reservoirs and a long diffusion path length, the mineralizing regime of the hydrogel matrix is targeted to a localized region comprising of only 10% of the total hydrogel volume.[7, 17] In contrast to a stagnant, non-constant-composition solution based system, a gel based system, with a constant solution/gel interface concentration, does not suffer a diminishing of the driving-force during the precipitation reaction. [7, 17] In vitro gel-based mineralization models rely on homogeneous nucleation for mineralization within the hydrogel matrix. The location of mineral growth is limited and dictated by the delivery ions and local supersaturations. The monitoring (qualification/quantification) of changes in these mineralization kinetics, as various additives are placed in the hydrogel, is how these gel-based models are usually used. [7, 10-12, 17-19, 28-31, 33-40, 42-46] We expand this model by introducing a surface that can be easily functionalized for targeted crystal growth.

In this work, we introduce a "nucleating" surface (functionalizable pSi membranes) into two different crystal growing microenvironments. For the solution based studies we expand upon the works that utilize substrates in solution-based *in vitro* models, and we move beyond an SBF based system, by making changes to the temperature and the concentrations of calcium and phosphate used. We examine pSi in solutions at both metastable and actively precipitating states. We compare some of the resulting morphologies of the crystal aggregates from these solution-based models to the

morphologies of crystal aggregates grown in a 10 w/v % gelatin hydrogel.

We have introduced these functionalizable, pSi substrates into a system that capitalizes on the unique temporal and spatial gradients that can be achieved in hydrogels, acting as a growth medium; while tight regulation of the diffusion boundary conditions impart predictable control on those gradients in the system. We have examined not only how an oxidized substrate would mineralize in such an environment but the role that substrates in general may play in biological mineralization. Adding proteins and polypeptides to both the pSi substrate and the hydrogel, we have created a model system that can be used to interrogate the role of the various organic components found in bone.

3.3 Design

3.3.1 Choice of Substrate

It is difficult to integrate solid, non-porous, substrates into a dynamic DDSs (Fig. 1.7) because the only orientation that can be facilitated is one where the plane of the precipitation-front lies perpendicular to the nucleating substrate, only allowing for a small area of the precipitation to exist on the substrate. To overcome the limitation which burdens the use of solid substrates we have explored the use of rigid, porous disks that can lie within the plane of the precipitation-front (Fig. 3.1). We introduce, for the first time, a fabrication method for the rapid, reproducible, production of thick (~200-250μm), mechanically stable, freestanding pSi lift-off films (disks) that can not only be readily handled, but maintain their patterned shape throughout the etching and electropolishing processes and subsequent functionalizing workups (Fig. 3.2-3.3). The structure and

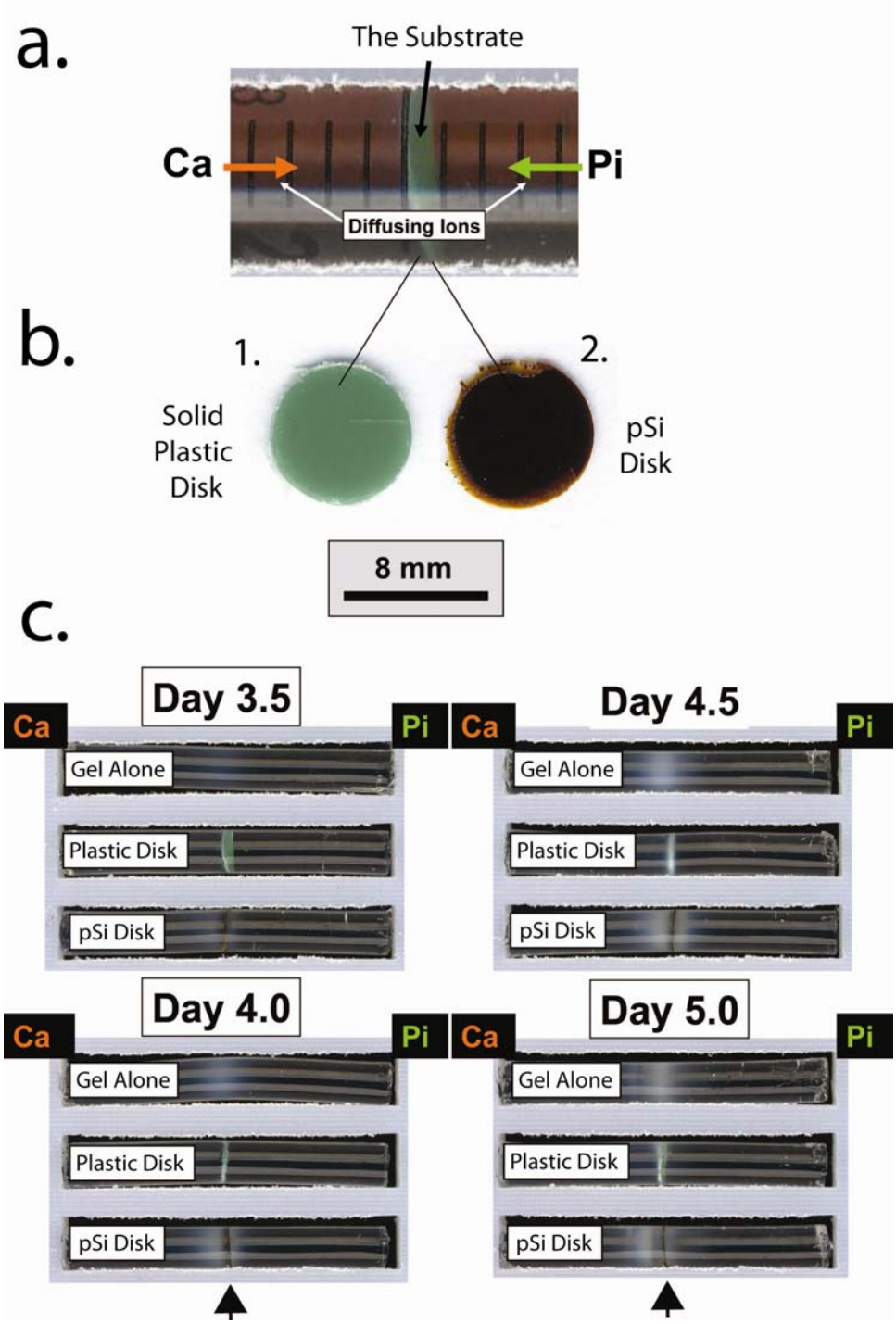

Figure 3.1 Examination of the ion permeability of porous silicon films in a circulating semi-infinite reservoir dynamic DDS. (a.) To compensate for geometric challenge of placing a substrate in a DDS a functionalizable, rigid porous membrane is fabricated. As a comparison (b1) a plastic disc the same size as the (b2) pSi disk is created to act as a negative control. (c.) 12 tubes are placed on a DDS, 4 just gelatin (positive control), 4 with the plastic discs, and 4 with pSi disks. Each set of tubes were taken off the DDS every 12 hours starting at 3.5 days.

design of pSi presents an excellent opportunity to introduce a nucleating substrate into hydrogel-based double diffusion system, and create a complete hydrogel-based *in vitro* model for the formation of HA.

Nanoporous silicon was used to construct porous membranes/substrates to allow for mass transport of ions through the substrate while at the same time providing a surface for nucleation and growth of HA.

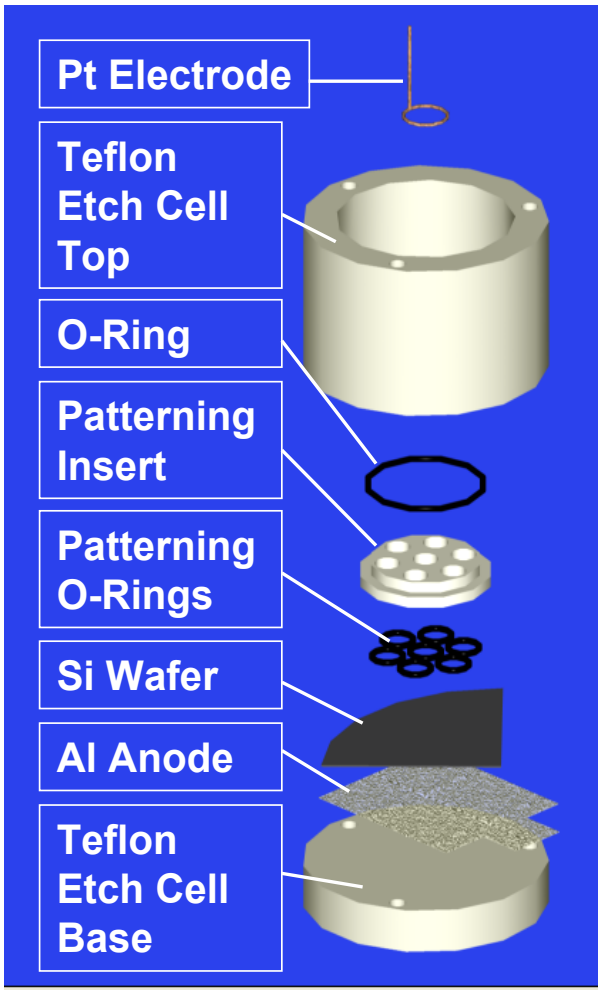

Figure 3.2 Custom designed porous silicon (pSi) etch cell to fabricate multiple pSi films. The removable insert provides the capability to adjust both the size and number of pSi films. Once fabricated, the modular configuration of the etch cell makes it possible electropolish and completely lift off the pSi substrate(s).

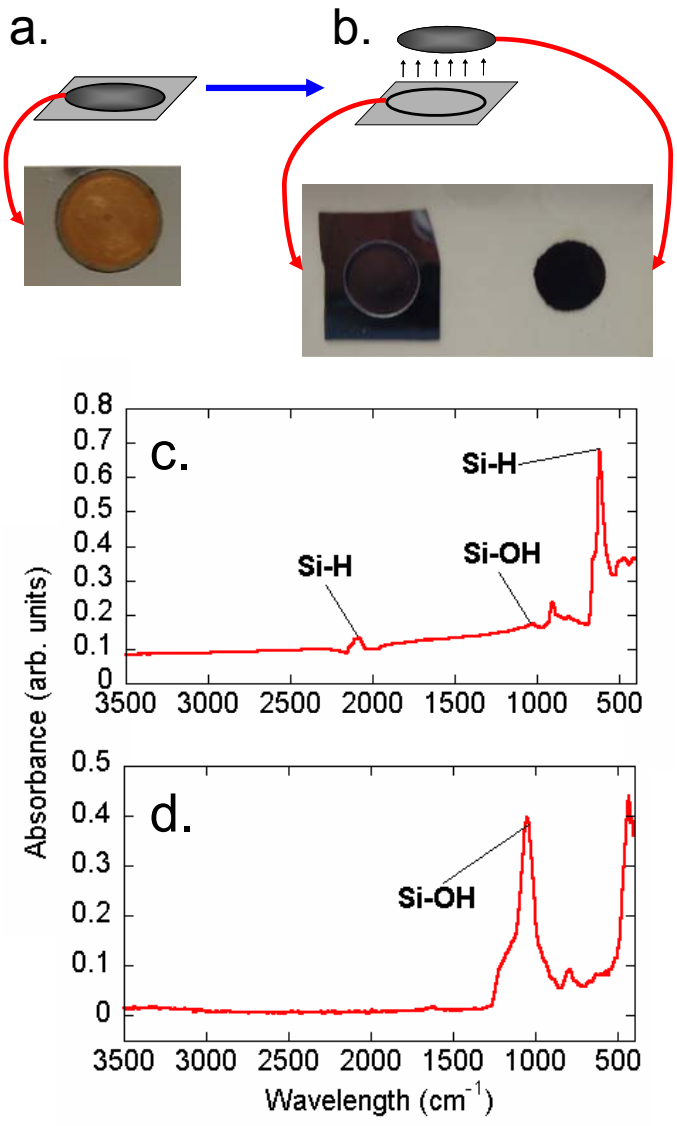

Figure 3.3 Schematic of the (a.) fabrication of porous silicon from P++ silicon with (100) orientation anodically etched in an 3:1 HF:Ethanol etchant with an applied current of 45 mA/cm^2, no illumination, for 150 minutes (to create a ~200 µm film). The porous silicon films were subsequently lifted off (b.) by electropolishing the disks in a 1:16, HF:Ethanol solution at a current of 6 mA/cm^2 for 10-15 minutes. Once etched, pSi films can be functionalized. The FTIR-ATIR spectra of (c.) freshly etch pSi and (d.) oxidized pSi are distinctly different.

3.3.2 Fabrication of pSi membranes

Porous silicon (pSi) is created by electrochemically etching the (100) face of a single-crystal, p-type Si wafer using a constant current. After the pSi layer is formed, the interface between the porous substrate and bulk silicon is electropolished to create a free

standing disk (Fig. 3.3b). The free standing pSi membranes (200-250 μm thick) can be carefully manipulated after removal from the bulk substrate. The disks are then thermally and aqueously oxidized to passivate the surface.

3.3.3 Introduction of pSi membranes into a solution model

Previous studies have addressed the nucleation and growth of HA on both oxidized and functionalized Si surfaces and pSi substrates in simulated body fluid (SBF), [102-106, 109] yielding an understanding of how these substrates mineralize in fluids with the same ion concentration as human blood plasma and at physiological temperatures. Using these studies and conditions as a foundation, we expand the scope of this solution based model to examine four variations in reagent concentrations/ratios at both 20 °C and 37 °C, for a total of 8 conditions (Table 3-1) The experiments were run for 3, 5 and 7 days, the resulting mineral on the substrates were examine with FE-SEM and a General Area Diffraction Detector system (GADDS) (Fig. 3.4).

3.3.4 Introduction of pSi membranes into DDS

After fabrication of the pSi membranes, the films are introduced into the gel-filled diffusion tubes that are placed into the DDS (Fig. 1.7). The gels are prepared in layers with the pSi substrates set at a prescribed location know to mineralize under normal conditions. Control gels are prepared in a similar fashion, but contain only buffered gel at the site of mineralization. After the gels are placed on the DDS, calcium and phosphate solutions are diffused through the hydrogel from opposing sides of the diffusion tubes.

Table 3-1: The conditions A-H, and results for solution growth of mineral on pSi substrates

Condition	Calcium Concentration (mM)	Phosphate Concentration (mM)	Temperature (°C)	Habit	Phase	Figure Location
A	2.5	1*	20	Prism	HA	3.4a, 3.5a, 3.8, 3.9
B	2.5	1.5**	20	Plate	HA	3.4b, 3.5b
C	5	2***	20	Plate	HA/OCP	3.4c, 3.5c, 3.6
D	5	3**	20	Plate	HA	3.4d. 3.5d
E	2.5	1[a]	37	Prism	HA	3.4e., 3.5e, 3.7
F	2.5	1.5**	37	Plate	OCP	3.4f, 3.5f
G	5	2***	37	Plate	HA	3.4g, 3.5g
H	5	3**	37	Plate	HA	3.4h, 3.5h, 3.10a

*The concentration of calcium and phosphate are the same as found in SBF
**The concentration of calcium and phosphate are stoichiometric with respect to hydroxyapatite
***The concentration of calcium and phosphate are twice the concentration found in SBF

In general, a DDS utilizes two semi-infinite reservoirs of reagents on either side of the gel medium. As reagents diffuse towards each other in the gel medium a gradient of concentrations of those reagents develops. Assuming that the same concentration of ions are set at either end of the diffusion tubes, the relative ratio ions at the site of mineralization, is based on the diffusivity of the individual salts from the reservoirs.[17] In a dynamic DDS the steepness of the ion gradients decreases over time as ions build up in the gel and the system slowly approaches equilibrium and the steady state condition. Regulation of the major reaction conditions required for calcium phosphate formation (pH, ratios, and ion product) will dictate which calcium phosphate phase is most-likely to form. The ability to predict the concentration of reagents and the nature of the gradients in the DDS is achieved by tightly controlling the boundary conditions of the system (such as maintaining a semi-infinite concentration source; see Chap. 1 section 1.2.4 and 1.3.2.2. Mineralization occurs both in the bulk gel as well as on the pSi surface. The experiment is terminated after 5 days.[17]

3.3.5 Proteins/peptides together with substrates

One set of solution based conditions was selected as a suitable scenario to account for the physical effects hydrogels have on crystal growth, and chosen to serve as a control for the hydrogel-based system. Under the conditions of the solution based control, proteins were added to the solution and the resulting change in crystal morphology was observed. As an initial exploration into the potential of this system as a hydrogel-based *in vitro* model, these proteins of sizes known to be immobile in a hydrogel based DDS were combined with the substrates. Proteins were added to DDS by either physisorption to the substrates themselves or placed in the gel surrounding the substrates. The resulting morphology of the crystal aggregates from both the gel and on the substrates were examined.

3.4 Results and Discussion:

3.4.1 Porous silicon substrates

As-fabricated porous silicon membranes are ~250 μm thick with surface pores 5-10 nm in diameter that coalesce underneath the surface into an interconnected network of 30 nm channels which form predominately perpendicular to the etch surface as it extends through the membrane. In the porous silicon etch cell, the size of the o-ring seals for the 7 film insert (Fig. 3.2) restricts the diameter of the resulting membranes to 7.8 mm, making the films small enough to be placed inside the 5/16 inch (7.9 mm) diameter gel filled diffusion tubes.

The color of the pSi films is a deep reddish brown resulting from the optical light envelope of the Fabry Perot fringes that develop in the film. [110] The growth of thick oxides on these films cause the center of this envelope to blue shift resulting in a more

orange/red color until the film reaches a yellow or even clear to frosty white color as the film turns completely to glass. In some instances the oxide layers may become so thick that they result in quantum confinement of the silicon in the films leading to a visible photoluminescence. [120] The films oxidized in this paper retain their reddish brown color and do not visibly photoluminesce indicating that the oxide layer, though complete (no more Si-H) is relatively thin.

These chemically robust films can be placed in solutions buffered to physiological pHs, and neither dissolve nor react directly with aqueous environment. The robust nature of these disks make them suitable for both solution- and hydrogel-based experiments. The thorough oxidation of the substrates imparts hydrophilicity to the substrate, allowing the pores to be filled with solution by capillary action. When introduced to an aqueous environment, the filling of the pSi pores facilitates the sinking of these otherwise low density substrates. Without the chemical passivation, these normally hydrophobic substrates would simply float on top of the aqueous solution. The porous nature of these disks subsequently allow for the ready diffusion of ions through the substrate when the films are placed in a hydrogel based DDS.

3.4.2 Solution based experiments:

There are 8 conditions for the surface induced crystal growth of HA on oxidized pSi substrates (Table 3-1). Each condition was run in a volume of 10 mL for 3, 5, and 7 days. For each condition, 5 ml of the calcium solution was added to the pSi substrate first, followed by 5 mL to the phosphate solution. The order of addition is critical, but will not be discussed here.

One of the advantages to examining crystal growth on a substrate is that by examining different regions of the substrate, crystals and aggregates of crystals at various

stages of growth can be seen. By examining multiple regions, of a number of substrates, at different time points a construction of the stages of crystal growth can be pieced together

For most of the solution based conditions, within the confines of each condition there was little to no variations in the crystal morphology from day 3 to day 7, figures 3.4 & 3.5 comprise of images taken from substrates at days 3, 5, and 7 for all conditions. With increased time there was visually (not quantified) an increased coverage of material on the substrate. In the case of condition C, however there were select regions where there was both a noticeable change in the crystal morphology, and a discontinuity in the crystal coverage because of changes in the crystal phase. As can be seen from figure 3.6 condition C presented a mixture of crystal phases octacalcium phosphate (OCP) and HA this determination is made by visual inspection since Condition C is a mixture of the morphologies seen in both Condition F (OCP by GADDS, Fig. 3.7) and Condition D. Over time the OCP appears to have been consumed by what is most likely a combination of Ostwald's rule of stages and dissolution-reprecipitation. The OCP crystals themselves are not changing into the more thermodynamically stable HA by some sort of solid-state transformation, but instead appear to be dissolving at the expense of the HA crystals growing in the surrounding area. This dissolution leaves a visible void on the HA coated substrate.

The aggregates of crystals from Conditions A and E, appear to be assembled from elongated crystals. The crystals grown in Condition E do not undergo a change in the crystal phase, but instead show a slight change in the crystal morphology over time, which can only be seen at high magnifications. As can clearly be seen in Fig. 3.8, the aspect ratio of the crystal spindles change from long flat crystals to long rounded crystals.

Figures 3.9 and 3.10 show the likely stages of grow for Condition A, that start from prismatic HA crystals, which assemble into bundles by either aggregation or overgrowth, and these bundles evolve in to dumbbells that subsequently become spherulites.[121] The elongated prismatic-character of the crystals that make up these spherulites are visible on the surface of the spheres and can be seen in figure 3.10 (j-l).

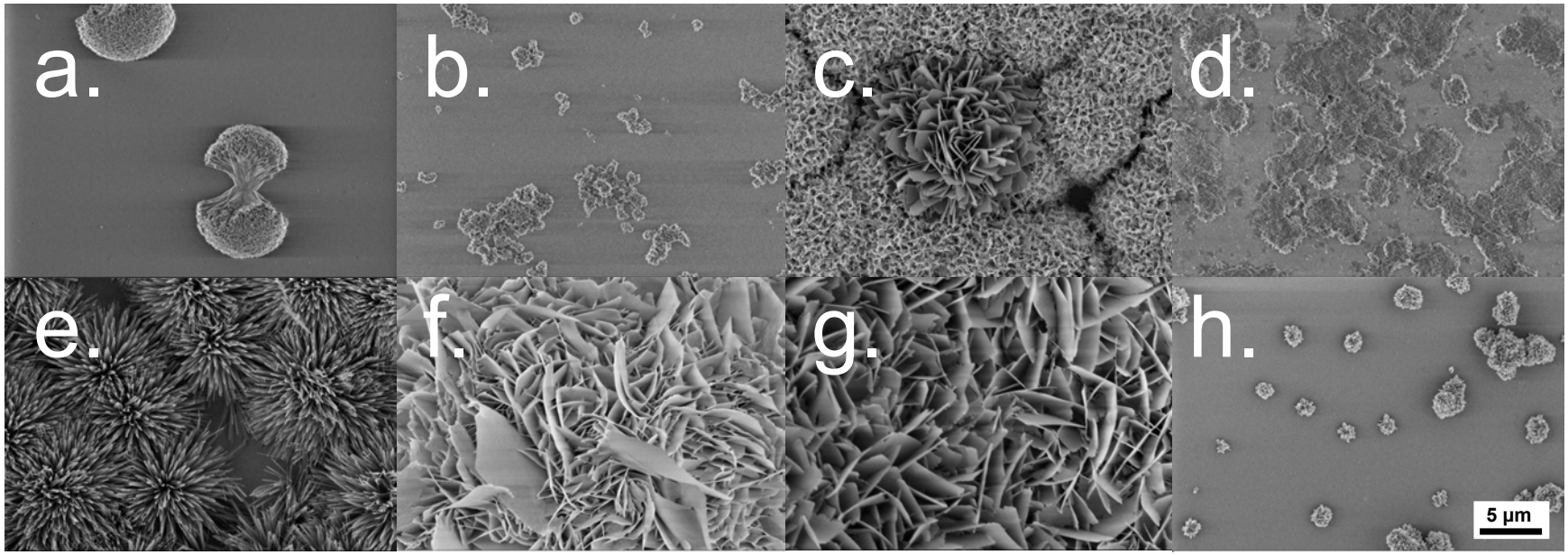

Figure 3.4 Low magnification of FE-SEM images of (a.) Condition A (HA), (b.) Condition B (HA), (c.) Condition C (HA/OCP), (d.) Condition D (HA), (e.) Condition E (HA), (f.) Condition F (OCP), (g.) Condition G (HA) and Condition H (HA).

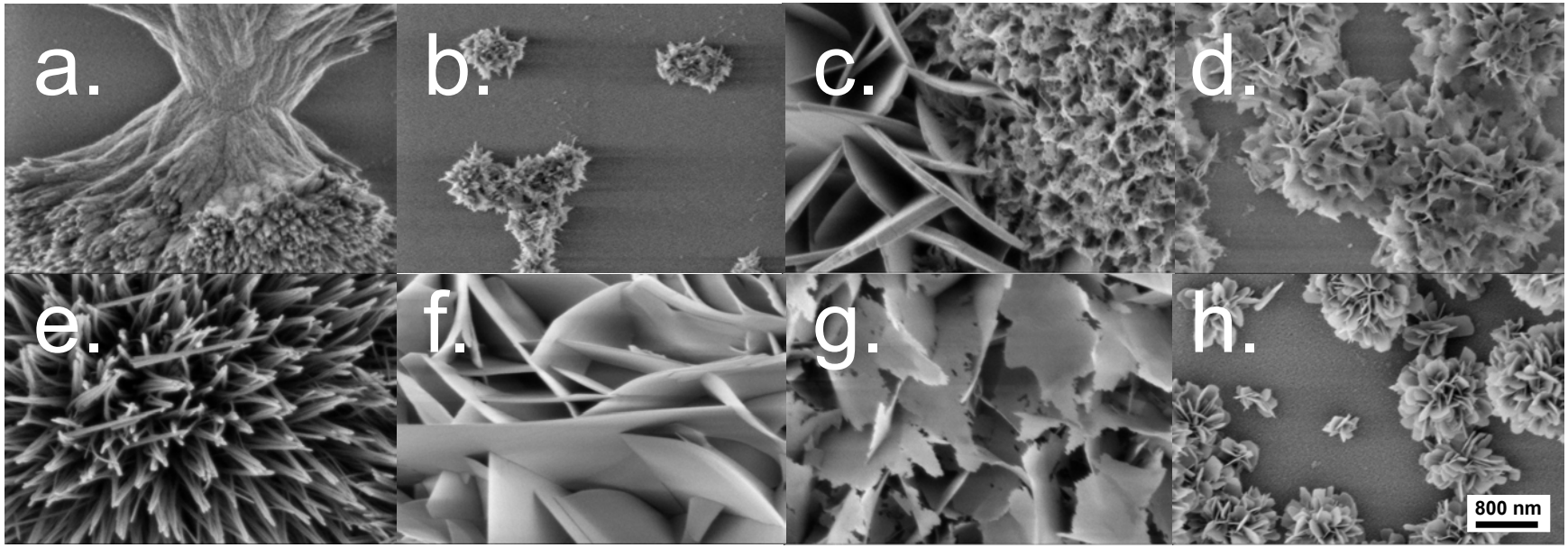

Figure 3.5 High magnification of FE-SEM images of (a.) Condition A (HA), (b.) Condition B (HA), (c.) Condition C (HA/OCP), (d.) Condition D (HA), (e.) Condition E (HA), (f.) Condition F (OCP), (g.) Condition G (HA) and Condition H (HA).

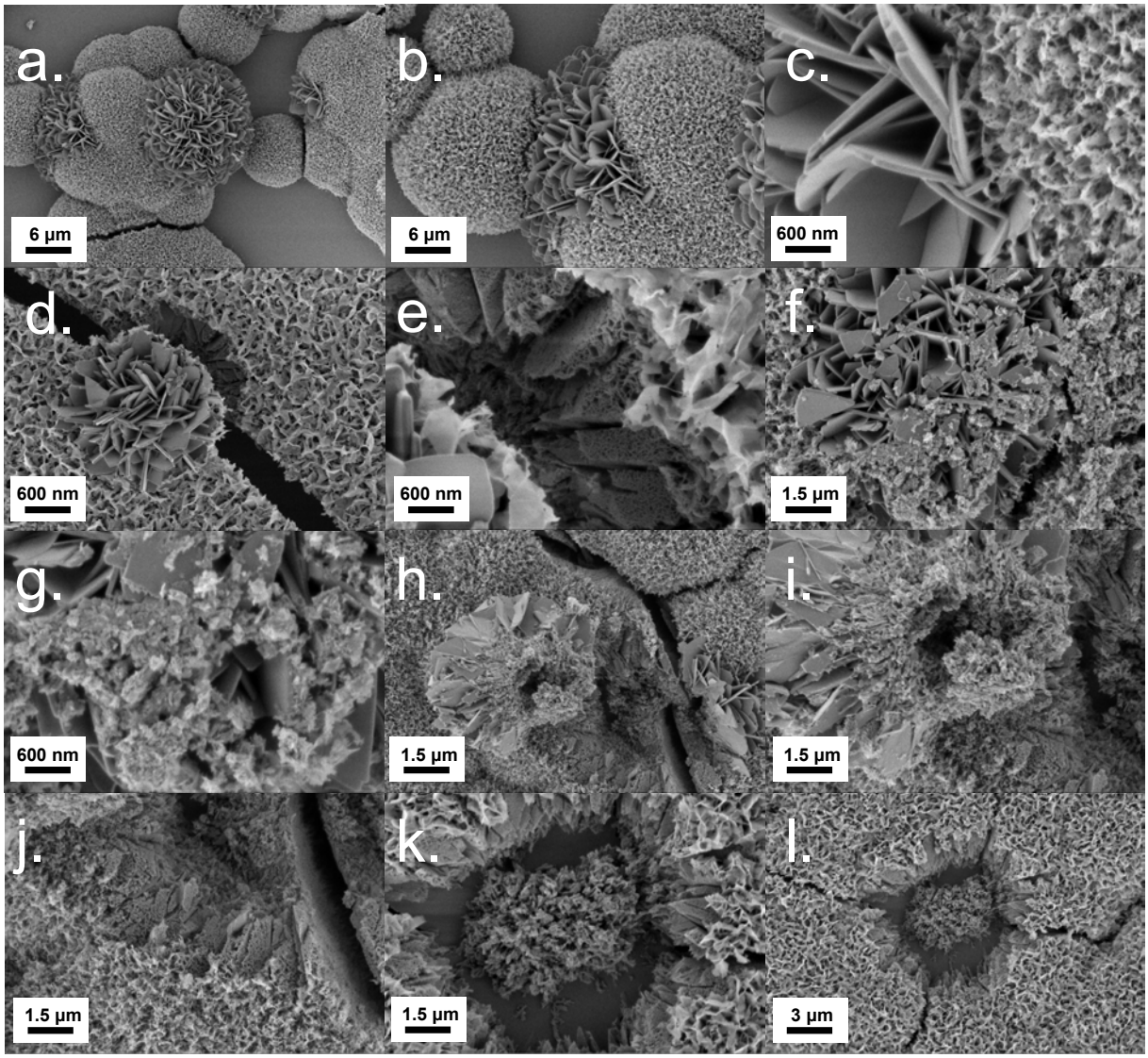

Figure 3.6 FE-SEM, images of calcium phosphate from Condition C, taken at multiple time points (3, 5 & 7 days), at multiple locations on the substrates. Images a-e show mixture of both HA and OCP (with its distinctly large and plate-like habit). From image f to i the dissolution of the OCP aggregate can be seen. In images a, b, & k the pores of the underlying pSi substrate can be seen.

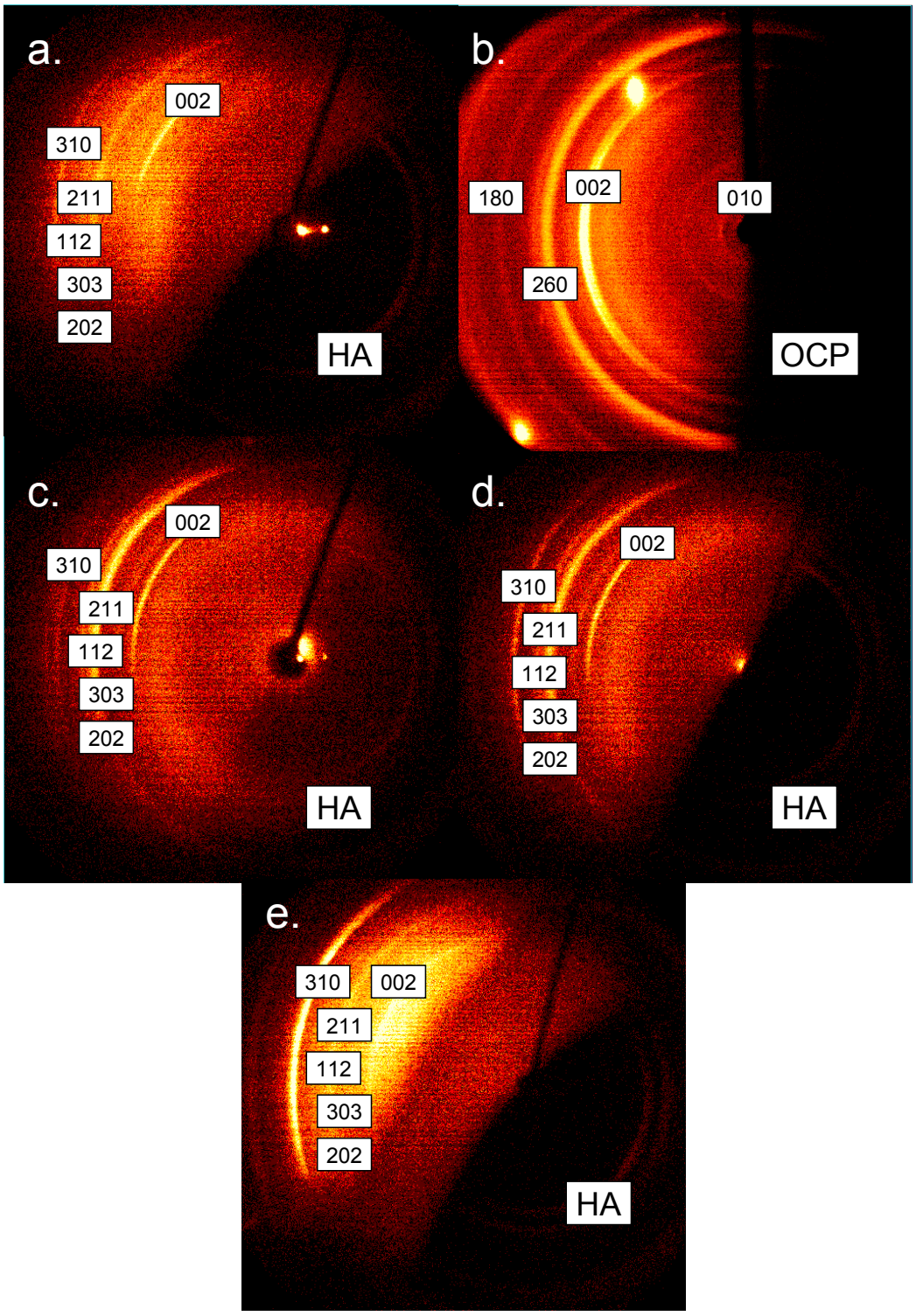

Figure 3.7 Representative spectra of General Area x-ray Diffraction of solution grown mineral on pSi substrates. (a.) condition A (HA), (b.) condition F (OCP), (c.) condition E (HA), (d.) condition H (HA), and condition G.

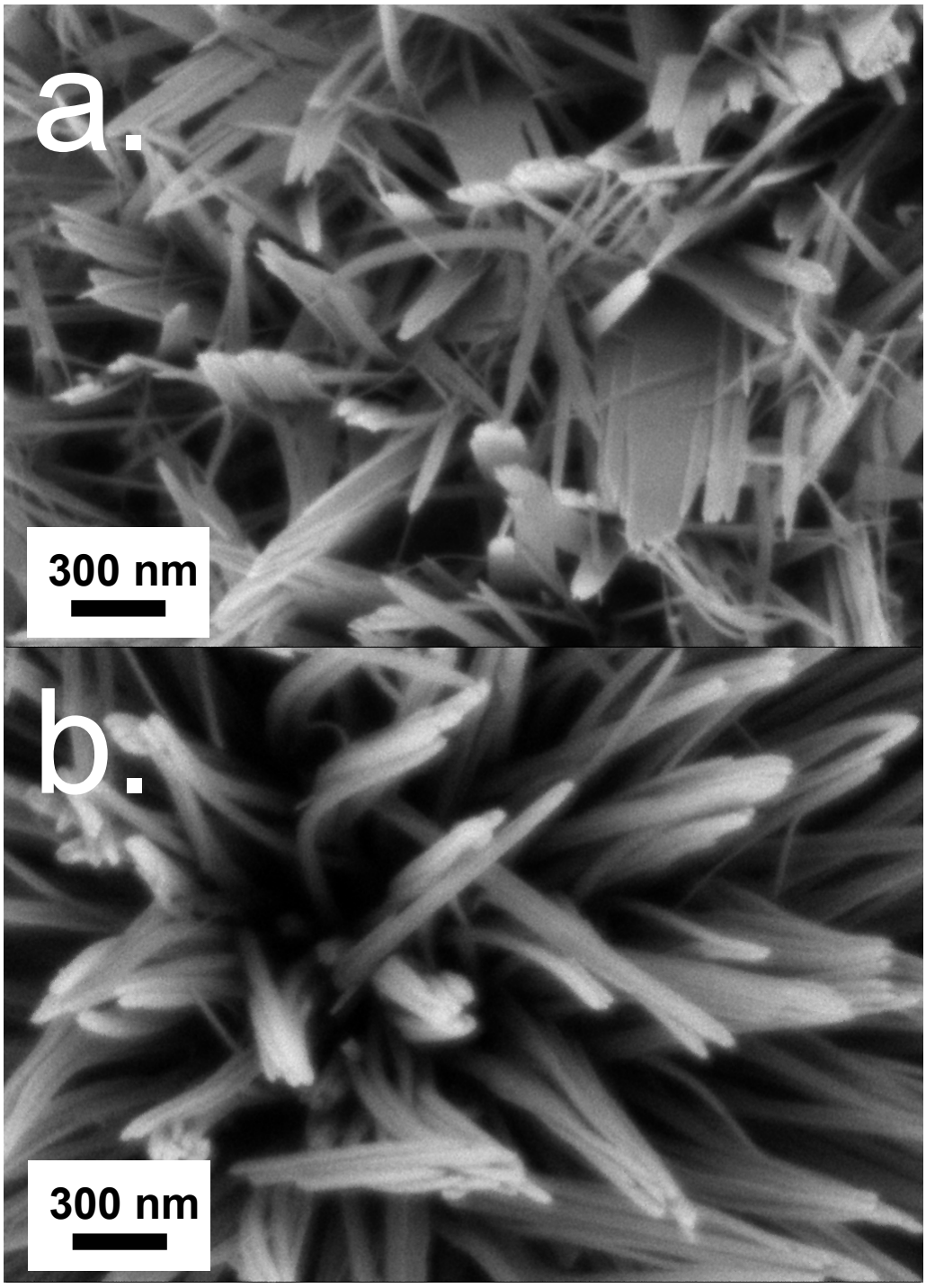

Figure 3.8 High magnification FE-SEM images of Condition E (HA), (a.) at 3 days the crystals show a flattened blade like morphology. (b.) 5 days the blade like morphology becomes rounded and more needle like in character

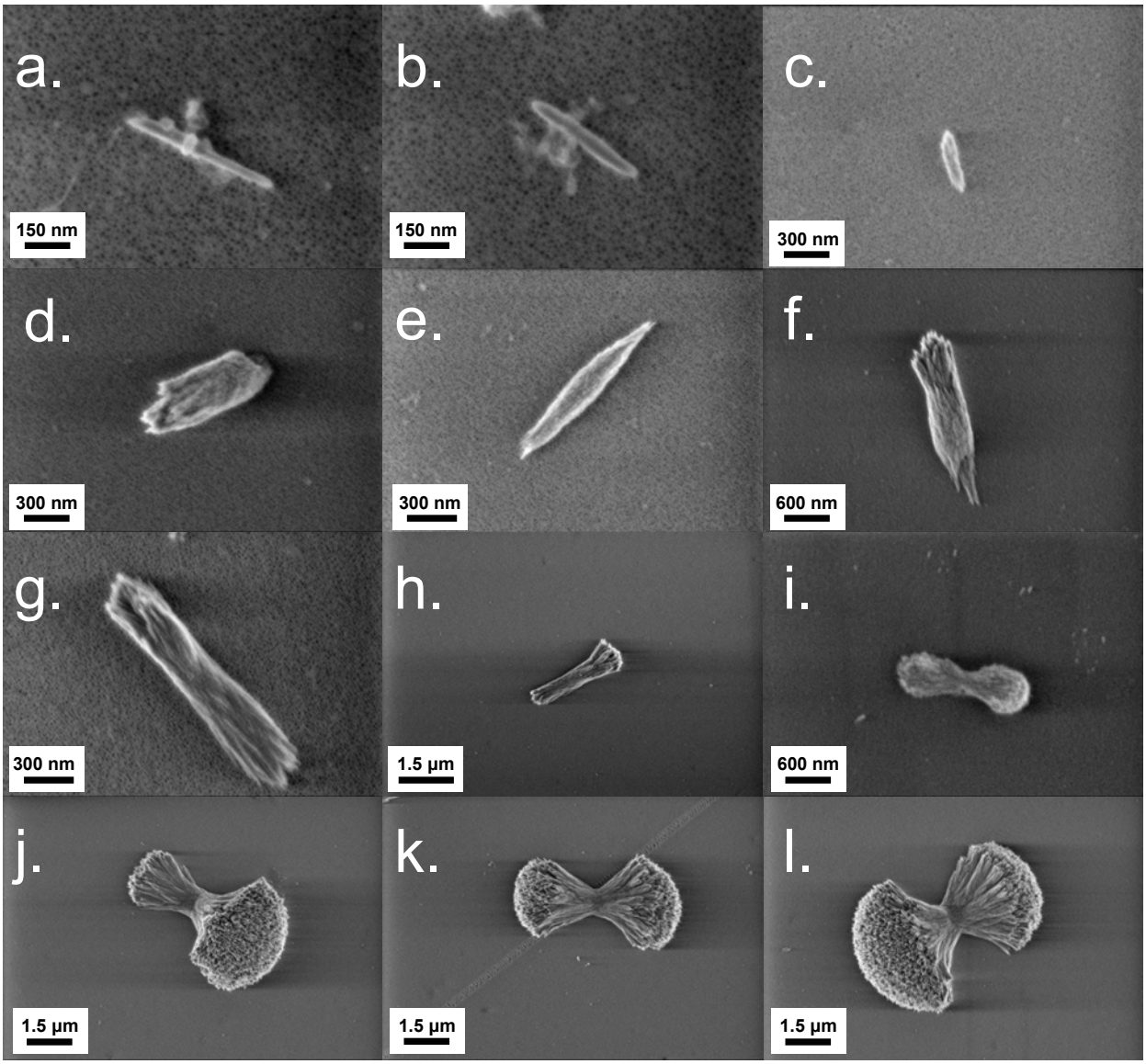

Figure 3.9 The first set of FE-SEM images for Condition A, taken at multiple times (3-7 days) at multiple locations on the substrate. These images demonstrate a possible mechanism for the formation of dumbbell shape aggregates of HA crystals. From the formation of (a & b) individual prismatic HA crystals to the bundling/over growth of these crystals into a (i-l) dumbbell morphology.

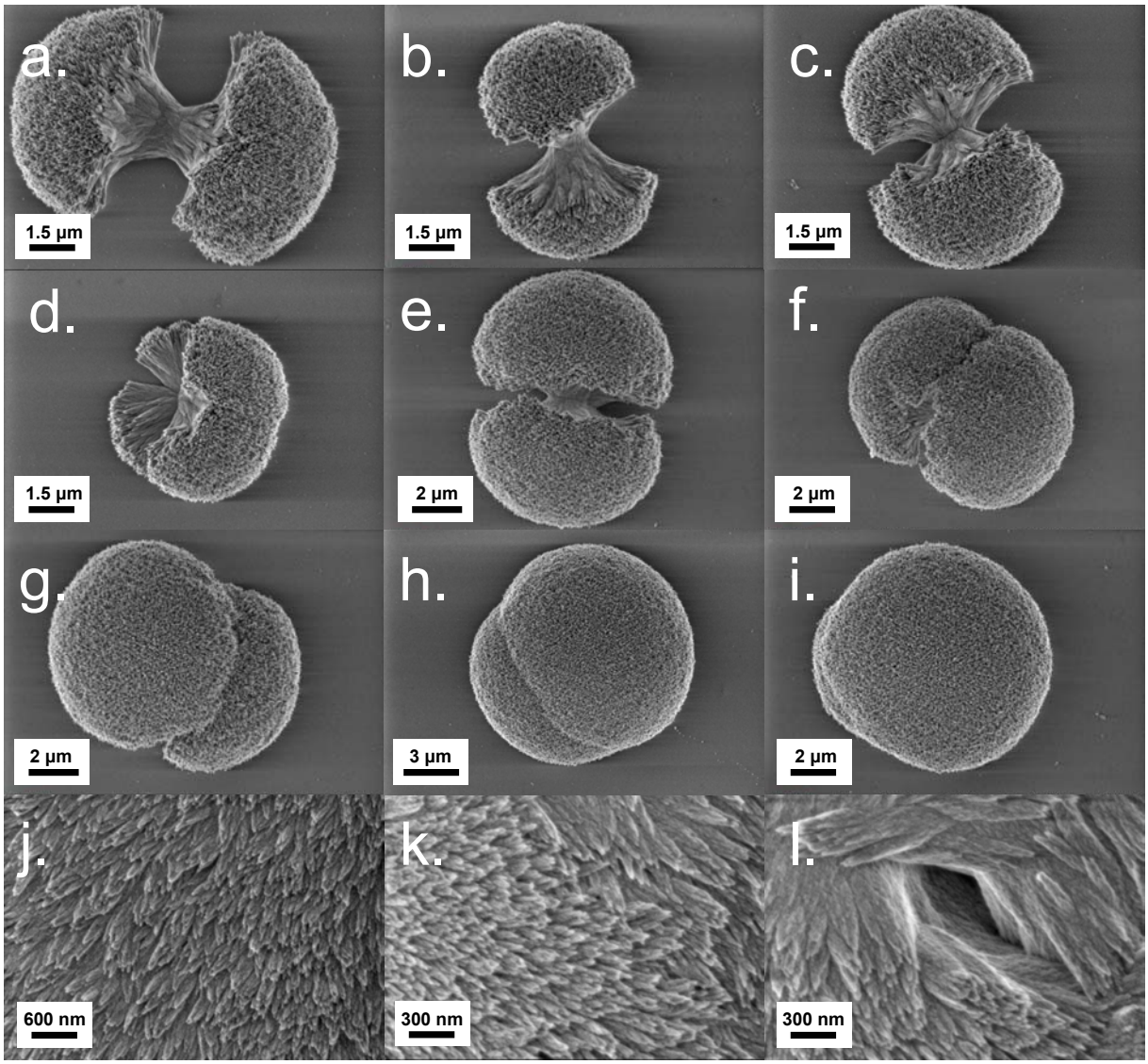

Figure 3.10 The second set of FE-SEM images for Condition A, taken at multiple times (3-7 days) at multiple locations on the substrate. These images demonstrate a possible mechanism for the formation of (i.) spherical aggregates from (a-h) dumbbell shaped aggregates of HA crystals. The surface of the spherical aggregates (j-l) continue to present the habit of the individual prismatic HA crystals.

To understand the changes in the crystal morphology we have seen from each condition, we must first step back and consider the driving forces for crystallization. The change in chemical potential of the crystallizing species $\Delta\mu$, is a measure of the change in free energy of the ions in the system as they move from a speciated state to a crystallized state. Therefore the larger $\Delta\mu$, the larger the driving force for

crystallization.[107, 122]. In the equations below (Eq. 3.1-3.2), it can be seen that the driving force for crystallization is strongly dependent on both the supersaturation σ of ions, the temperature T in the system and Boltzmann's constant k_B. The supersaturation of the system is dependent on the concentration of ions in the system in terms of the ion product, *IP*.

$$\sigma = \ln \frac{IP}{Ksp} \qquad \text{(Eq. 3.1)}$$

$$\Delta\mu = k_B T\sigma \qquad \text{(Eq. 3.2)}$$

The ion product for a unit cell of HA, $Ca_{10}(PO_4)_6(OH)_2$ can be determined as $[Ca]^{10}[PO_4]^6[OH]^2$, and for OCP $Ca_8H_2(PO_4)_6{\cdot}5H2O$ can be determined as $[Ca]^8[H]^2[PO4]^6$. The ratio of the *IP* of the system to the equilibrium constant *Ksp* of crystal (HA at 25 °C is 10^{-115}, OCP at 25 °C is $1.01*10^{-94}$) [123]dictates the relative supersaturation σ of the system.

The HA crystal morphologies seen in conditions A and E, are examples of HA crystals that appear elongated and prismatic, while the morphologiess of the OCP crystal in conditions C, and F, and the HA crystals in the remaining conditions B, C, D, G and H appear plate-like. From condition A to D and from condition E to F there is an increase in the concentrations of calcium and phosphate. This trend correlates to an increase in the ion-product (*IP*), which translates to an increase in σ (as seen in Eq. 3.1) and thus the driving force in crystal formation (as seen in Eq. 3.2). The difference from conditions A through D to conditions E through H is an increase in temperature,

which also translates into an increase in σ and the driving force in crystal formation. Thus as the driving force in crystal formation increases, the phases and morphologies of the crystals formed change from HA crystals that are prismatic in character, to OCP crystals that are plate-like in character; as σ is increased further the crystal phase once again becomes HA and the morphology remains plate-like.

Considering the morphologies seen, in terms of Ostwald's "Rule of Stages," as a competition between kinetics and thermodynamics, we can give a possible explanation in correlation between changing the driving force for crystal formation and the changes in both crystal phase and morphology. At low σ (conditions A and E) the driving force is relatively low. The concentration of ions in both condition A and E is equivalent to the concentration of calcium and phosphate found in SBF (without the additional salts). At this concentration the solution is in a metastable state. Even though the *IP* of the solution is well above the value of the *Ksp* (dissolution equilibrium constant) visible precipitation does not occur. But with the addition of pSi, the substrate acts as a heterogeneous nucleation site and destabilizes the solution to initiate crystal growth. Once crystal growth is initiated, the driving force is still low, and rather than witnessing one of the more unstable, kinetically driven (in terms of Ostwald's rule of stages) phases form first, such as the more soluble amorphous calcium phosphate, brushite and/or OCP,[124, 125] we instead see HA form. In conditions A and E the HA formed is elongated and prismatic in character, a morphology that one would expect from HA's hexagonal crystal structure. Since these crystals, in this solution, likely form by a relatively slowly process the addition of material may be mediated by ion-by-ion addition, or in the very least by a fast transformation from a less stable phase (not seen in these studies).

In contrast, OCP is known to grow as thin blades[126-128] or plates, which can clearly be seen in the images of conditions C and F (Fig. 3.5-3.6 and 3.8). In each of these conditions both the concentration of ions, and ratios of calcium to phosphate in solution have changed relative to conditions A and E. These changes alone should not change the favored phase in the system from HA to OCP since the ratio of Ca:P is only changed from 2.5 to 1.67 still within the range (above 1.5) to promote the formation of HA. However since the system is not stirred and calcium and phosphate are not added at the same time there may be local regions of high phosphate concentration that, upon initial mixing, promote the formation of the plate-like OCP, this may be the case since these conditions are also metastable at 20 °C. Additionally, condition F occurs +17 °C higher than condition C (which presents a mixture of both OCP and HA with HA being the majority phase, Fig. 3.8).

Conditions B, C, D, G and H all present plate-like HA crystals and this maybe a result of first forming an unstable kinetically driven phase which is then slowly transformed to the more thermodynamic phase, but the morphology of the original phase is maintained. An example of such a kinetic phase would be amorphous calcium phosphate (ACP). [109, 129, 130] ACP constitutes many forms from hydrated clusters of ions, to calcium poly-phosphate glasses, [131] to small clusters of ions of specific formulas,[126-128] specific calcium to phosphate ratios,[128] and stabilized by a surrounding layer of hydration.[109] Whatever the form, ACP it is the most unstable phase. In aqueous solutions at pH 7.4 ACP converts to HA, but the resulting morphology of the HA crystals has an OCP, plate-like character.[125, 128, 132] The supposition is that there is a transitory phase between ACP and HA that is OCP-like.[124, 125] OCP contains both apatitic layers and hydrated layers. [133] OCP can

contain various amounts of water that can easily enter or leave through the structure through the hydrated channels in layer.[124, 125] The removal of water and this hydration layer would lead to the formation of an HA crystal structure,[124, 125] this would be considered a solid state transformation, where all that is needed to transform the crystal structure is the removal of water. This solid-state transformation due to the loss of water is what likely occurred in the case of condition G, since in the low magnification FE-SEM (Fig. 3.5) both conditions G and F look the same. Closer examination of condition G, through higher magnification FE-SEM (Fig. 3.6), shows that these large plate-like crystals are made of individual blade-like crystals,[124, 125, 134] which could still be considered OCP, but the GADDs information on condition G confirms that the crystal phase is in fact HA.

However, the apparent dissolution of the OCP phases seen in condition C (Fig. 3.8) would suggest a combination of Ostwald's rule of stages and dissolution-reprecipitation where the growth of the stable HA occurs at the expense of the relatively unstable OCP, yet the underlying crystal structure of the HA produced is still plate like.[8] In light of this information, the creation of plate-like HA may be the result of the solid state transformation of small OCP-like crystallites to small crystallites of HA through the loss of water, followed by a dissolution step. Once these small yet stable HA crystallites have formed with the underlying plate-like character, a competition begins and the less stable OCP and OCP-like crystals begin to redissolve feeding the growth of the new plate-like HA.

Condition H, presents small aggregates, of HA crystals, 300-700 nm in size (Fig. 3.12). Unlike most of the other conditions, the aggregates in this condition do not completely cover the substrate, and in some cases present discrete aggregates of HA

crystals that can be more closely examined. For a series of control experiments for the experiments performed within the hydrogel, a solution-based *in vitro* control needs to be established which compensates for the physical effects that the hydrogel has with regards to the growth of crystals.[8, 17]

Condition H is most closely related to growth in a hydrogel environment. Hydrogels regulate the concentration and ratio of calcium and phosphate, via diffusion.[8] In condition H, the ratio of ions and concentration of the reagents is set at the start of the experiment. In hydrogels crystal growth is dominated by surface diffusion.[8] In condition H the temperature of the reaction was raised from 20 °C (laboratory temperature) to 37 °C, to promote surface diffusion in the growth of the crystals. Finally hydrogels suppress nucleation.[8] Condition H achieves the suppression of nucleation on the substrate by using concentrations of reagents (5mM Ca and 3mM PO_4) so high that the nucleation of crystals and the formation of a precipitate begins as soon as the solutions are mixed. As a result the relative frequency of nucleation events on the substrate is in competition with the nucleation events occurring in the solution. In this case of course there is not a question as to whether or not crystals first nucleate in solution or on the substrate. Here crystals first nucleate in solution by design. The suppression of gravity and convection found in hydrogels could not be accounted for in these experiments. For these solution-based control experiments (to be compared to crystals grown in the gel) substrates were removed and examined under an SEM at 5 days of growth.

Condition H provides a control for comparison against solution-based growth on porous silicon experiments found in the literature;[102, 103] and establishes a solution-based equivalent to the hydrogel system to coincide with the morphology and

amount of growth/coverage seen in hydrogel based experiments on the same time scale. The solution-based experiments presented here bridge the two methods (solution-based found in the literature; [102-106] and hydrogel based) of crystal growth.

3.4.2.1 Oxidized pSi in solution control.

Results from Condition H (Fig. 3.4, 3.5 and 3.11) show floret-like aggregates The crystalline aggregate "petals" (for lack of a better term), have a rounded character. Due to the similarity in the size of the crystal aggregates seen in preliminary hydrogel-based experiments (see Section 3.4.3) and the ability to examine these aggregates as discrete packets on the surface, confirms that Condition H is a suitable control for mineral grown on a substrate in a hydrogel.

3.4.2.2 BSA physisorbed to pSi in solution:

The globular BSA protein was chosen as a control protein for a couple of reasons, first it is inexpensive and readily available, second it is rather "sticky" in character making it easy to physisorb (attach/adsorb via intermolecular forces of attraction) to a substrate and third, there are reports in the literature on BSA's ability to either promote or inhibit HA formation in hydrogel,[135] which gives us a baseline to work from. The BSA protein was physisorbed with a total amount of 40 μg per pSi film. Results from the BSA pSi substrates (Fig. 3.11c) placed in solution again show the floret-like aggregates of similar size and clustering to the oxidized pSi in solution control, but at what appears to be a greater level of coverage than bare pSi (not quantified). The crystalline aggregate petals seem to be slightly elongated compared to the ones from the control substrates.

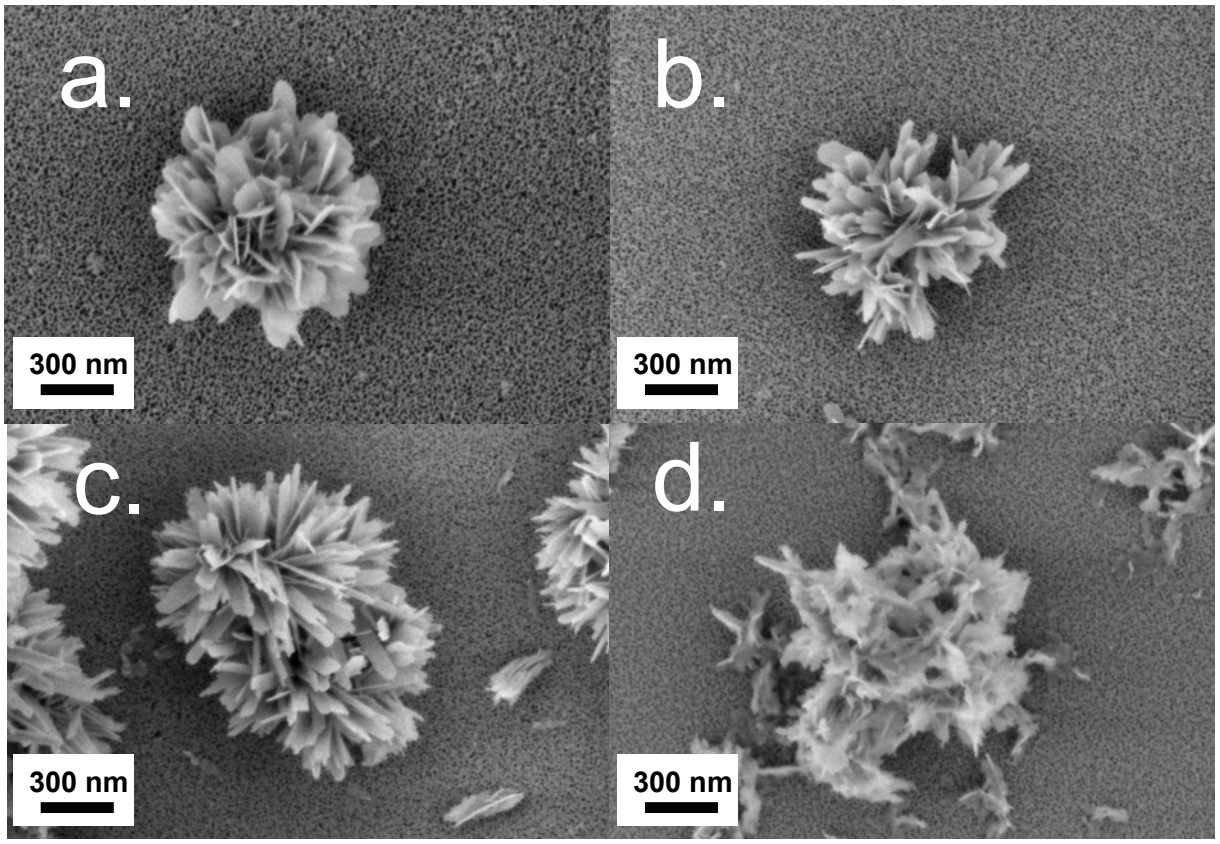

Figure 3.11 FE-SEM images of HA crystal aggregates grown in solution on pSi (a.) bare-oxidized, (b.) pSi+BSA, (c.) pSi+Casien, and (d.) pSi+Gelatin. Run for 5 days in 5 mM calcium and 3 mM phosphate in Tris buffer at pH 7.4 at 37°C.

3.4.2.3 Casein physisorbed to pSi in solution:

Milk casein is a globular phosphoprotein know to inhibit HA precipitation in solution.[135] The milk casein protein was physisorbed onto pSi substrates, with a total amount of 40 μg per pSi film. Results from the casein pSi substrates (Fig. 3.11b) placed in solution also show the floret-like aggregates of similar size and clustering to the BSA pSi in solution substrates, and at what appears to be a similar if not greater level of coverage (not quantified). The crystalline aggregate petals also seem to be slightly elongated compared to the ones from the control substrates.

3.4.2.4 Gelatin physisorbed to pSi in solution in solution:

To physisorbed gelatin onto pSi substrates, pSi films were placed under gelatin (275 Bloom 10 w/v % in Tris buffer pH 7.4), left to set and the hydrogel was then removed by simply melting away the gel at 50 °C but not rinsing the surface. Results show (Fig. 3.11d) that the overall structure of the HA aggregates are similar to the oxidized pSi and protein based controls, but the crystal morphology is distinctly different than either the control or the substrates with proteins physisorbed, exhibiting tapered crystal petals that appear less distinct from one another. These petals also seem to be blended/fused together.

There is no reason to believe that all of the protein/peptide material originally physisorbed to the surface of the oxidized pSi, remained on the substrate while in solution. In fact we surmise that though much of the material remained on the surface, as indicated by the increased coverage by HA on the protein-coated surfaces relative to the presence of HA on bare pSi, that some of the material did indeed release into solution as evident by the apparent changes in crystal morphology. Since nucleation determines coverage and phase, while growth conditions determine morphology/habit[108] the apparent change in crystal morphology for not only the substrates with physisorbed proteins/peptides but the physisorbed gelatin, suggest that morphology of the crystal aggregates were affected by the medium into which they grew which would contain some eluted organics. And as demonstrated by the solution-based experiment seen in figure 3.11, the presence of the gelatin seems to have a significant effect on crystal morphology. The effect of gelatin seems to change the aggregate morphology from a series of distinct blades of crystals (sprouting radially out from a central location), to a less distinct, blended, more tapered, plate-

like character.

3.4.3 DDS Based Experiments

Increasing the complexity of the *in vitro* model and broadening the applicability of pSi to study HA crystal growth, we introduce pSi substrates into a hydrogel-based DDS (Fig.1.7). The basis of this hydrogel-based *in vitro* model is a circulating infinite-reservoir dynamic DDS.[17] The constant concentration of calcium and phosphate, at the respective solution/gel interfaces, are maintained using reservoirs of large volumes (1L) relative to that of the gel filled reaction tubes, that are changed frequently, peristaltic pumps (circulating solution at rate of 42mL/min), short reservoir circuits (<200mL), and short reaction times (3-5 Days). The nature of the dynamic DDS restricts the ratios of ions in the resulting precipitation reaction to values which coincide with the relative diffusivity of the reagent salts within the hydrogel matrix ($6.0 \pm 0.5 \times 10^{-6}$ cm^2/s for calcium chloride dihydrate and $3.9 \pm 0.2 \times 10^{-6} cm^2/s$ for ammonium phosphate dibasic, (1.49 to1.76):1).[17] The reaction environment, kept at a pH of 7.4 and a temperature of 20 °C, helps to restrict the calcium phosphate product formed to that of HA.

3.4.3.1 HA in the control hydrogel:

The HA (as confirmed by pXRD) obtained from the control gels (absent of proteins/substrates) were examined by FE-SEM, appear as floret-like polycrystalline aggregates composed of small plate like crystals (Fig. 3.12-14). Each group/petal-shaped-cluster of polycrystalline-aggregates extends out radially from the center of the aggregate and ends in a taper to yield the floret-like morphology. Again the morphology of these HA aggregates correlate with the morphology seen in HA

aggregates on the oxidized pSi substrates placed in the hydrogel and physisorbed with gelatin and placed in solution. The distortion of the HA aggregates from the presentation of distinct crystallites (as seen in the solution based controls section 3.4.1.1) is likely because a of strong interaction between the growing crystals and the organics that makeup gelatin matrix.

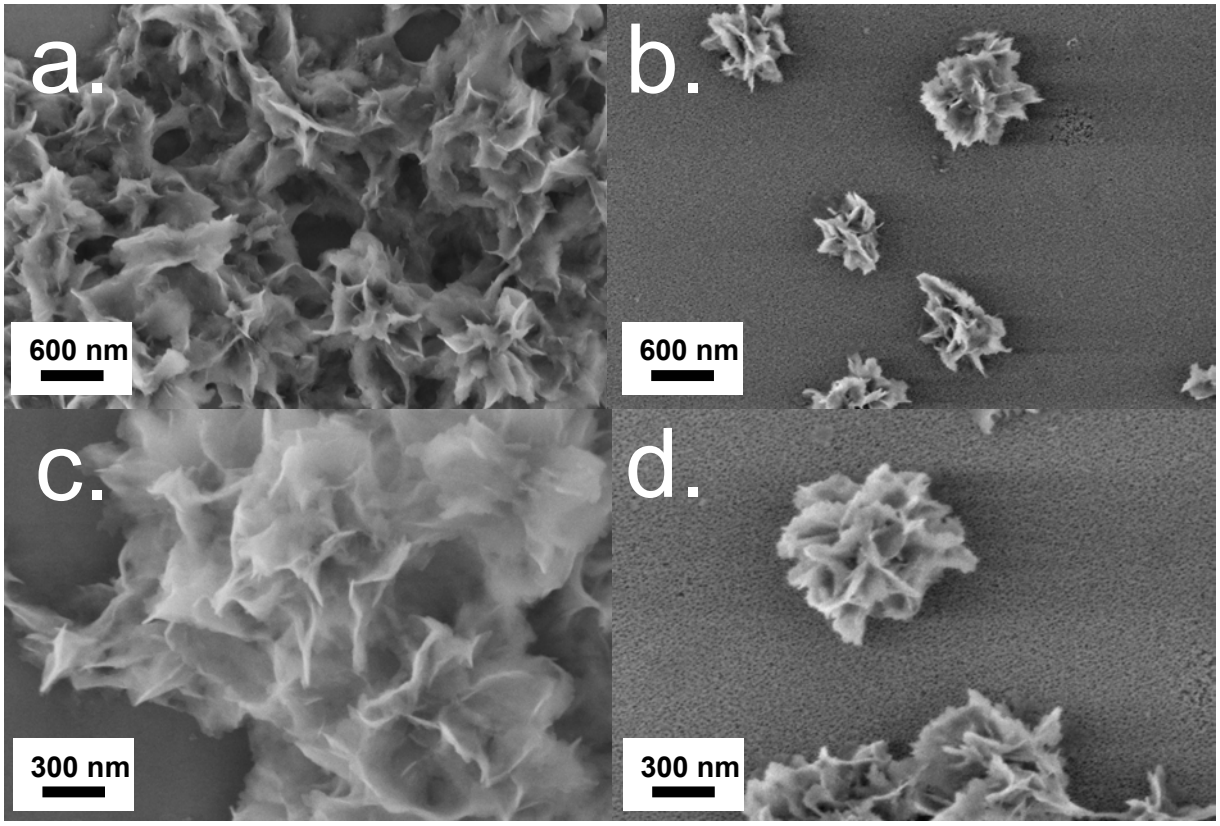

Figure 3.12 FE-SEM images of HA crystal aggregates grown (a & c) in gelatin hydrogel (mounted on a silicon substrate), and (b & d) on oxidized pSi in a gelatin hydrogel, (the pores of pSi visible) in a dynamic DSS at 20 °C, run for 5 days. These images of the HA crystal habit serve as controls for HA crystal grown in the presence of proteins.

3.4.3.2 HA in the protein loaded hydrogel:

Proteins in the hydrogel at concentrations of 20 µg (200 µg/mL) were suspended in the hydrogel within a 2 mm (0.1 mL) space at the location of known

mineralization using techniques as describe by Boskey.[17] The results of only having BSA and casein in a hydrogel (Fig. 3.13) demonstrate that the crystal morphology seen on substrates in the gel with physisorb proteins have a significant change relative to each protein by itself in the gel with respect to BSA but not with respect to casein. The morphology of the crystal aggregates grown in the presence of BSA in the hydrogel still appear blended together as seen in the gelatin control, while the aggregates grown in the presence of casein in the hydrogel have appear blended as well more fused appearance than the mineral formed in the presence of BSA.

The HA (as confirmed by pXRD, Fig 3.14) crystal aggregates obtained from the gels containing BSA exhibit similar floret-like morphology as the HA grown in the control gels but have a more "fused" or blended like appearance where the petal-like crystallites have less distinction from each other. Rather than each group/petal-shaped-cluster of polycrystalline-aggregates extending out radially from the center of the aggregate the aggregates seem to melt into spread out and "melt" into the mounting substrate.

The HA (as confirmed by pXRD) obtained from the gels containing Milk Casein has a seemingly exaggerated crystal morphology as the crystals seen in the BSA loaded gels with a "fused" floret-like morphology. The resulting similar morphology between the casein-loaded and BSA-loaded gels, suggests that these proteins, with a gelatin matrix, have a similar effect on the growth morphology of HA. The lack of significant/drastic HA morphology change (such as those seen by changing σ in the solution model) between gelatin, BSA and casein proteins in the hydrogel, indicates that the gelatin hydrogel dominates in dictating the crystal morphology. Though there was not a drastic change in the morphology or phase (Fig.

3.13) there are some subtle differences. Moving from a blank gelatin gel, to a BSA loaded gel to, to a casein gel, the crystal morphology appears to become more and more “fused” in appearance. This gradual decrease in the “quality” of the crystal morphology is likely because of a relative increase in the interaction between the growing crystals and the organic components of the gelatin hydrogel as facilitated by these proteins. Based on these assumptions, it seems that the interaction between the growing crystals and the added proteins is greater for the milk casein than for the BSA. This conclusion is supported by the solution-based experiments were the addition of casein to the substrates placed in solution resulted in more elongated crystals relative to the oxidized control substrates, and substrates with BSA physisorbed to the surface.

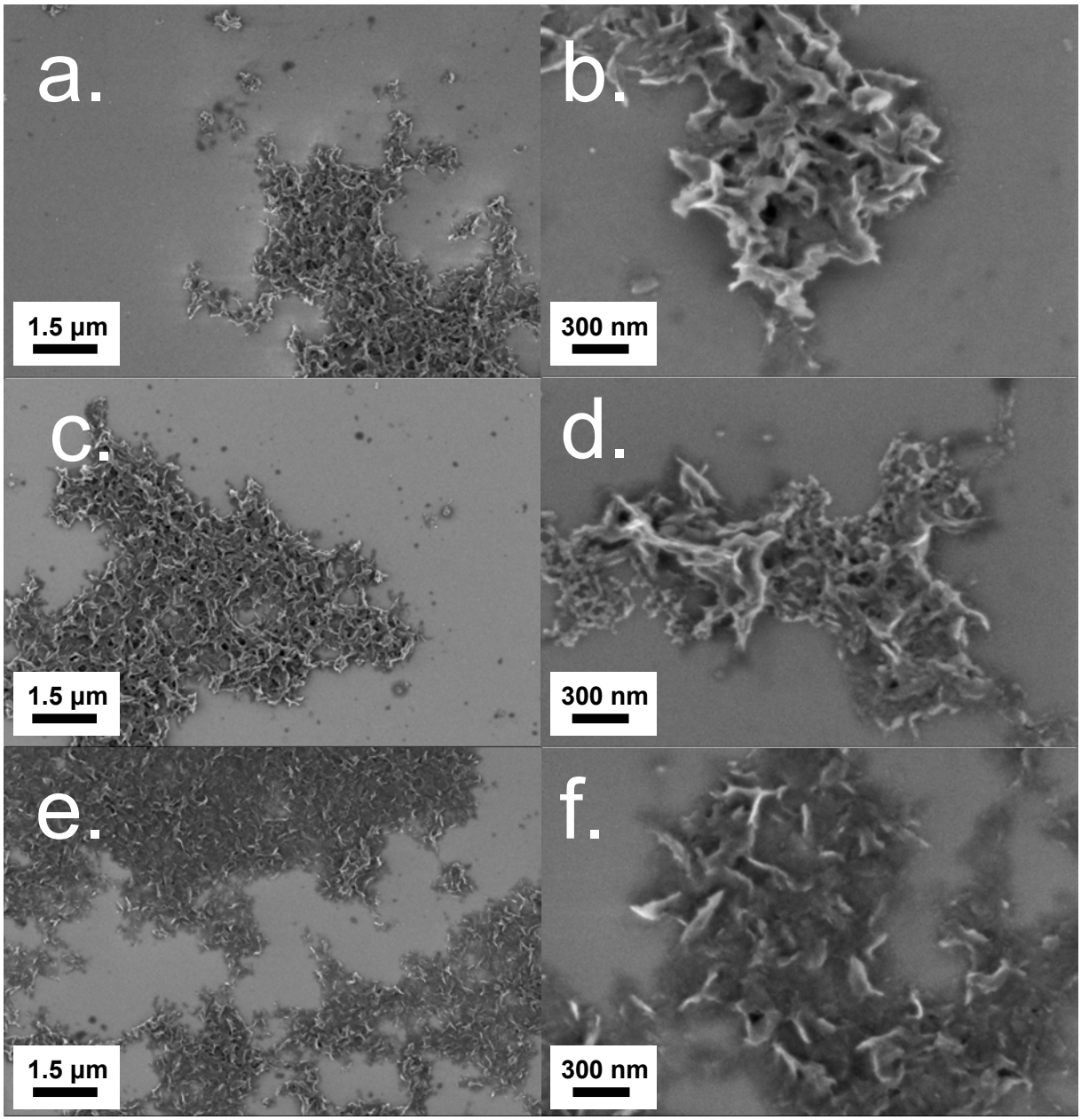

Figure 3.13 FE-SEM of HA crystals grown in (a & b) bare gelatin gel, (c & d) BSA in gelatin, (e & f) Casein in gelatin. Isolated from the gelatin hydrogel after being in a dynamic DSS at 20 °C, run for 5 days.

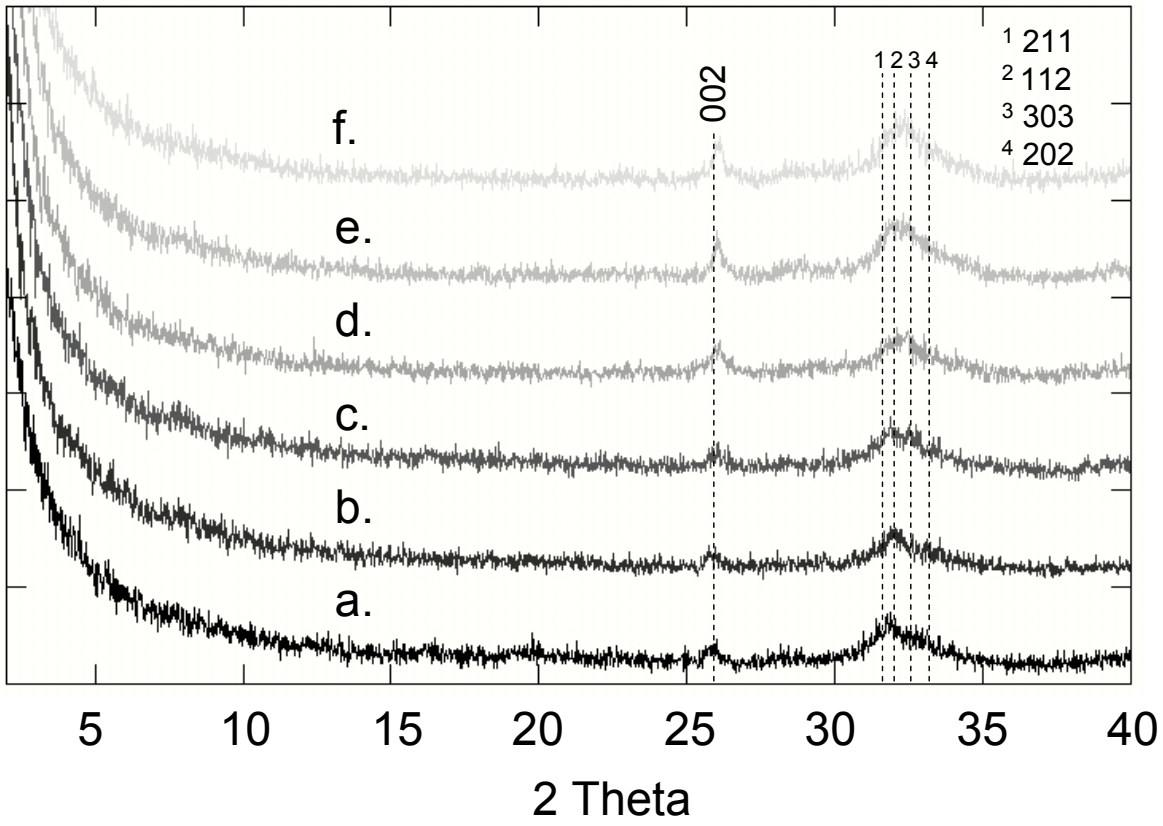

Figure 3.14 pXRD confirming the HA crystal phase of mineral from: (a.) gelatin with no additives (crystal length = 32 nm)[a], (b.) gelatin with BSA (crystal length = 10 nm)[a], (c.) gelatin with casein (crystal length = 21 nm)[a], (d.) gelatin with oxidized pSi (crystal length = 20 nm)[a], (e.) gelatin with BSA near pSi (crystal length = 18 nm)[a], and (f.) gelatin with casein near (crystal length = 15 nm)[a] pSi.

[a] crystal length along the c-axis was determined by Sherrer analysis, instrument peak broadening was compensated for using a corundum standard.. The background was corrected using a manual spline fit.

3.4.3.3 pSi substrates in the hydrogel.

The ability for these nano-porous films to facilitate the free, unrestricted diffusion of ions and to assure that the clearance between the membrane and the tube wall would not result in a bypass of the porous substrate, a control experiment was done with plastic discs of the same size and compared to bare gel and gel with pSi substrates (Fig. 3.1). Results show that the nanoporous films allow for the free

movement of ions and do not retard the precipitation reaction, while plastic discs of the same size do in fact inhibit precipitation in the tubes. The only precipitation seen in the tubes containing plastic discs occurred along the edge of the disc between the disc and the tube, the precipitation did not extend beyond this edge, neither across the disc surface nor any wider than the thickness of the disc itself.

When removed from the gelatin matrix, the stress from the removal of the tubes and the slicing of the gelatin matrix tends to result in cracking and breaking of the stiffer, more brittle, immobilized 250μm thick disks. These films and film fragments are still robust enough to be handled and mounted on SEM stubs, but due to the adhesive and mechanical properties of the gelatin hydrogel, very few films survive the experiment in completely one piece (Fig. 3.15).

Initial precipitation of mineral in the hydrogel occurs at 3 days, using a 6 cm long (3 mL volume) tube filled with 10 w/v % 275 Bloom gelatin in Tris buffer pH 7.4, with reservoir concentrations at 100 mM calcium chloride dihydrate, and 100 mM ammonium phosphate dibasic both in Tris buffer pH 7.4, respectively. On day 5 the matured precipitation band is excised, the hydrogel is melted away and the crystals are analyzed with pXRD, and FE-SEM.

3.4.3.3.1 Oxidized pSi in the hydrogel:

In this dynamic DDS the oxidized pSi substrates alone do not seem to provide for a heterogeneous nucleation situation where the crystals preferentially nucleate on the substrate over that of nucleating in the bulk hydrogel. The very nature of the nucleation suppression qualities of the hydrogel and the speed of addition of the reactions via an exponential concentration profile, create a narrow window of time (a

few hours) in which initial nucleation can take place at a given point. In short, the very nature of the dynamic DDS and 5 day target of the experimental design handicaps the system in such a way that visible precipitation in the hydrogel dominates over clearly visible precipitation on the relatively small substrate. As soon as precipitation is seen on the substrate it has already appeared in the gel.

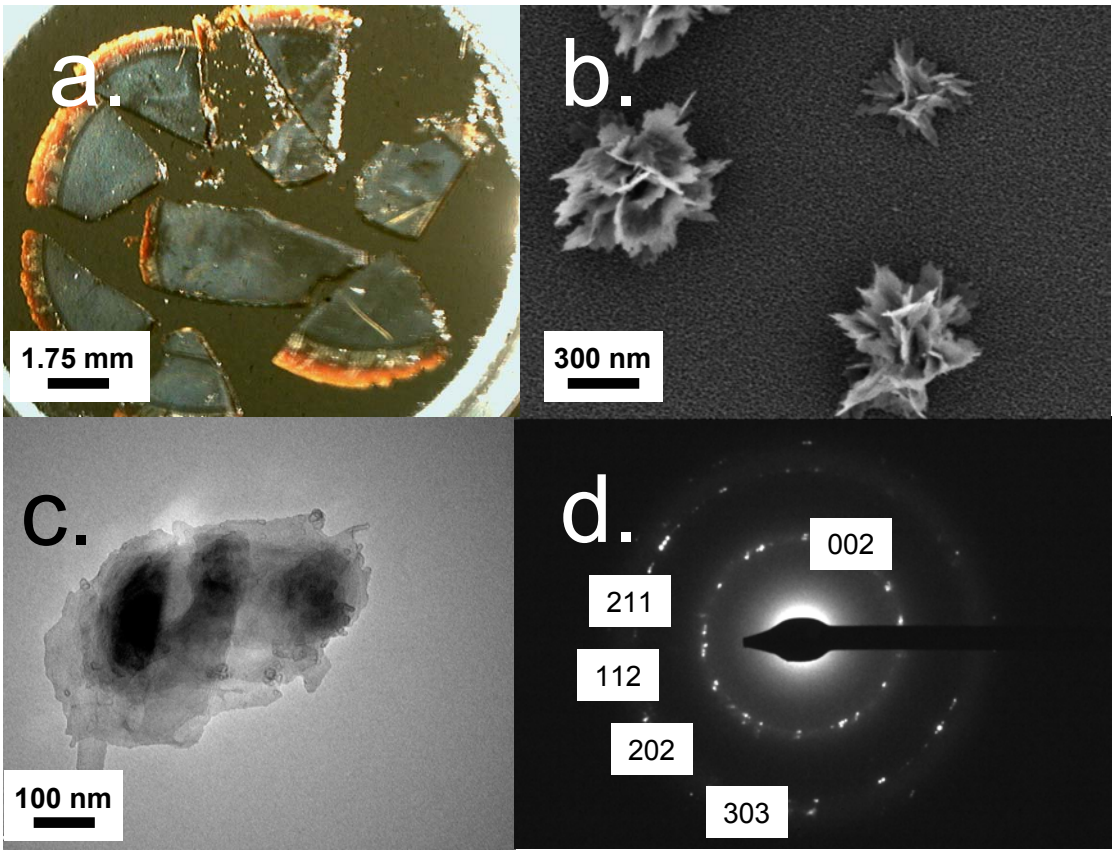

Figure 3.15 Characterization of mineralized pSi disks, after 5 days in a DDS. Examined by (a.) optical microscopy, (b.) FE-SEM, showing the floret-like crystal aggregates, with pores of the underlying pSi substrate visible (c.) TEM (light-field) and (d.) SAED to confirm that the crystalline aggregates are HA. Samples for optical microscopy and FE-SEM were examines as-is, while preparation for TEM and SAED required that the crystalline aggregates be sonicated off of the pSi substrate.

Although it appears that the exclusive restriction of crystal growth to only the pSi substrate is not currently feasible with this system, the use of the pSi substrate

allows for the excision and examination of crystals that have grown at a specific location within the hydrogel. The control of the crystal nucleation and growth elements about a given location can be witnessed using these strategically placed substrates that can be subsequently removed and examined.

The presence of the otherwise unmodified oxidized pSi substrate does not seem to have an effect on the crystal morphology when compared to crystals grown in just the hydrogel (Fig. 3.13). The crystal morphology of HA aggregates grown in both the gel on the oxidized pSi in the gel have strong correlations to the crystal morphology seen when HA was grown on oxidized pSi, with physisorbed gelatin, in solution (section 3.4.1.4).

The physisorption of proteins such as BSA and Milk Casein on to pSi substrates placed in the DDS, not only effect the crystal morphology resulting in a more flattened morphology of the crystal aggregates (Fig. 3.14), but also increase the overall coverage of HA on the substrate (not quantified).

3.4.3.3.2 Proteins and pSi in the hydrogel:

Proteins in a hydrogel can have an effect on the morphology [10, 11, 19, 39, 40, 42-46] and the total concentration of crystals grown in those gels. [12, 13, 17, 18, 28-31, 33-38] The remaining question is what is the effect of introducing a substrate to this protein, hydrogel dynamic, on the formation of HA. Two permutations of including a substrate with a protein and a hydrogel were explored. In one system the proteins are physisorbed directly onto the substrate prior to being loaded into the gel. In the second system the proteins are placed in the hydrogel in a layer just about the substrate in the gel.

3.4.3.3.2.1 Proteins on the pSi substrates in the hydrogel:

BSA and casein proteins were physisorbed onto oxidized pSi surfaces at concentrations of 40 μg/film. After 5 days the mineralized films were examined by FE-SEM. The images in figure 15 show the morphology of the HA crystal aggregates grown with proteins physisorbed onto oxidized pSi placed in a hydrogel. As can be seen in the comparison to the oxidized pSi control the substrates, the BSA coated substrates present a morphology that can best be described as "fused" (compared to the oxidized control substrates) floret-like morphology. Where the crystals do not appear to grow up and out in all directions but rather appear to grow out along the substrate surface. In the case of the casein protein on pSi, there is no longer any sign of the original pSi substrate. There seems to be complete coverage of the substrate with a morphology that appears the same as the morphology as the crystals grown on the BSA coated substrate.

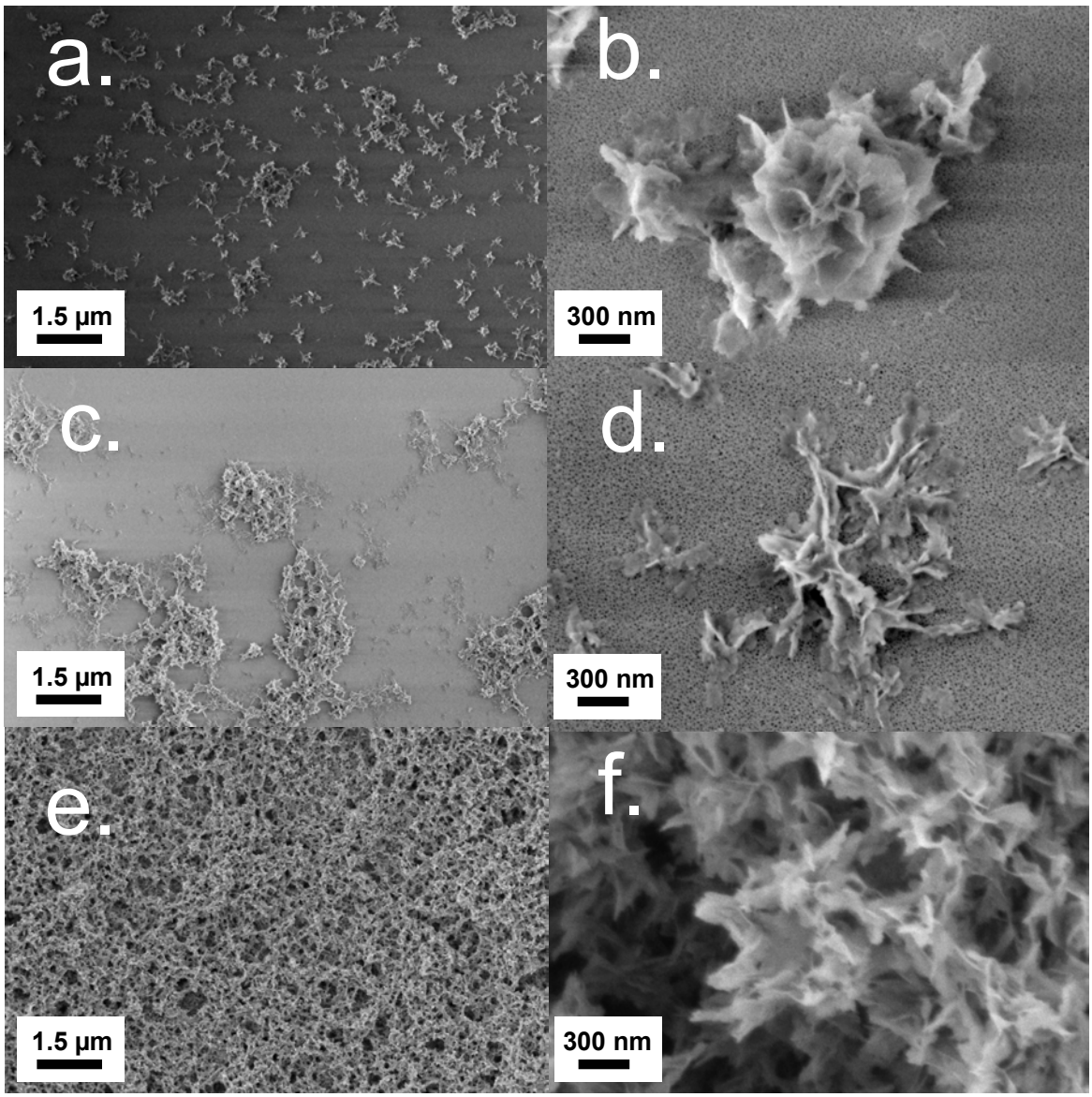

Figure 3.16 Mineralized pSi from substrates placed in a hydrogel. (a & b) oxidized pSi, (c & d) BSA physisorbed to pSi, (e & f). (a-d) On both the oxidized pSi and pSi with BSA, the pores of the pSi substrate are still visible (e & f), in the case of casein on pSi , the pore of the pSi substrate can no longer be seen.

3.4.3.3.2.2 Proteins near the pSi substrates in the hydrogel:

BSA and casein proteins were place in a 0.1 mL (2 mm) hydrogel layer just about the oxidized pSi substrate at a concentration of 200 μg/mL (20 μg total). Examination of the HA crystals via pXRD confirmed that the crystals are HA (Fig 3.14). The inclusion of a substrate to this dynamic seems to enhance this effect of interaction between the growing crystals, the BSA protein and the gelatin hydrogel, leading to a more flattened character of the crystal aggregates on the substrate. In the case of casein, the addition of the substrate does not seem to enhance this observed flattening of crystal aggregates on the substrate. The crystal morphology does not seem to deviate from the morphology seen with BSA physisorbed to the surface, but there seems to be an increase in coverage. In substrates with casein physisorbed to the surface and placed in the hydrogel, it is no longer possible to see the pores of the porous silicon as seen in the FE-SEM of the other substrates. The masking may be the result of a couple of factors such as either gelatin strongly interacting with the casein proteins on the substrate or a surface layer of calcium phosphate.

3.4.4 Concentration data

Table 3-2 highlights the percent change in calcium and phosphate (relative to HA grown in a gelatin gel) of all crystal growing conditions in the hydrogel. BSA alone in the gelatin gel and BSA physisorbed to the pSi substrate, both seem to have little effect (neither promotes or inhibits) on mineralization, which coincides to what has been reported in the literature.[7] In contrast, milk casein alone in the gelatin gel and milk casein physisorbed to the pSi substrate, differ in there ability to promote mineralization. While milk casein alone neither inhibits nor promotes mineralization

in the hydrogel, casein physisorbed to the pSi substrate seems to promote mineral formation. The introduction of the pSi substrate on average has a noticeable effect on the concentration of HA in the hydrogel.

Table 3-2: The effect of additives in the hydrogel on the resulting calcium and phosphate concentration as compared to a gel without additives. The conditions with proteins near the pSi substrate were compared to oxidized pSi alone.

Additives in the hydrogel	Change in Calcium Concentration Relative to no additives (%)	Change in Phosphate Concentration Relative to no additives (%)	Promote v. Inhibit
No additives	N/A ± 7.29	N/A ± 0.45	N/A
40 ug BSA alone	7.45 ± 6.46	5.37 ± 0.30	Neither
40 µg milk casein alone	5.19 ± 4.79	5.05 ±.017	Neither
Oxidized pSi	-5.29 ± 3.55	-7.55 ± 0.622	Inhibit
BSA on pSi	5.33 ± 4.26	5.33 ± 0.30	Neither
Milk Casein on pSi	9.43 ± 0.61	8.28 ± 0.43	Promote
40 µg BSA near pSi	-9.03 ± 16.16[a]	-6.52 ± 0.33[a]	Inhibit
40 µg milk casein near pSi	3.62 ± 0.82[a]	7.49 ± 0.52[a]	Neither

[a] relative to oxidized pSi

Oxidized pSi alone in the hydrogel appears to inhibit mineral formation. When considering the effect of proteins near the pSi substrate the differences in concentrations reported are relative to oxidized pSi as the control. The presence of BSA near the pSi, on average, has a significant effect on the formation of mineral relative to the pSi control and subsequently the gelatin hydrogel, though the values of calcium are within error of both controls, the difference in the values of phosphate are significant. In this case it seems that the substrate may play a dominant role leading to the inhibition of mineralization. With the introduction of milk casein next to the pSi, there is likely a competition taking place, which results in a cancellation in the effect generated by the pSi alone. This competition may arise from a partial adsorption of casein to the pSi substrate, giving way to sections on the substrate that a bare, oxidized pSi, and sections coated with casein (which as seen with "casein on pSi" condition

leads to mineral promotion). In conclusion the presence of a substrate has an effect on the role of the protein in the hydrogel

3.4.5 Contributions to the *in vitro* model for bone formation

The similar morphology of HA crystals grown in a gelatin hydrogel as compare crystals grown in solution in the presence of gelatin (< 4ppm), strongly suggests that the ECM-like matrix acts as not only a growth medium but as a growth modifier as well. Since within the hydrogel based DDS mineral forms in both the gel and on the pSi at the same time, mineral does not exclusively nucleate or form on the substrate. Both the concentration data and the FE-SEM data suggests that the presence of a substrate has an effect on the role of the proteins the hydrogel. In the case of crystal morphology, proteins in the hydrogel enhance the chemical effects of the hydrogel on the crystal morphology. The introduction of a substrate heightens these changes in crystal morphology. Examining both the concentration data and FE-SEM data it seems that casein a known inhibitor in solution, has little to no effect on mineralization alone in the hydrogel but becomes a promoter once attached to a substrate. This data indicates that the roles of both proteins and substrates change as these two components are brought together and depend on the context in which these two components are combined.

3.5 Conclusion

We have expanded the role of porous silicon as a substrate to study crystal growth in both solution-based and hydrogel-based *in vitro* models for biomineralization. The introduction of pSi as a nucleating substrate into a variety of mineralizing solutions has resulted in a map of crystal morphologys and has enhanced

our understanding of how HA forms in solution. We have demonstrated a system by which a functionalized substrates can be placed in a hydrogel-based double diffusion system to study the nucleation and growth of HA. This pilot study has elucidated the combined role of proteins and substrates in mineralization within in an ECM-like microenvironment.

In the future, these surfaces will provide us with the ability to: immobilize small molecules and peptides not previously accessible in the gel system and examine surfaces important for implants in a biologically relevant (i.e., hydrogel matrix) mineralization assay. Unfunctionalized pSi is reported to be biologically compatible and able to support the growth of mammalian cells[136] leaving room for the expansion of this work beyond that of acellular systems. This platform allows for the development and study of surface functionalities and how those functionalities may interact with a hydrogel matrix in the presence proteins to form mineral

3.6 Supplemental Information

3.6.1 Materials and Methods:

3.6.1.1 Gel preparation:

Gelatin: 30g of 275 Bloom Type A Gelatin (Fisher) was mixed with 300 mL Tris Buffer pH 7.4, heated to 50°C in a hot water bath and pH balanced using 2M NaOH until the pH was 7.4.

3.6.1.2 Fabrication of pSi

Porous silicon is fabricated via an anodic etch process. Boron doped P++ silicon (0.8-2 mohm-cm, Siltronix), 525 μm thick, with (100) orientation was

anodically etched in an HF/Ethanol etchant to produce nanopores that form perpendicular to the polished crystal face.

A silicon wafer was cleaved into quarters. One quarter of the wafer was placed in a uniquely designed Teflon etch cell (Fig. 2) with a 7 hole-patterned (0.78cm) interchangeable insert, then filled with 60 mL of 3:1 volume of HF (Hydrofluoric Acid 48% aqueous Mallkroct Baker) to 100% Ethanol (Absolute ACS/USP Pharmco) solution, with an applied current of 45 mA/cm^2, no illumination, for 150 minutes (to create a ~200 μm film). The challenge in creating a porous silicon film on a substrate, to later be used as a membrane, is to create a film thick enough to later be handled once released. To minimize cracking due to electropolishing the etch solution was changed every 30 minutes. To reduce the likely hood of etchant ion depletion due to diffusion limitations the etch solution was mixed continuously using a peristaltic pump, with a 0.3mL throw and an agitation rate of 1-2 Hz.

The porous silicon films were then prepared to be removed from the bulk silicon substrate to produce a porous silicon lift-off film/membrane. In releasing the membrane from the bulk silicon, care needs to be taken to make sure that the porous silicon releases as an intact film. In order to assure that the entire film was undercut by the electropolishing process, the 7 hole-patterned insert was removed and the silicon wafer was placed under an o-ring large enough to provide an etch area that encompassed the entire etched pSi pattern (larger than the 7 hole-patterned insert) . The wafer was etched again in 3:1 HF:Ethanol at $19mA/cm^2$ for 1. This pre-electropolishing, etch-step generates as starting point, that extends lateral beyond the pSi film which allows for complete undercutting across all of the porous silicon films.

After the second etch step, the etch solution was replaced with 1:16,

HF:Ethanol solution, the entire expanded etch area was electropolished slowly at a current of 6 mA/cm^2 for 10-15 minutes. Once electropolished the solution surrounding the films was agitated with a plastic transfer pipette until the films broke free from the substrate. If the films did not freely lift-off with-in 2-3 agitation cycles, the process was repeated with fresh electropolishing solution until the films lifted off.

The porous silicon films were then treated to create an oxide on the surface. Once fabricated the highly reactive silicon hydrides on the surface of the pSi film need to be passivated. To maintain the structural integrity of the lift-off film, only a surface layer of oxide needs to be grown while preserving the underlying silicon structure. Complete oxidation, the complete conversion of all of the Si-Si bonds to Si-O-Si bonds, would place too much stress on the film and cause it to shatter.

The freshly etched films were initially rinsed with 100% ethanol and left to air dry. Once dry, the films were oxidized in air at 200°C in air (oven model no. OV12A, GS Blue M Electric) for two days, to provide a thin thermal oxide. Thermal oxidation alone is not enough to completely oxidize these films to protect them against solutions buffered physiological pH. To protect the films with a level of oxidation that would normal require long term (month long time scales) exposure to create, an additional workup using a hyper-aqueous oxidation technique was applied. After thermal oxidation the pSi films were submersed in a borax (alkaline buffer) solution 5mg/mL in water for two days, to create a more complete oxide layer. Applying a thermally oxidized layer prior to the hyper-aqueous oxidation step, guards against the growth of a thick oxidized layer throughout the film, which could destabilize the membrane. This hyper-aqueous oxidation step is important to quickly and completely oxidize a thin layer of silicon while avoiding complete dissolution of the film and preserving the

underlying silicon structure. After hyper-aqueous oxidation treatment the films were rinsed three times with DI H_2O and twice with 100% ethanol and left to dry.

3.6.1.3 Treatment of pSi with protein suspensions

Protein suspensions of BSA and Casein where prepared by suspending/dissolving the target protein in 0.15M Tris buffer at pH 7.4 (preserved with 0.1% sodium azide) at a concentration of 2mg/mL. Once mixed the solutions were dispensed at 20uL on oxidized porous silicon substrates sitting on #4 whatman filters, yielding 40ug of protein on each surface. The substrates were then left to dry. The capillary actions of the pSi and the whatman filter to wicked away excess fluid. Once dry, the pSi films were placed in gelatin filled double diffusion tubes.

3.6.1.4 *Loading of the hydrogel into the reaction tubes*

To prepare tubes for filling, 3mL polystyrene serological pipette sections (cut with a hotwire cutter) were capped with a polyethlyne disc and sealed with parafilm. For experiments without either proteins or pSi, the 3mL tubes were simply filled with 10% w/v gelatin in Tris buffer pH 7.4 and left to set. For experiments using proteins, the protein solutions were first mixed 1:1 with 20 w/v % gelatin in Tris buffer pH 7.4, and then diluted to the desired concentration with 10 w/v % gelatin in Tris buffer pH 7.4. The 3 mL pipette tubes were then filled to the 1.45mL mark (2.9cm, measured from the bottom) with 10 w/v % gelatin in Tris buffer pH 7.4, and left to set. Then 100uL of the protein in a 10 w.v % gelatin mixture was added on top of the first layer and left to set. Finally the last layer of 10% w/v gelatin in Tris buffer pH 7.4, was placed in the tube to fill the remaining balance, and left to set.

For experiments using the pSi substrates, the pipette tubes were filled with 10

w/v % gelatin in Tris buffer pH 7.4 until the top edge of the meniscus along the edge of the tube reached the 1.5 mL (or halfway) mark and then left to set. The remaining volume of the tube was then filled with 0.15M Tris buffer pH 7.4. Using air tweezers, the porous silicon discs were placed on top of the Tris buffer solution. Capillary action causes the porous membrane to fill with solution and a gentle nudging with the plastic transfer pipette breaks the surface tension of the solution causing the pSi to gentle float to the bottom of the solution alighting on top of the gel/solution interface.

The Tris buffer solution was then removed with a transfer pipette and replaced with 10 w/v % gelatin in Tris buffer pH 7.4. The molten gelatin solution was gently and repeatedly agitated with a transfer pipette and then removed to help dilute/remove any excess Tris buffer solution left behind. A fresh layer of 10 w/v % gelatin in Tris buffer pH 7.4 was then placed in the tube to fill the balance of volume between the pSi and the top of the tube.

For experiments with both substrates and proteins/peptides, a layer of gelatin was poured first, followed by the placement of pSi, followed by a 100ul layer of protein/peptide in 10% gelatin, followed by a final layer of 10% gelatin.

3.6.1.5 Pre-hydration:

Once the gels were set, all tubes were uncapped and place in 15 mL centrifuge tubes filled with 6 mL of Tris buffer at pH 7.4 and left to set at 25°C for 2 days.

3.6.1.6 Calcium and Phosphate Solutions for the DDS:

2 liter solutions of calcium and phosphate were prepared in 0.15 M Tris buffer, with 39.7g Tris HCl (Sigma), 5.82 g Tris Base (Sigma), 0.4g sodium azide (Fisher), and either 29.4g (calcium chloride dihydrate (Sigma-Aldrich)) or 26.4g (Ammonium

phosphate dibasic (Sigma-Aldrich)) to make 100mM solutions in Tris bluffer pH 7.4. Solutions in the DDS reservoirs were changed at 2.5 days to preserve the semi-infinite condition.

3.6.1.7 System placement:

Tubes were placed on the DDS and in cases were there was more than one type of additive in the gel (relative to the other tubes) the tubes were set alternating the tubes with condition made in triplicate.

3.6.1.8 Removal of tubes from the system:

When tubes were removed from the double diffusion system they were placed in the refrigerator for 30-45min to firm up the gels for handling.

3.6.1.9 Concentration analysis:

The gels were sectioned in to 9 nine equal slices and the center section (0.333 mL) containing the mineral and target gel was isolated, and soaked/washed for 45 min in 10 ml of 0.15 M NH_4OH, changing the solution every fifteen minutes. The gels were then pat dry and hydrolyzed in 10 mL of 0.8 M HNO_3 at 70°C for 2 days. Once hydrolyzed the solutions were then run through an axially viewed ICP trace analyzer emission spectrometer (model ICAP 61E trace analyzer, Thermo Electron, Waltham Ma). The transfer optics had been replaced with a short depth of field transfer optics to reduce matrix effects.

3.6.1.10 Calcium and Phosphate Solutions for Solution based experiments

Solutions of calcium and phosphate were prepared in 0.15M Tris buffer at concentrations of 10mM and 5 mM calcium (calcium chloride dehydrate (Sigma-

Aldrich)) in 500 mL, and 6 mM and 3mM phosphate (Ammonium phosphate dibasic (Sigma-Aldrich)) each in 500mL of solution.

3.6.1.11 Placement of pSi into the solution based experiments:

Porous silicon substrates were each placed in 20 mL vials (72 total), and then filled with 5 ml of calcium solution (via a syringe) followed by 5 mL of phosphate solution (via a syringe). Half of the vials were placed ion the bench top at laboratory temperature (20 °C), the other half were set in an incubator (37 °C). One-third of the vials were removed, after 3, 5, and 7 days. Once removed, the solutions were decanted, and the substrates were washed three times 0.15 M NH_4OH, and then rinsed twice with acetone.

3.6.1.12 Analysis of crystal morphology:

3.6.1.12.1 FE-SEM of solution base experiments:

Once dry, the substrates were mounted to aluminum SEM stubs with carbon pasted. The substrates were not coated before being examined with a Leica 1550 FE-SEM. Substrates were examined at 1 kV with an aperture of 7.5 μm.

3.6.1.12.2 GADDs of solution base experiments:

Substrates already mounted on SEM stubs. Where placed on a GADDs (Bruker Instruments) with the detector set a Theta = 10, and Omega = 5. Samples were examined for 100-300 seconds.

3.6.1.12.3 Preparation of samples from the hydrogel:

The gels were simply cut with a razor blade to excise both sections of just mineral and sections of pSi and mineral. One isolated, each gel section was place in 1.5 ml of 0.15 M NH_4OH, and heated in a hot water bath at 50°C for 5 min. The solutions were then agitated on a vortex and centrifuged at 16,000 G for 5 min. The supernatants were then decanted-off the resulting pellets. The pellets were then resuspend in 1.5 mL of 0.15 M NH_4OH and the heating and centrifuging steps were repeated twice more. Once washed, the pellets were rinse with acetone twice to remove the water and left to dry in air. The resulting powders were then analyzed by pXRD (Scintag Theta-Theta Xray Diffractometer), ATR-FTIR (Bruker Optics - Vertex80v) and FE-SEM (LEO 1550). The pSi substrates were analyzed only with FE-SEM (LEO 1550). To examine the crystal grown on the oxidized pSi control substrates from the gel the cleaned, mineralized substrate was sonicated in acetone for 10 minutes in a Bronsan model sonicator and 10 μL of the supernatant was dispensed onto a carbon coated copper TEM grid (Electron Microscopy Sciences) and left to dry, TEM samples were then examine in FEI T12 TWIN TEM.

3.6.1.12.4 pXRD

For pXRD, the washed and centrifuged mineral samples were powdered with a pestle and mortar and place on zero a background hold (single crystal quartz cut-off-axis) and scanned (in an Scintag Theta-Theta Xray Diffractometer) between $2\theta = 2°$ to 40°. The size of the crystallites along the *c*-axis was determined using Scherrer analysis of the $2\theta \approx 26°$, and by comparing the sample spectra to a corundum standard to correct for any instrument broadening. Two different methods of background correction were used (Spline-fit and Box-fit (with a 1.5 degree width)) to account for

the poor quality of spectra obtained.

3.6.1.12.5 ATR-FTIR

For ATR-FTIR, a background was taken of the chamber under vacuum before the powdered samples (from XRD) were placed on the diamond ATR stage and then scanned (in a Bruker Optics - Vertex80v, vacuum FTIR) at a resolution of 4 cm^{-1} with 32 scans, using a liquid nitrogen cooled detector. The SF of the phosphate *v4* peak was calculated using the established technique[94, 95] as the sum of the ~562 cm^{-1} and ~600 cm^{-1} peak heights divided by the height of the minimum between this doublet.

3.6.1.12.6 FE-SEM

For FE-SEM, after extraction of the mineral from the hydrogel, but prior to the final centrifuging and decanting of the acetone wash solution the mineral suspension in acetone was pipetted on to a silicon substrate and left to dry. The samples of pSi were glue directly to an SEM stub using carbon adhesive. The samples were place in the FE-SEM without coating and examined at 1 kV and an aperture setting of 7.5 μm.

CHAPTER 4

4 The Effects of Inhibitor Gradients on the Formation of Mineral in a Hydrogel-Based Double Diffusion System

4.1 Introduction

Physical gradients of mineral density and mechanical properties occur in many mineralized tissues, including the growth plate, the ligament-bone interface, and the dentin-enamel junction in teeth. [98, 137-139] The osteochondral interface is an example of an interface found in Nature that demonstrates a transition over a small distance (~100 μm) from a stiff tissue with high mineral content (bone) to a more compliant tissue with a low mineral content (cartilage). [140] The transition zone between these dissimilar tissues has mechanical properties that bridge them.[137, 141-143] In the field of biomineralization there are a number of theories as to how such an interface is formed.[144-146] The most prominent and accepted idea is that this mineralized interface forms as a result of a competition between mineralization promoters and mineralization inhibitors.

There is a growing need to understand the formation mechanisms of these interfaces to apply to engineered tissues. Tissue engineered constructs for a variety of systems (e.g., osteochondral, bone-tendon, bone-ligament, teeth) all require the development of physical gradients within the synthetic tissue to prevent delamination of the stiffer materials from the more compliant materials.[137, 141-143] The current generation of biomaterials are usually homogenous materials and one of the biggest challenges in the area of tissue engineering is the successful integration of the cartilage

constructs with the subchondral bone.[141-143] A few of these tissue engineering-based strategies for osteochondral defect repair have relied on the placement of chondrocytes in composite scaffolds that contain large Pi gradients, coaxing biology into engineering the complex biomaterial.[147, 148] The formation mechanisms of mineralized interfaces can be investigated through the implementation of an *in vitro* model. A proper *in vitro* model for this task not only provides a platform to systematically test theories and ideas in biomineralization, but also serves as means through which engineering strategies can be implemented and explored. For our *in vitro* model, we have chosen a hydrogel-based circulating semi-infinite reservoir dynamic double diffusion system (DDS) (see Chap. 1). This DDS affords us control over a strategically targeted site of mineralization, while providing a hydrogel microenvironment similar to the ECM. The reproducible and predictable location for mineralization is programmed into the design of this DDS, and our ability to change that programming gives us the freedom to engineer the location and the shape of the resulting mineralized precipitation band. In the current work, we have established spatial gradients of a mineralization inhibitor, pyrophosphate, in cylinders of gelatin gel. This chemical gradient, in turn, is converted into a physical gradient of mineral density within the gels.

4.2 Background: Mineral Gradients in Biology

Gradients of inhibitors of mineralization may play a role in creating the gradients of mineralization at the osteochondral interface. The release, by cells, of matrix vesicles containing the mineralization inhibitor pyrophosphate (PPi), and the enzyme alkaline phosphatase (ALP), some distance from the osteochondral interface

suggests that the location of the mineralized tidemark is defined in part, by chemical gradients.[144, 146, 149] The mineralization inhibitor PPi, a phosphate dimmer, can be converted to inorganic phosphate (Pi) via enzyme assisted hydrolysis using ALP**.** This balance of PPi production and Pi conversion performed by chondrocyctes may be responsible, in part, for the mineral gradient seen at the osteochondral interface. A disruption of this balance in cartilage can lead to either over mineralization of this region or the promotion of the pathological mineral calcium pyrophosphate dihydrate, which is associated with pseudogout.[146, 149] Creating analogous gradients found in this region, with respect to composition and rate of change, in an acellular *in vitro* model is difficult. The control/study of this region using chemical gradients would help to determine (*in vitro*) the right balance between these two outcomes.

4.3 Experimental Design

Precipitation of HA within a 6 cm hydrogel using reservoirs of 100 mM Calcium and 100 mM Phosphate in the DDS occurs within a specified region within the gel (Fig. 4.1). The region of precipitation is dictated by both the concentration and ratio of ions to each other, inside the gel. The values of these ion concentrations and ratios are dependent on the diffusivities of these ions through the hydrogel. The visible band of precipitation seen in the diffusion tube after 3 days exists in this specified region, with the edges of the band defining the borders of this region. Outside the area occupied by the visible precipitation band, mineral formation does not occur. By carefully controlling when, where, and eventually, the concentration of inhibitor delivered to this location, the size and shape of the allowable region for precipitation can also be controlled.

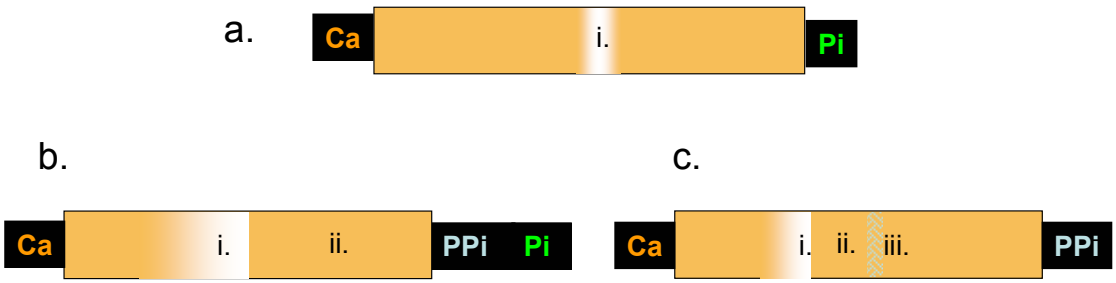

Figure 4.1 Schematics of the experimental design (a.) the classic HA formation experiment with serving as the control with reservoirs of calcium and phosphate forming a band of HA (i), the (b.) global regulation of (ii) inhibitor gradients using reservoirs and (c.) the regulation of inhibitor gradients using enzymes (iii).

We have introduced gradients of PPi into a hydrogel-based DDS [17] to modify the nucleation and growth of HA crystals. The restrictive nature of the hydrogel matrix provides the first step in facilitating the regulation of the chemical gradients by limiting mass transport to a diffusion-only process. With diffusion as the principle regulator of ion delivery the resulting chemical gradient is well-defined, and evolves predictably over time. We hypothesize that these chemical gradients can be converted into physical gradients of mineral content, which in turn could result in gradients of mechanical properties, similar to the properties found in natural tissues. In this work we determined the effect of PPi gradients on the location, density, size, and shape of the band of HA formed in an ECM-like hydrogel.

In this study two approaches were used to create inhibitor gradients. A system of global regulation is achieved using a reservoir filled with a mixture of Pi (promoter) and PPi (an inhibitor), which is diffused through a gelatin hydrogel in each sample tube, and towards an opposing reservoir of calcium attached to the other end of the sample tube (Fig 4.1). A system of local regulation is achieved by using a reservoir of 100% PPi, and diffusing the inhibitor through the gelatin hydrogel, which contains a band of ALP. The strategically placed band of ALP converts the diffusing PPi into Pi,

acting as an inhibitor sink and a Pi source. By varying the concentrations of immobilized enzymes we effectively modulate a gradient of inhibitors and demonstrate the ability to control the formation of the mineral/hydrogel interface. The resulting mineral band was observed by visual inspection, the phase identified via pXRD, the habit examined by FE-SEM, the chemical composition determined by FTIR-ATR, and the mineral density gradient quantified by micro-CT.

4.4 Results and Discussion

4.4.1 Forms of calcium pyrophosphate

Calcium pyrophosphate has a number of polymorphs and pseudo-polymorphs (hydrates). The pseudopolymorph most commonly found pathologically in biological systems is calcium pyrophosphate dihydrate (CPPD), as a mixture of two different polymporphs, triclinic (t-CPPD) and monoclinic (m-CPPD). Synthetically there are dozens of forms of calcium pyrophosphate[51, 150] and of those forms, only a few are pure calcium and pyrophosphate (with water), the rest have various monovalent and divalent ion substitutions/additions. Of these pure calcium pyrophosphate forms there are amorphous, triclinc, monoclinic, orthorhombic, and hexagonal polymorphs. Of these polymorphic crystal forms there are two pseudopolymorphs, the dihydrates and tetrahydrates. The triclinic form is exclusively a dihydrated, but the monoclinic form can be either dihydrate or tetrahydrate. The orthorhombic (o-CPPT) form is exclusively a tetrahydrate (unless heated to the anhydrous form) but can convert to either the triclinic or monoclinic form and even a hexagonal (h-CPPD)[51] form, which is also a dihydrate. The number and degree of hydration in these hydrate forms can be expanded and the list made more complicated through the addition or

substitution of hydrogen into the formula, but that changes the phase of the pyrophosphate being discussed. Such substitutions can lead to the formation of anhydrous forms, tri-hydrates and even hexa-hydrates. In our investigation we found that the calcium pyrophosphate produced in this gelatin system (as seen by pXRD) is a mixture of triclinic, monoclinic and orthorhombic forms (Fig. 4.2g & 4.2h) and is therefore a mixture of the di- and tetra-hydrate forms, as such we will use the convention of CPPx to indicate the calcium pyrophosphate mineral produced.

4.4.2 Ca/PPi system

In this first iteration of experiments we examine the formation of a calcium pyrophosphate precipitate in a gelatin hydrogel. One reservoir is filled with a solution of calcium ions, and the other reservoir is filled with a solution of pyrophosphate ions. By varying the concentration of ions in each reservoir we can vary the starting ratio of reagents which will then, thereby demonstrating that we can in-turn, vary the location of the precipitation band. In a control experiment (no ALP), using 100mM calcium in one reservoir and 100mM pyrophosphate in the other reservoir, a band of calcium pyrophosphate hydrate (CPPx) forms near the center of the tube (Fig. 4.2b). [9, 53-55] The mineral band appears after 4 days and the exact location of the band is 3 mm from

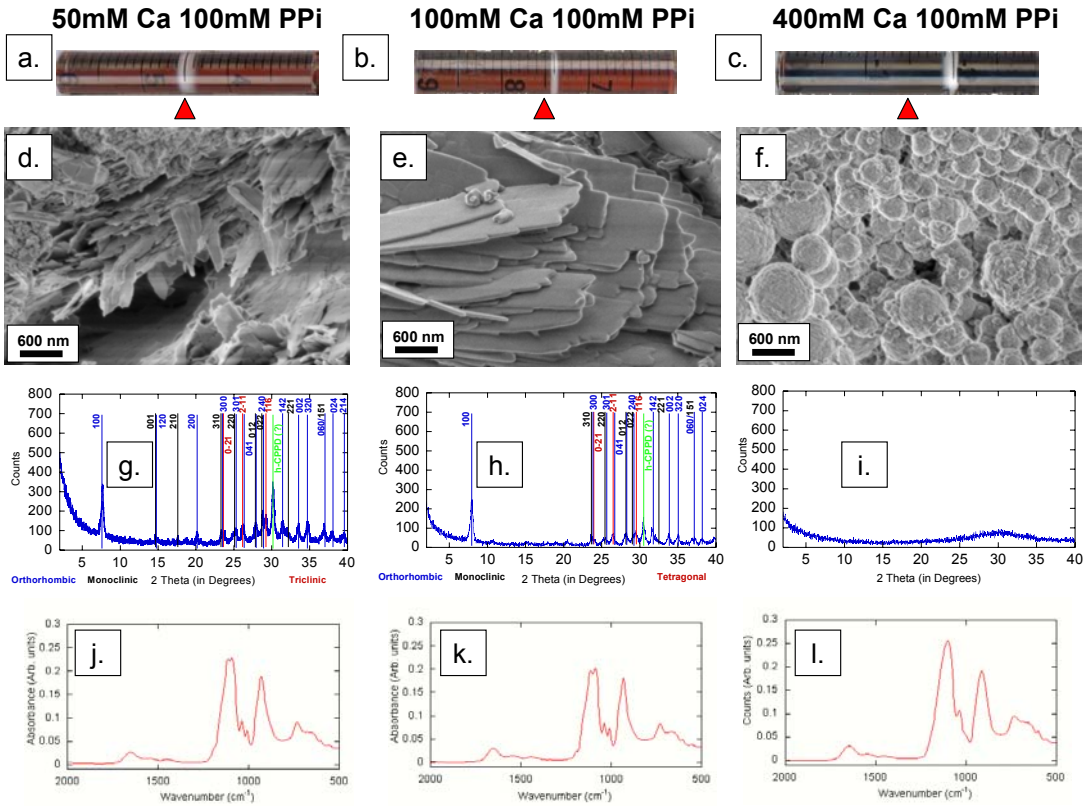

Figure 4.2 The results of changing the concentration of the calcium reservoir presented as (a-c) scanned images (arrows indicate the center of the tube, and nominal location of a HA band when using reservoirs of calcium and pjospjate, (d-f) FE-SEM images, (g-i) pXRD patterns (indexing was made using powder diffraction cards #: 70-0881, 41-0489, 41-0490, 22-0537, 09-0345 and references [51, 150] and (j-l) FTIR-ATR spectra.

the center of the tube, towards the PPi side of the tube (Fig. 4.2b). In comparison, the classic setup of the DDS [17] where a Pi reservoir is used and HA is produced, the mineral band appears at 3 days in the center of the tube (Fig. 4.3a). In the Ca/PPi system, adjusting concentrations in the calcium source reservoir from 100 mM to 50 mM while keeping the PPi reservoir at 100 mM, moves the CPPx band to the center of the tube and increases the width of the band from 1 mm to ~4 mm (Fig. 4.2a). The mineral produced with a 50 mM calcium reservoir and a 100 mM PPi reservoir is still a mixture of the orthorhombic, monoclinic and the triclinic CPPx. When the calcium

reservoir is changed to 400 mM and the PPi reservoir is maintained at 100 mM, the CPPx band moves to a position 9 mm from the center towards the PPi side with a width of ~3 mm (Fig. 4.2c.). Examination of the precipitates with FE-SEM shows a change in crystal morphology as a function of calcium concentration: a spherical morphology lacking facets (at 400 mM Ca) to thin blade like crystals (at 50 mM Ca) (Fig. 4.2d-f). Examining both the FTIR-ATR and pXRD for all three conditions (Fig. 4.2 g-i and j-l, respectively), there is a progression of increasing crystallinity with decreasing calcium concentration (400 mM to 50 mM), indicating that decreases in relative supersaturation within the hydrogel leads to an increase in the crystallinity of the precipitation produce (Fig 4.2j-l). In pXRD, the increase in crystallinity can be seen by an increased prominence of peaks that were either not initially present or were originally close to the level of "noise" in the spectrum. In the FTIR-ATR spectra, as the peaks become sharper and more distinct, the vibrations represented by those spectral peaks are themselves becoming more and more distinct as vibrations become coupled to the crystal lattice.

4.4.3 Ca/PPi/Pi system: Global regulation

Using the CPPx control experiments as a foundation, 100 mM of Pi was added to the source reservoir and the concentration of PPi in the reservoir was varied. This modification introduces an HA promoter into the system and facilitates the creation of a promoter-inhibitor gradient starting from the solution/gel interface. Two conditions were compared to the 100 mM Ca/100 mM PPi control where the concentration of calcium in the Ca source reservoir was kept at 100 mM and the concentrations in the opposing reservoir were: 100 mM Pi : 100 mM PPi, and 100 mM Pi : 25 mM PPi. By

regulating the concentration of ions in the reservoirs, the promoter-inhibitor gradient is dictated by the diffusion of ions from the reservoir through the hydrogel from the gel/solution interface and every tube in the experiment has the same gradient. The condition 1:1 Pi:PPi, presents a precipitation band with a sharp mineral to hydrogel interface starting 3 mm (toward the calcium side) from the center of the diffusion tube and the band extends an additional 3 mm in the direction of the calcium reservoir (Fig. 4.3). The precipitation band, (as determined by pXRD) is HA, and under this condition there is no appearance of the CPPx band at the expected location 3 mm (from the center) towards the Pi:PPi reservoir. Decreasing the concentration of PPi in the source reservoir so that the ratio of Pi:PPi is 4:1, the precipitation band appears closer to the center of the tube, with the mineral/hydrogel interface laying at the center of the tube, and the precipitation band extending 4 mm towards the calcium reservoir. This band (as confirmed by pXRD) is HA and has less of a sharp interface as compared to the 1:1 Pi:PPi condition. Again there is no appearance of the CPPx band at the expected location.

Adjusting the concentration of PPi in the source reservoir changes the driving force for diffusion, this change in driving force affects the rate at which material is delivered to a given location within the gel. The rate of ion delivery dictates how much material is at a given point in the gel at a given time, changes in these ion concentrations have a direct effect on the local supersaturation/ion-product of both CPPx and HA at a given location. The higher the concentration of PPi, the more supersaturated a region becomes with respect to the formation of CPPx, conversely the supersaturation of HA is compromised and calcium becomes sequestered by increased concentrations of PPi. The competition for calcium and the resulting formation of a

mineral product contributes to the relative sharpness of the resulting precipitation band. The higher the inhibitor concentration, the sharper the edge (mineral/gel interface) of the precipitation band. The steepness of the inhibitor gradient is increased by either raising the inhibitor source concentration (as done in the set of experiments) or by shortening the gradient path-length (see Section 4.4.4). The steeper the inhibitor gradient, the sharper the mineral/hydrogel interface.

4.4.4 Ca/PPi/ALP system

As stated earlier, the introduction of ALP into the system creates both a "point sink" for PPi and a "point source" for Pi. When ALP is present in the system, asymmetric bands of HA crystals form within the gel. The side of the band closest to the ALP band is sharp, while the far side has a more gradual transition to mineral-free gel similar to the globally regulated system (Fig. 4.3). We interpret this result to mean that the excess PPi, which was not hydrolyzed by the immobilized enzymes, acts as an inhibitor of apatite growth, creating the sharp interface closest to the beads. Changes in the sharpness of the mineral interface can be made by changing the concentration of ALP.

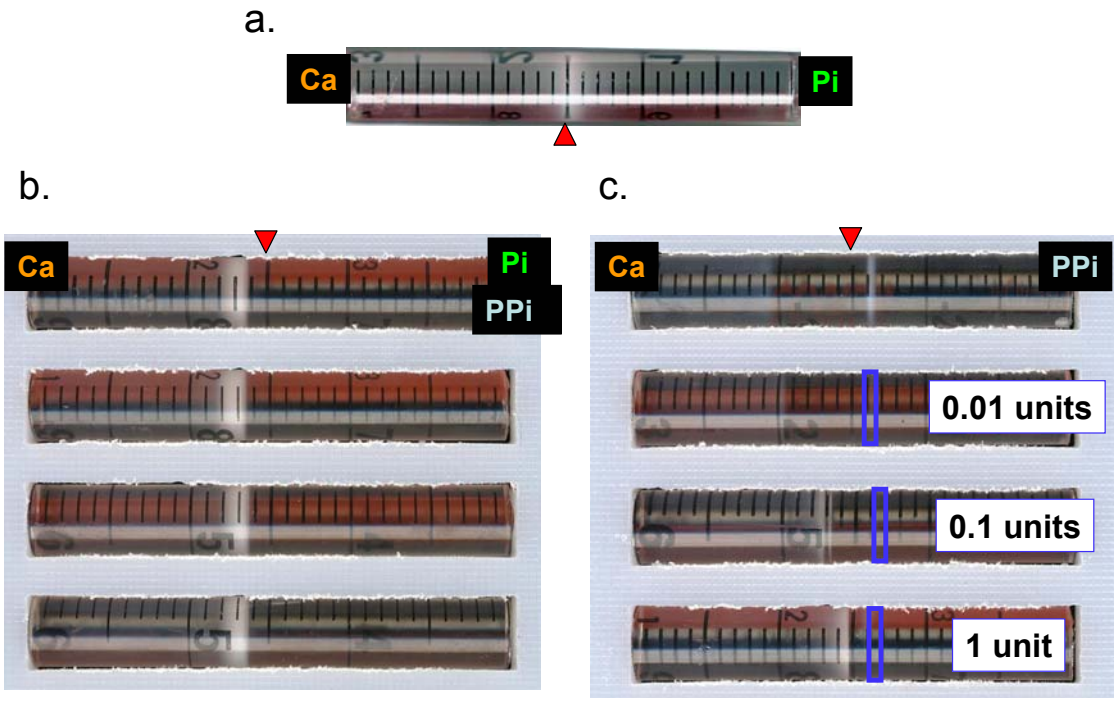

Figure 4.3 Actual scans of completed experiments (a.) the calcium and phosphate based control experiment used to make HA, the (b.) global regulation of inhibitor gradients using reservoirs 100mM calcium, 100mM phosphate with 100 mM pyrophosphate and (c.) the regulation of inhibitor gradients using enzymes (ALP on agarose beads, at concentrations of 0.01 units, 0.1 units and 1 unit).

4.4.4.1 ALP on beads

ALP immobilized on agarose beads were mixed into 10 w/v % gelatin in Tris buffer and then placed at the location where the CPPx band is known to form. The ion reservoirs were kept at Ca = 100 mM and PPi = 100 mM, and the bands of ALP were prepared at concentrations of: 0.001, 0.01, 0.1, 1, 2.5, 5, 10, and 25 units. One unit of ALP on agarose beads has the activity at pH 9.4 such that it will hydrolyze 1 milli-mole of p-nitrophenyl phosphate per minute.

As the concentration of ALP is increased from 0 units to 1 unit the appearance of the CPPx band begins to diminish (Fig. 4.3c). With ALP concentrations higher than 0.1 unit, a HA band begins to appear. As the HA band forms, the edge of the band

facing both the PPi reservoir and the ALP band, appears truncated with a sharp mineral/hydrogel interface on that side. As ALP concentration increases the band shifts closer to the center of the tube and the sharp mineral/hydrogel interface becomes increasingly more diffuse. Both FE-SEM and XRD show that the HA formed in the presence of lower ALP concentrations (higher PPi levels) has a lower crystallinity and poorly defined facets (Fig. 4.4 and 4.5). Examination of the crystal morphologies (by SEM, Fig. 4.5) and sizes (by Scherrer analysis of XRD peak widths, Table 1) show that in the presence of low ALP concentrations (therefore high PPi concentrations), the apatite crystals were smaller and less crystalline as compared to those crystals formed at high ALP concentrations. Examining the FTIR-ATR (Fig. 4.6) spectra we find that the mineral precipitation band at the condition of 0.1 unit of ALP has an FTIR signature that is a convolution of both CPPx and HA (HA: characteristic symmetric (*v1*) and asymmetric (*v 3*) P-O stretching modes 900-1200 cm^{-1}, primarily peaks at 1020, 1050, and 1110 cm^{-1}; CPPx: characteristic P-O-P stretching modes, 1037-1147cm^{-1}). This FTIR data suggests that the mineral is contaminated by the presence PPi in the precipitate. The pXRD of this precipitate (Fig. 4.5) is inconclusive, examination of the spectrum in a zoomed-in window between 2-theta = 22-35 degrees suggests that the phase may be HA, but not convincingly. As the concentration of ALP is increased to 1 unit and the relative intensity of the pXRD peaks from mineral precipitate also increases, the FTIR spectra shows the distinctive signature of HA, indicating that contamination by PPi goes away (Fig 4.6). This data demonstrates that not only does the inhibitor dictate the location of the mineral band, it also has an effect on the relative crystallinity and chemical composition of the band.

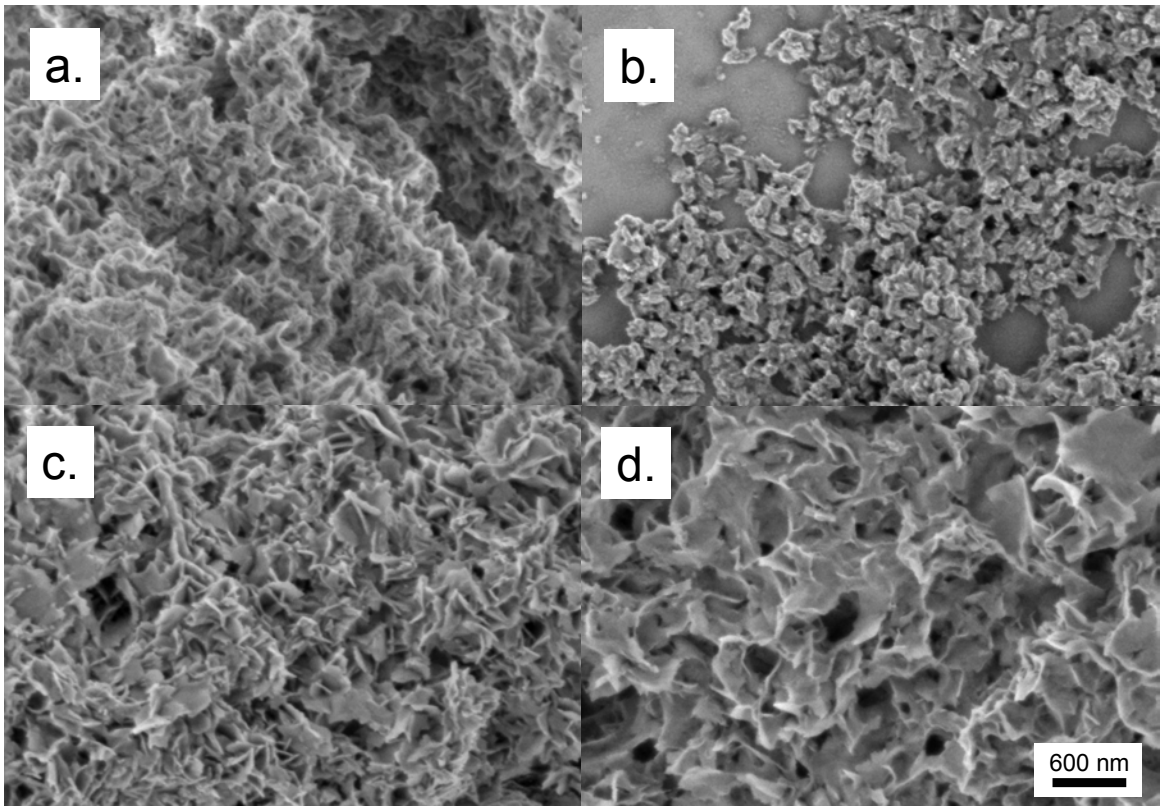

Figure 4.4 FE-SEM images of middle mineral precipitation band using: (a.) 0.1 units of ALP on beads, (b.) 0.1 units of ALP as powder, (c.) 1 unit of ALP on beads and (d.) 1 unit of ALP as powder.

All three of the techniques used to characterized the mineral precipitates in these gels are based on average sampling and do not yield precision with regards to how the mineral gradient changes with location. The amount of precipitate in these gels is so small per cross-sectional area that using Raman microscopy [151] or light microscope histology, [140] on sections of these mineralized gelatin samples is not practical. To properly examine the quality of the gradient we examined the mineral precipitate using microCT of unmodified gelatin cylinders to produce a density map across the sample. All three of the techniques used to characterized the mineral precipitates in these gels are based on average sampling and do not yield precision with regards to how the mineral gradient changes with location. The amount of

precipitate in these gels is so small per cross-sectional area that using Raman microscopy [151] or light microscope histology, [140] on sections of these mineralized gelatin samples is not practical. To properly examine the quality of the gradient we examined the mineral precipitate using microCT of unmodified gelatin cylinders to produce a density map across the sample.

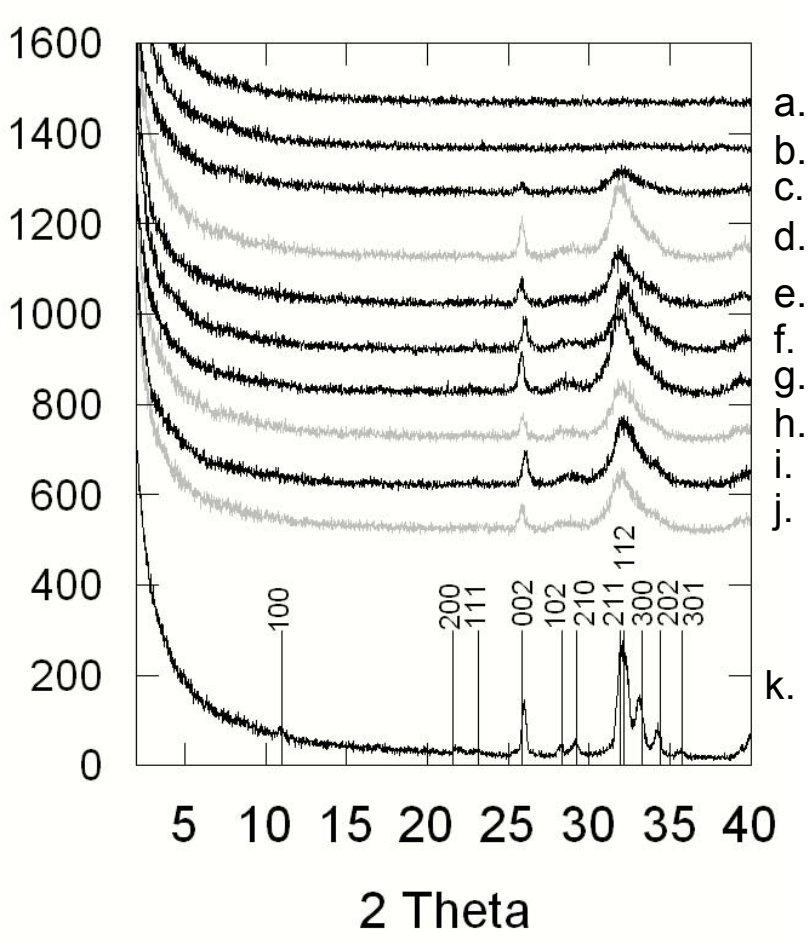

Figure 4.5 XRD plots of the middle precipitation band taken from experiments using both ALP on beads (a-c, e-g, i) and ALP as a powder (d, h, j) as compared to a (k.) hydrothermally prepared HA standard. a. = 0.01 units, b. = 0.1 units, c.& d. = 1 unit, e. = 2.5 units, f. = 5 units, g. & h. = 10 units, i. = 25 units, j. = 100 units.

Table 4-1: Tabulation of the number and the width of the precipitation bands as determined by both optical and microCT scans

Conditions		No. of Bands by sight	No. of Bands by µCT	Width of Bands by µCT (mm)	
Global Regulation	**Local Regulation**			**Ca side**	**Pi Side**
100 Ca to 100 Pi	N/A	1	1	9460	--
50 Ca to 100 PPi	N/A	1	N/A	N/A	N/A
100 Ca to 100 PPi	N/A	1	N/A	N/A	N/A
400 Ca to 100 PPi	N/A	1	N/A	N/A	N/A
100 Ca to 100 PPi 100 Pi	N/A	1	N/A	N/A	N/A
100 Ca to 25 PPi 100 Pi	N/A	1	1	4.00	--
N/A	0.001 Unit ALP Beads	1	1	--	3.94
N/A	0.01 Unit ALP Beads	1	1	--	4.50
N/A	0.1 Unit ALP Beads	2	1	--	4.00
N/A	1 Unit ALP Beads	2	2	2.00	4.10
N/A	2.5 Units ALP Beads	1	1	2.87	1.24
N/A	5 Units ALP Beads	1	1	5.11	1.95
N/A	10 Units ALP Beads	1	1	6.69	--
N/A	25 Units ALP Beads	1	1	10.10	--
N/A	0.1 Units ALP Powder	2	1	--	5.12
N/A	0.25 Units ALP Powder	2	1	--	3.85
N/A	0.5 Units ALP Powder	2	1	--	2.98
N/A	0.75 Units ALP Powder	2	1	--	4.10
N/A	1 Unit ALP Powder	2	2	3.39	2.15
N/A	10 Units ALP Powder	2	1	8.60	--
N/A	100 Units ALP Powder	2	N/A (gel fell apart)	N/A	N/A

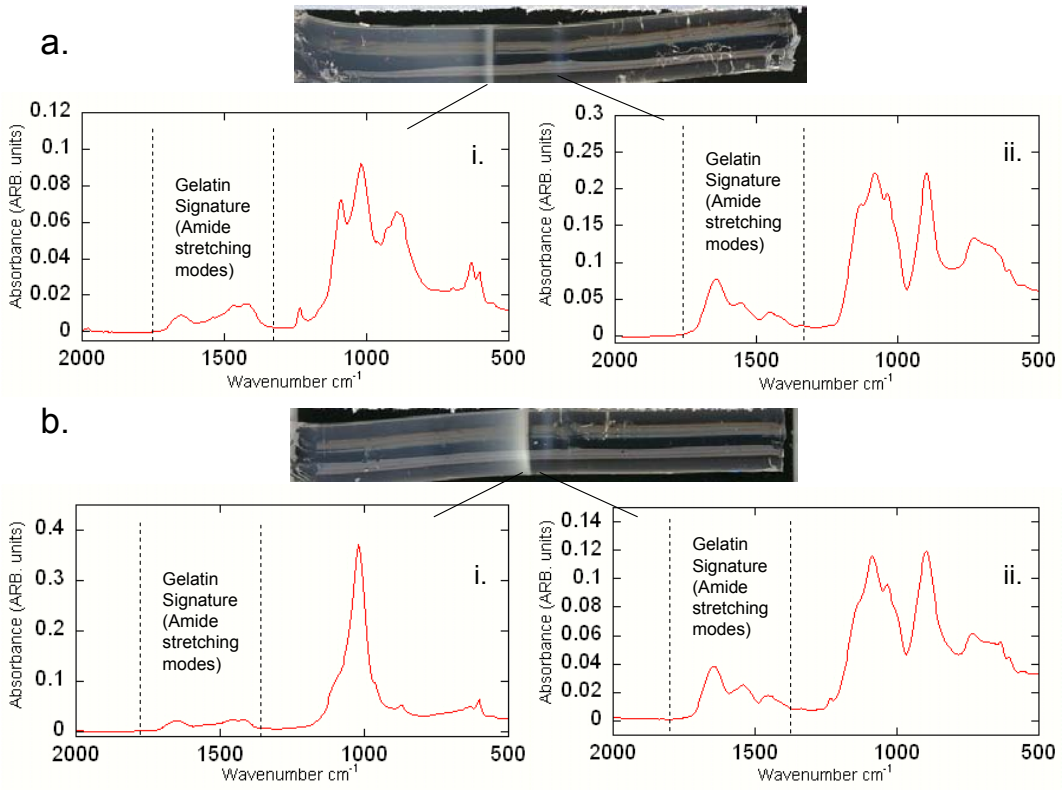

Figure 4.6 Scanned images and FTIR-ATR spectra of precipitation bands formed using (a.) 0.1 units of ALP on beads and (b.) 1 unit of ALP on beads. FTIR-ATR spectra of (i.) the middle band shows that the mineral band created under 0.1 ALP is contaminated with some PPi, and that this contamination is removed as the ALP is increased to 1 unit. The FTIR-ATR spectra of (ii.) the CPPx band confirm that the mineral is CPPx but poorly crystalline (the peaks are not a sharp or well defined as they are for the more crystalline samples).

Examination by microCT confirms that the condition required to promote the formation of a second band composed of HA is 1 unit of ALP, loaded into the enzyme band. As seen in Fig. 4.7, optically, two bands can be seen when using either 0.1 units or 1 unit of ALP, but when measuring the relative mineral density of the samples this appears to not be the case. Two bands can be clearly seen in both the microCT density image and the density line scan when examining tubes using 1 unit of ALP, but not when using 0.1 units of ALP. HA can not be identified in the secondary band found using 0.1units of ALP and the microCT can not register a change in density within that

region above the baseline of the gel. With both the FTIR and the XRD confirming that the center-band is HA (when using 1 unit of ALP), and the miroCT verifying that a relatively dense mineral band is formed when using 1 unit of ALP; we can conclude that 1 unit of ALP

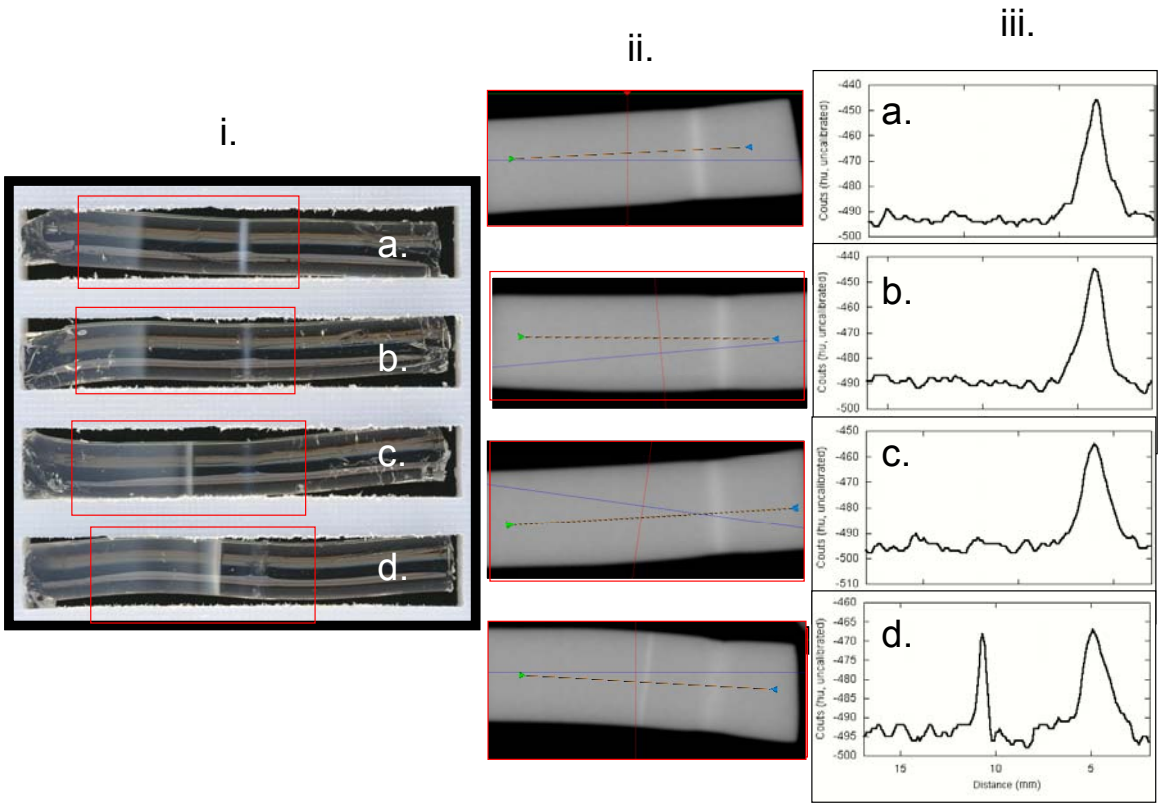

Figure 4.7 Examining the precipitation bands formed using (a.) 0.001 units of ALP on beads, (b.) 0.01 units of ALP on beads, (c.) 0.1 units of ALP on beads, and (d.) 1 unit of ALP on beads. The data is presented as (i.) scanned images, (ii.) micro CT images, and (iii.) line scans of the density gradients as measured by microCT. The data shows that despite the fact that two precipitation band can be seen in the (i.) scanned I, mages of using (c & d) 0.1 units of ALP and 1 unit of ALP, the (ii. & iii.) microCT data shows two bands in only the tube using (d) 1 unit of ALP

is the minimum concentration of ALP required to form the HA band. For the 1 unit of ALP condition, the steepness of the HA band's mineral density was measured (via microCT) and Fig. 4.8 shows that the gradient in the mineral density from the center

of the HA band to the gel is 500 microns.

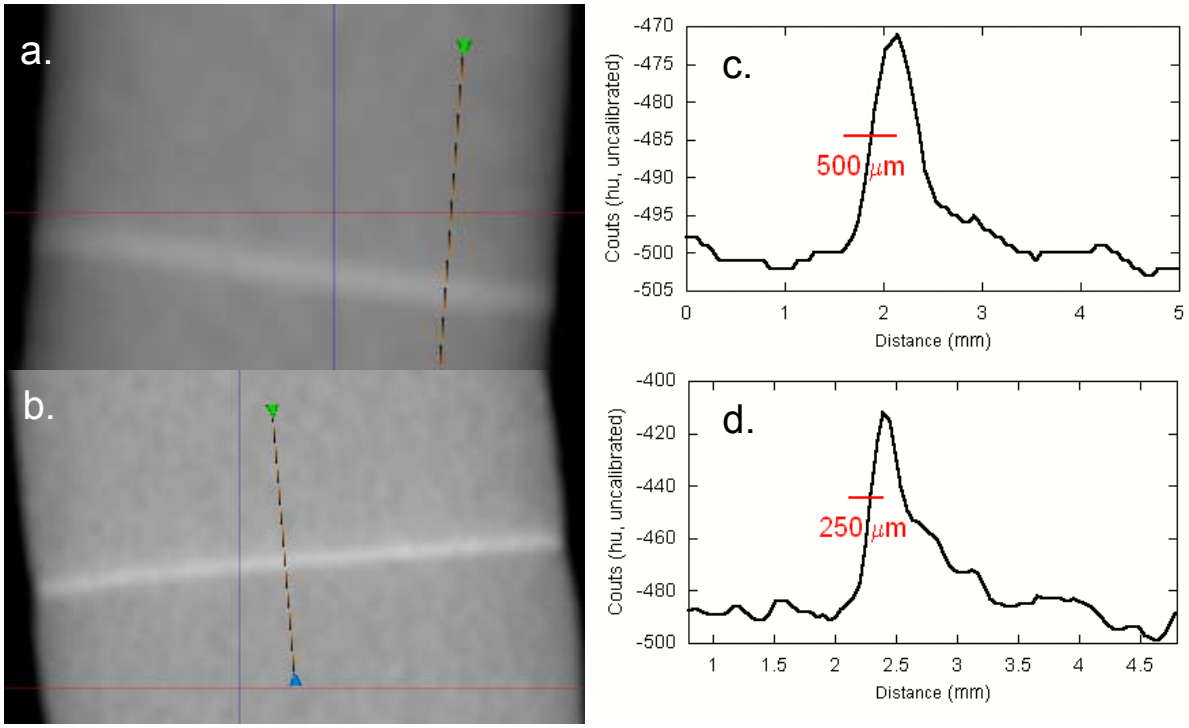

Figure 4.8 MicroCT images (a & b) and line scans (c & d) of the density across samples using (a & c) 1.0 unit ALP on beads and (b & d) 1.0 unit ALP as a powder. These line scans show that the mineral gradient as measured by density from the center of the band to the mineral free gel is the smallest (250 μm) for the system using 1.0 ALP as a powder

Using ALP immobilized on agarose beads, high concentrations of enzymes can be placed in the hydrogel (25 units) and this does not compromise the integrity of the gel. The downside of using ALP on beads, is that the distribution of beads within the hydrogel is not homogeneous. Improper/ineffective mixing of the enzyme loaded beads with the gelatin hydrogel can lead to localized aggregation of the beads within the gel. In addition, if a few beads are lost in transferring the beads within gel to the diffusion tubes then the effective concentration of enzymes in the ALP becomes compromised, this issue is particularly relevant for low concentrations of ALP.

4.4.4.2 ALP lyophilized powder

An alternative to ALP on beads is the use of an ALP powder. ALP as a lyophilized powder is dissolved in a solution of Tris buffer and is then mixed 1:1 with 20 w/v % gelatin in Tris buffer. This ALP/gelatin mixture is then placed at the location where the CPPx band was known to form (Ca = 100 mM and PPi = 100mM) at concentrations of: 0.1, 0.25, 0.5, 0.75, 1, 10, and 100 units. One unit of the lyophilized powder of ALP has the activity at pH 9.4 such that it will hydrolyze 1 micro-mole of p-nitrophenyl phosphate per minute. As a free enzyme, ALP has a MW of ~80 kDa and the dimer found in the lyophilized powder has a MW of ~160 kDa (as reported by Sigma-Aldrich), both sizes are well above the ~3 kDa cutoff required for proteins to stay within the gelatin hydrogel and not diffuse away. [17]

The advantages of using ALP powder over using ALP on beads are the increased homogeneity within the gel and the increased accuracy of the concentration. The increased resolution allows for the exploration of concentrations between 0.1 and 1 unit. With the lyophilized ALP in the gel, as was seen in the conditions using ALP on agarose beads, increasing ALP concentration from 0 to 1 units yields a diminishing of the CPPx band, but this destruction of the CPPx band is not gradual. The CPPx band is clearly seen in conditions of 0.1 to 0.75 units of ALP but disappears with 1 unit of ALP. At concentrations higher than 10 units the concentration of free ALP enzyme was so high that the gel integrity was compromised and began to simply fell apart upon handling after the experiment.

With ALP powder mixed into the gel there was a different trend in the crystallinity of the HA precipitation band with an increase in ALP, as compared to the conditions using ALP on beads. With ALP as a powder mixed into the gel there is a

more homogenous distribution of the enzyme, and the probability of ions encountering an enzyme as it diffuses across the ALP boundary is higher than if ALP on beads were used in the hydrogel. For a given activity of ALP, with this increased probability of ions interacting with enzymes less PPi is likely to "escape" and interact with the forming precipitation band. As shown in the FTIR spectra (Fig. 4.9) the resulting diffuse/faint band for conditions of 0.1 to 1 units of ALP is apatitic. This idea of a more homogenous band resulting in less PPi escaping the enzyme band and contaminating the HA precipitate is not obvious by the FE-SEM images of the mineral precipitate

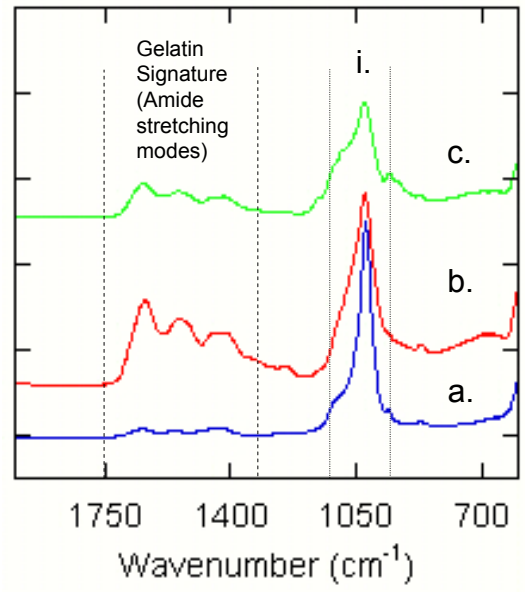

Figure 4.9 FTIR-ATR spectra of the middle precipitation band taken from tubes that used (a.) 1.0 unit of ALP as powder, (b.) 0.75 units of ALP as powder and (c.) 0.1 units of ALP as a powder. All three spectra have apatitic character in the (i.) *v1, v 3* phosphate bands which becomes sharper with the increase in ALP concentration.

using 0.1 units ALP powder versus the mineral precipitate using 0.1 units ALP beads (Fig. 4.4), but is confirmed in comparing the use of 1 unit ALP powder versus 1 unit

ALP on beads. The HA crystal aggregates formed using the ALP powder are more similar to the HA crystal aggregates seen in the HA control experiment (using 100 mM Ca and 100 mM Pi) and not similar to the crystals seen in the precipitate using ALP on beads.

The spatial distribution of enzymes on beads within the gel versus the distribution of free enzyme dispersed within the gel may be a contributing reason why there are similar trends in the HA band size, shape and location between the two systems (Fig 4.10). As stated earlier, 1 unit of ALP on beads has an activity that is 1000–fold greater than the activity of the lyophilized enzymes, yet the same number of units between the two systems produces the same result with respect to the appearance of the HA band. The inhomogeneous distribution of enzyme bound beads may hinder this activity, additionally the activity reported by Sigma-Aldrich for these enzymes is measured at a pH of 9.4, and since these experiments are performed at a pH of 7.4, there may also be an effect of the pH on the activity of both forms of the enzyme.

4.4.4.3 ALP with a mixed Pi:PPi reservoir

In exploration into an even more biologically relevant scenario, the complexity of the system was increased to take into account the presence of Ca, Pi, PPi and ALP, all together. In these experiments, the introduction of Pi is not solely dependent on the conversion of PPi to Pi by ALP. To facilitate this increased level of complexity the local regulation of the inhibitor gradient is combined with the global regulation of a mixed reservoir. In this experiment the reservoirs are kept at 1:1 Pi:PPi with 100 mM concentration of each. The ALP immobilized on acrylic beads (with an activity of at pH 9.4 such that one unit will hydrolyze 1 micro-mole of p-nitrophenyl phosphate per

minute) is again placed at the location of known CPPx formation.

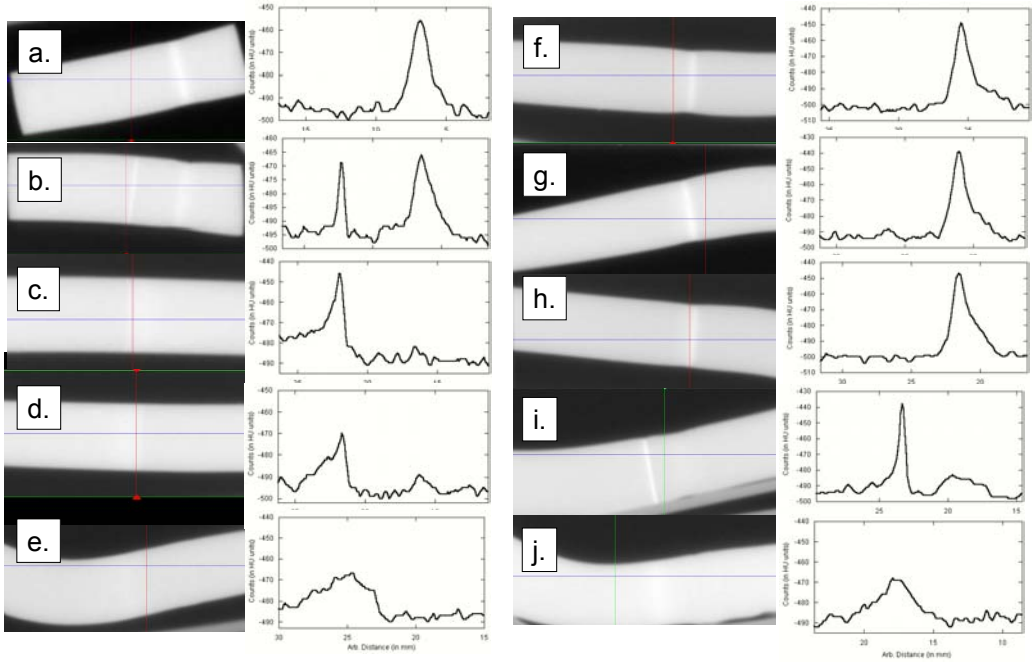

Figure 4.10 MicroCT images and line scans of mineralized bands made with (a-e) ALP immobilized on beads and (f-j) ALP as lyophilized powder. The condition for mineralization where ALP on beads were used, examined at concentrations of (a.) 0.1 units, (b.) 1 unit, (c.) 2.5 units, (d.) 5 units, and (e.) 10 units of ALP. The (a-e) line scans show that at (b.) 1 unit of ALP produces two mineralized bands, while (c.) 2.5 units shows only one band. The condition for mineralization where ALP as a lyophilized powder was used, examined at concentrations of (f.) 0.1 units, (g.) 0.25 units, (h.) 0.75 units, (i.) 1 unit, and (j.) 10 units of ALP. The (f-j) line scans show that at (i.) 1 unit of ALP produces one dominant mineralized band and one faint mineralized band, while (j.) 10 units shows only one broad, low density band.

With no ALP beads, a band of truncated hydroxyapatite band with a sharp mineral/gel interface on the PPi/Pi side forms with a 2 mm offset (from center) on the calcium side of the tube as seen with the global regulation condition of Ca:Pi:PPi 1:1:1. Again a faint band can be seen in the position where CPPx would normally be found. With the inclusion of ALP on beads the HA band moves closer to the center and the sharpness of the mineral/gel interface becomes more diffuse and the change from mineral to empty gel becomes more gradual in appearance

4.5 Conclusion

We have demonstrated, acellularly, that a gradient of inhibitors and control over that gradient can translate into a controlled gradient in mineralization. We have created an experimental model to study and tune the formation of a mineralizing interface via the modulation of acellular components. While the goal of these studies is to test the hypothesis that gradients of mineralization can be created enzymatically in the DDS, in the future, a similar set-up could be used to model disease states such as pseudogout, which results from the precipitation of calcium pyrophosphate dihydrate crystals in articular cartilage.[144-146] In future work, we will create a cell-based version of this system by replacing the phosphatase beads with a band of chondrocytes, which produce PPi, proteoglycans, and other inhibitors of apatite nucleation and growth.

4.6 Material and Methods

A circulating semi-infinite dynamic DDS was setup with 12 double diffusion tubes (6 cm long) in 10 w/v % in 275 Boom Type A Gelatin (Fisher) in Tris buffer pH 7.4, and reservoirs with 100 mM Calcium Chloride Dihydrate (Sigma-Aldrich) and Pyrophosphate Tetrabasic Decahydrate (Sigma) and/or Ammonium Phosphate dibasic (Sigma-Aldrich), at varying concentrations, in Tris buffer pH 7.4. All buffered solutions for both the gels and the reagents were treated with 0.05 w/v % sodium azide (Fisher).

At a location 2 mm towards the PPi side from the center of the tube (the site of normal CPPx precipitation) bands of immobilized ALP enzymes 28.09 units/mL of lyophilized powder (Sigma-Aldrich) or 267 units/mL on agarose beads (Sigma-

Aldrich), were set within the gel at varying concentrations, or 667 units/mL on acrylic beads (Sigma-Aldrich). After 7 days, the resulting mineral band was excised with a razor blade. The excised bands were melted out by placing the band in 1.5 mL of 0.15 M NH_4OH, and heated for 5 min in a 50 °C waterbath, vortexed and centrifuged for 5 min at 16000 G. After centrifugation, the solution was decanted and replaced with 0.15 M NH_4OH, and the process repeated twice more. Once washed, the pellet was then rinsed twice with acetone to remove the water, and then left to dry.

For FE-SEM, the pellet was suspended in acetone and deposited onto a silicon substrate. For pXRD, the pellet was powdered with a pestle and mortar before being placed on a zero background holder (a slide of single crystal quartz, cut off-axis). For FTIR-ATR the powdered samples from pXRD were placed on an ATR stage.
For microCT, the gels were removed from their tubes by cracking the polystyrene plastic with pliers. Once the tubes were cracked the hard plastic was chipped or peeled away and the gels were place in 10 mL of 0.15 M NH_4OH and placed on a rocker table for 45 minutes changing the solution every 15 minutes. The resulting ion free gels were then patted dry and set in dry centrifuge tubes and remained in the tubes and were scanned either the same day or within 12 hours. Imaging studies were performed at Cornell Imaging (Cornell University, Ithaca, NY). Centrifuge tubes containing the hydrogel samples were transferred to the micro-CT imaging system (GE eXplore CT120, GE Healthcare). Volumetric imaging was performed by digitizing 720 projections over 360° (0.5°/step), and averaging two projections per angle, resulting in 50 μm isometric spatial resolution. Image stacks were then processed and reconstructed into 3D datasets using a modified Feldkamp algorithm (GE internal reconstruction software). The field of view for the data acquisition was 75 × 75 × 45

mm. Post-processing, visualization, and image quantification was then performed using Microview (GE healthcare) and Osirix (Osirix).

REFERENCES

1. Veis, A., *Biomineralization. From Nature to Application*. Metal Ions in Life Sciences, ed. A. Sigel, H. Sigel, and R.K.O. Sigel. Vol. 4. 2008, West Sussex: John Wiley & Sons Ltd. 671.
2. Tomson, M.B. and G.H. Nancollas, *Mineralization Kinetics - Constant Composition* Science, 1978. **200**(4345): p. 1059-1060.
3. Koutsoukos, P., et al., *Crystallization of calcium phosphates - constant composition study* Journal of the American Chemical Society, 1980. **102**(5): p. 1553-1557.
4. Boskey, A.L. and R. Roy, *Cell Culture Systems for Studies of Bone and Tooth Mineralization.* Chemical Reviews, 2008. **108**(11): p. 4716-4733.
5. Hunter, G.K., et al., *Inhibition of hydroxyapatite formation in collagen gels by chondrotin sulfate.* Biochem. J., 1985. **228**: p. 463-469.
6. Hunter, G.K., S.C. Nyburg, and K. Pritzker, *Hydroxyapatite Formaton in Collage, Gelatin and Agarose Gels.* Collagen and Related Research, 1986. **6**(3): p. 229-238.
7. Silverman, L. and A.L. Boskey, *Diffusion systems for evaluation of biomineralization.* Calcified Tissue International, 2004. **75**(6): p. 494-501.
8. Henisch, H.K., *Crystal growth in gels*. 1970, University Park: Pennsylvania State University Press.
9. Mandel, G.S., et al., *Calcium pyrophosphate crystal deposition - a kinetic-study using a type-I collagen gel model.* Scanning Microscopy, 1990. **4**(1): p. 175-180.
10. Iijima, M., et al., *Elongated growth of octacalcium phosphate crystals in recombinant amelogenin gels under controlled ionic flow.* Journal of dental research, 2002. **81**(1): p. 69-73.
11. Iijima, M., et al., *Crystal growth of octacalcium phosphate in bovine amelogenins and recombinant amelogenin.* Journal of Dental Research, 2000. **79**(5): p. 1248-1248.
12. Boskey, A.L., et al., *Osteopontin-Hydroxyapatite Interactions in-Vitro - Inhibition of Hydroxyapatite Formation and Growth in a Gelatin-Gel.* Bone and Mineral, 1993. **22**(2): p. 147-159.
13. Gericke, A., et al., *Importance of phosphorylation for osteopontin regulation of biomineralization.* Calcified Tissue International, 2005. **77**(1): p. 45-54.
14. Baht, G.S., G.K. Hunter, and H.A. Goldberg, *Bone sialoprotein-collagen interaction promotes hydroxyapatite nucleation.* Matrix Biology, 2008. **27**(7): p. 600-608.
15. J.R.D, A.L.B, and L.A.E, In Preparation.
16. Glimcher, M.J., et al., *Recent studies of bone mineral Is the amorphous calcium-phosphate theory valid.* Journal of Crystal Growth, 1981. **53**(1): p. 100-119.
17. Boskey, A.L., *Hydroxyapatite Formation in a Dynamic Collagen Gel System - Effects of Type-I Collagen, Lipids, and Proteoglycans.* Journal of Physical Chemistry, 1989. **93**(4): p. 1628-1633.
18. Hunter, G.K. and H.A. Goldberg, *Nucleation of Hydroxyapatite by Bone*

Sialoprotein. Proceedings of the National Academy of Sciences of the United States of America, 1993. **90**(18): p. 8562-8565.
19. Iijima, M., et al., *Effects of bovine amelogenins on the crystal morphology of octacalcium phosphate in a model system of tooth enamel formation.* Journal of Crystal Growth, 2001. **222**(3): p. 615-626.
20. Pokric, B. and Z. Pucar, *Precipitation of Calcium Phosphates under Conditions of Double Diffusion in Collagen and Gels of Gelatin and Agar.* Calcified Tissue International, 1979. **27**(2): p. 171-176.
21. Alfrey, A., Gurnee, E. F. and Lloyd, W.G., *Diffusion in glassy polymers.* Journal of Polymer Science Part C: Polymer Symposia, 1966. **12**(1): p. 249-261.
22. Crank, J., *The Mathematics of Diffusion*. 1975: Clarendon Press.
23. Kirkaldy, J.S. and D.J. Young, *Diffusion in the Condensed State*. 1987: The Institute of Metals.
24. Shewmon, P.G., *Diffusion in solids*. 1963, New York, NY [u.a.: McGraw-Hill.
25. Kumar, M.R., et al., *Collagen-Membrane-Induced Calcium Phosphate Electrocrystallization.* Crystal Growth & Design, 2011. **11**(1): p. 26-28.
26. Wada, Y., et al., *Electrophoretic gels of dentin matrix proteins as diffusion media for in vitro mineralization.* Journal of Dental Reserach, 1996. **75**(6): p. 1381-1387.
27. Watanabe, et al., *Novel biomineralization for hydrogels: Electrophoresis approach accelerates hydroxyapatite formation in hydrogels.* Biomacromolecules, 2006. **7**(11): p. 3008-3011.
28. Goldberg, H., et al., *Determination of the hydroxyapatite-nucleating region of bone sialoprotein.* Connective Tissue Research, 1996. **35**(1-4): p. 385-392.
29. Hunter, G.K., et al., *Nucleation and inhibition of hydroxyapatite formation by mineralized tissue proteins.* Biochemical Journal, 1996. **317**: p. 59-64.
30. Hunter, G.K., C.L. Kyle, and H.A. Goldberg, *Modulation of crystal-formation by bone phosphoproteins-structural specificity of the osteopontin -mediated inhibition of hydroxyapatite formation.* Biochemical Journal, 1994. **300**: p. 723-728.
31. Hunter, G.K., et al., *Induction of collagen mineralization by a bone sialoprotein–decorin chimeric protein.* Journal of Biomedical Materials Reserach, 2000. **55**(4): p. 496-502.
32. Balluffi, R.W., S.M. Allen, and W.C. Carter, *Kinetics of Materials*. 2005: Wiley-Intersceince.
33. Boskey, A., et al., *Dentin sialoprotein (DSP) has limited effects on in vitro apatite formation and growth.* Calcified Tissue International, 2000. **67**(6): p. 472-478.
34. Boskey, A.L., et al., *Studies of Matrix Vesicle-Induced Mineralization in a Gelatin Gel.* Bone and Mineral, 1992. **17**(2): p. 257-262.
35. Boskey, A.L., B.D. Boyan, and Z. Schwartz, *Matrix vesicles promote mineralization in a gelatin gel.* Calcified Tissue International, 1997. **60**(3): p. 309-315.
36. Boskey, A.L., M. Maresca, and J. Appel, *The Effects of Noncollagenous Matrix Proteins on Hydroxyapatite Formation and Proliferation in a Collagen Gel System.* Connective Tissue Research, 1989. **21**(1-4): p. 501-508.

37. Boskey, A.L., et al., *Multifunctional Effects of Phosphophoryn on Mineralization in a Gelatin Gel.* Journal of Dental Research, 1990. **69**: p. 270-270.
38. Boskey, A.L., et al., *Effects of bone CS-proteoglycans, DS-decorin, and DS-biglycan on hydroxyapatite formation in a gelatin gel.* Calcified Tissue International, 1997. **61**(4): p. 298-305.
39. Iijima, M. and Y. Moriwaki, *Lengthwise and oriented growth of octacalcium phosphate crystal in polyacrylamide gel in a model system of tooth enamel apatite formation.* Journal of crystal growth, 1998. **194** (1): p. 125-132.
40. Iijima, M., Y. Moriwaki, and Y. Kuboki, *Effect of some physico-chemical properties of matrix on lengthwise and oriented growth of octacalcium phosphate crystal.* Connective Tissue Research, 1998. **38**(1-4): p. 171-179.
41. Iijima, M., K. Hayashi, and Y. Moriwaki, *Effects of the Ca2+ and PO43- ion flow on the lengthwise growth of octacalcium phosphate in a model system of enamel crystal formation with controlled ionic diffusion.* Journal of Crystal Growth, 2002. **234**(2-3): p. 539-544.
42. Iijima, M., et al., *Control of apatite crystal growth by the co-operative effect of a recombinant porcine amelogenin and fluoride.* European Journal of Oral Sciences, 2006. **114**(Suppl. 1): p. 304-307.
43. Iijima, M., et al., *Tooth Enamel Proteins Enamelin and Amelogenin Cooperate To Regulate the Growth Morphology of Octacalcium Phosphate Crystals.* Crystal Growth & Design, 2010. **10**(11): p. 4815-4822.
44. Iijima, M. and J. Moradian-Oldak, *Control of octacalcium phosphate and apatite crystal growth by amelogenin matrices.* Journal of Materials Chemistry, 2004. **14**(14): p. 2189-2199.
45. Iijima, M. and J. Moradian-Oldak, *Interactions of amelogenins with octacalcium phosphate crystal faces are dose dependent.* Calcified Tissue International, 2004. **74**(6): p. 522-531.
46. Iijima, M. and J. Moradian-Oldak, *Control of apatite crystal growth in a fluoride containing amelogenin-rich matrix.* Biomaterials, 2005. **26**(13): p. 1505-1603.
47. De Jong, A.S.H., T.J. Hak, and P. Van Duijn, *The dynamics of calcium phosphate precipitation studued with a new polyacrylamide steady state matrix-model: Influence of pyrophosphate, collagen and chondrotin sulfate.* Connective Tissue Research, 1980. **7**(2): p. 73-79.
48. Graeme Hunter and Harvey Goldberg, *Personal Communication*. 2008, 2010.
49. Mandel, G.S., P.B. Halverson, and N.S. Mandel, *Calcium pyrophosphate crystal depostion - the effect of soluble iron in a kinetic-study using a gelatin matrix model.* Scanning Microscopy, 1988. **2**(2): p. 1177-1188.
50. Mandel, G.S., P.B. Halverson, and N.S. Mandel, *Calcium pyropohsphate crystal deposition - the effect of monosodium urate and apatite crystals in a kinetic-study using a gelatin matrix model* Scanning Microscopy International, 1988. **2**(2): p. 1189-1198.
51. Mandel, G.S., et al., *Calciuim pyrophosphate crystal deposition disease - preparatuion and characterization of crystals.* Journal of Crystal Growth, 1988. **87**(4): p. 453-462.
52. Mandel, N. and G.S. Mandel, *Calcium pyrophosphate crystal deposition in*

model systems Rheumatic Disease Clinics of North America, 1988. **14**(2).
53. Mandel, N.S. and G.S. Mandel, *A Model For Human Calcium Pyrophosphate Crystal Deposition Disease - Crystallization Kinetics In A Gelatin Matrix.* Scanning Electron Microscopy, 1984: p. 1779-1792.
54. Mandel, N.S., et al., *Calcium Pyrophosphate Crystal Deposition - An Invitro Study Using A Gelatin Matrix Model.* Arthritis And Rheumatism, 1984. **27**(7): p. 789-796.
55. Mandel, N.S.M.a.G.S., *A Model For Human Calcium Pyrophosphate Crystal Deposition Disease Crystallization Kinetics in a Gelatin Matrix.* Scanning Electron Microscopy, 1984: p. 1779-1792.
56. Henisch, H.K., *Crystal Growth in Gels and Liesegang Rings*. 1988, Cambridge: Cambridge University Press.
57. Henisch, H.K., *Crystals in Gels and Liesegang Rings*. 1988, New York: Cambridge University Press. 197.
58. Henisch, H.K., J. Dennis, and J.I. Hanoka, *Crystal Growth in Gels.* Journal of Physics and Chemistry of Solids, 1965. **26**(3): p. 493-&.
59. Henisch, H.K., J.I. Hanoka, and J. Dennis, *Growth Rate and Defect Structure of Gel-Grown Crystals.* Journal of the Electrochemical Society, 1965. **112**(6): p. 627-&.
60. Lee, K., Mooney, DJ, *Hydrogels for tissue engineering.* Chemical Reviews, 2001. **101**(7): p. 1869-1879.
61. A single batch can be prepared by mixing several kg of gelatin purchased at one time in a large vat, although when using hydrogels at concentrations as low as 10 w/v%, a 1 kg bottle of gelatin powder tends to go a long way.
62. Veis, A., *The Macromolecular Chemistry of Gelatin*. Molecular Biology, ed. N.O.K. Bernard Horecker, Harold A. Scheraga. 1964: Academic Press - New York and London.
63. Guiseley, K.B., *Modified agarose and agar and method of making same*, U.P. Office, Editor. 1976, Marine Collids, Inc.: United States.
64. Young, R.J. and P.A. Lovell, *Introduction to polymers*. 1991, Cheltenham: Nelson Thomas Ltd. 443.
65. Lide, D.R., *CRC Handbook of Chemistry and Physics, 90th Edition*. 2009: CRC Press. 2804.
66. Cornell, S., Droz, M, Chopard, B, *Role of Fluctuations for inhomogeneous reaction-diffusion phenomena.* Physical Review A, 1991. **44**(8): p. 4826-4832.
67. Cornell, S., Koza, Z, Droz, M,, *Dynamic multiscaling of the reaction-diffusion front for mA+nB -> 0.* Physical Review E, 1993. **52**(4): p. 3500-3505.
68. Cornell, S., Droz, M, , *Steady-state reaction-diffusion front scaling for mA+nB-> inert.* Physical Review Letters, 1993. **70**(24): p. 3824-3827.
69. Galfi, L., Racz, Z, *Properties of the reaction front in an A+B->C type reaction-diffusion process.* Physical Review A, 1998. **38**(6): p. 3151-3154.
70. Ham, F., *Theory of diffusion-limited precipitation.* Journal of Physics and Chemistry of Solids, 1958. **6**(4): p. 335-351.
71. Koo, Y., Kopelman, R, *Space-resolved and time-resolved diffusion-limited binary reaction-kinetics in capillaries-experimental-observation of segregation, anomalous exponentsm and depletion zone.* Journal of statistical physics, 1991. **65**(5-6): p. 893-918.

72. Koza, Z., *The long-time behavior of initially seperated A+ B -> 0 reaction-diffusion systems with arbitrary diffusion constants.* Journal of statistical physics, 1996. **85**(1-2): p. 179-191.
73. Koza, Z., *Motion of the reaction front in the A+B->C reaction-diffusion system.* Physical Review E, 1996. **54**(2): p. R1040-R1043.
74. Srzic, D., B. Pokric, and Z. Pucar, *Precipitation in Gels under Conditions of Double Diffusion - Critical Concentrations and Solubility Products of Salts.* Zeitschrift Fur Physikalische Chemie-Frankfurt, 1976. **103**(1-4): p. 157-164.
75. Li, H.Y. and L.A. Estroff, *Porous calcite single crystals grown from a hydrogel medium.* Crystengcomm, 2007. **9**(12): p. 1153-1155.
76. Li, H.Y. and L.A. Estroff, *Hydrogels coupled with self-assembled monolayers: An in vitro matrix to study calcite biomineralization.* Journal of the American Chemical Society, 2007. **129**(17): p. 5480-5483.
77. Li, H.Y. and L.A. Estroff, *Calcite Growth in Hydrogels: Assessing the Mechanism of Polymer-Network Incorporation into Single Crystals.* Advanced Materials, 2009. **21**(4): p. 470-+.
78. Li, H.Y., et al., *Visualizing the 3D Internal Structure of Calcite Single Crystals Grown in Agarose Hydrogels.* Science, 2009. **326**(5957): p. 1244-1247.
79. Grassman, O. and P. Lobmann, *Morphogenetic control of calcite crystal growth in sulfonic acid based hydrogels.* Chemistry, 2003. **9**(6): p. 1310-1316.
80. Grassman, O., et al., *Biomimetic control of crystal assembly by growth in an organic hydrogel network.* American Mineralogist, 2003. **88**(4): p. 647-652.
81. Keene, E.C., J.S. Evans, and L.A. Estroff, *Silk Fibroin Hydrogels Coupled with the n16N-beta-Chitin Complex An in Vitro Organic Matrix for Controlling Calcium Carbonate Mineralization.* Crystal Growth & Design, 2010. **10**(12): p. 5169-5175.
82. Keene, E.C., J.S. Evans, and L.A. Estroff, *Matrix Interactions in Biomineralization: Aragonite Nucleation by an Intrinsically Disordered Nacre Polypeptide, n16N, Associated with a beta-Chitin Substrate.* Crystal Growth & Design, 2010. **10**(3): p. 1383-1389.
83. Eastoe, J.E., *The Amino Acid Composition of Mammalian Collagen and Gelatin.* Biochemical Journal, 1955. **61**(4): p. 589-600.
84. Clerici, E., A. Bairati, and P. Mocarell, *Structure and chemical composition of collagen gel.* Experientia, 1962. **18**(5): p. 241-243.
85. Arnott, S., et al., *Agarose Double Helix and Its Function in Agarose-Gel Structure.* Journal of Molecular Biology, 1974. **90**(2): p. 269-284.
86. Stellwagen, J., Stellwagen, NC, *Internal structure of the agarose-gel matrix.* Journa of Physical Chemistry, 1995. **99**(12): p. 4247-4251.
87. Chen, J.L., et al., *In vitro mineralization of collagen in demineralized fish bone.* Macromolecular Chemistry and Physics, 2005. **206**(1): p. 43-51.
88. Glimcher, M., *Mechanism of calcification-role of collage fibrils and collagen phosphoprotein complexs invitro and invivo.* Anatomical Record, 1989. **224**(2): p. 139-153.
89. Glimcher, M., *The possible role of collagen fibrils and collagen-phosphoprotein complexes in the calcificaiton of bone invitro and invivo.* Biomaterials, 1990. **11**(S): p. 7-10.
90. Silver, F.H. and W.J. Landis, *Mineral deposition in the extracellular matrices*

of vertebrate tissues: Identification of possible apatite nucleation sites on type I collagen. Cells Tissues Organs, 2009. **189**(1-4): p. 20-24.
91. Silver, F.H. and W.J. Landis, *Deposition of apatite in mineralizing vertebrate extracellular matrices: A model of possible nucleation sites on type I collagen.* Connective Tissue Research, 2011. **52**(3): p. 242-254.
92. Barbour, M.E., et al., *An investigation of some food-approved polymers as agents to inhibit hydroxyapatite dissolution.* European Journal of Oral Sciences, 2005. **113**(6): p. 457-461.
93. Wise, E.R., et al., *The organic-mineral interface in bone is predominantly polysaccharide.* Chemistry of Materials, 2007. **19**(21): p. 5055-5057.
94. Mahamid, J., et al., *Amorphous calcium phosphate is a major component of the forming fin bones of zebrafish: Indications for an amorphous precursor phase.* Proceedings of the National Academy of Sciences of the United States of America, 2008. **105**(35): p. 12748-12753.
95. Weiner, S. and O. Baryosef, *States of preservation of bones from prehistoric sites in the near-east - a survey.* Journal of Archaeological Science, 1990. **17**(2): p. 187-196.
96. Deshpande, A.S. and E. Beniash, *Bioinspired synthesis of mineralized collagen fibrils.* Crystal Growth & Design, 2008. **8**(8): p. 3084-3090.
97. Deshpande, A.S., et al., *Amelogenin-Collagen Interactions Regulate Calcium Phosphate Mineralization in Vitro.* Journal of Biological Chemistry, 2010. **285**(25): p. 19277-19287.
98. Verdelis, K., et al., *Spectroscopic imaging of mineral maturation in bovine dentin.* Journal of Dental Research, 2003. **82**(9): p. 697-702.
99. Beniash, E., et al., *Amorphous calcium carbonate transforms into calcite during sea urchin larval spicule growth.* Proceedings of the Royal Society of London Series B-Biological Sciences, 1997. **264**(1380): p. 461-465.
100. Beniash, E., et al., *Transient amorphous calcium phosphate in forming enamel.* Journal of Structural Biology, 2009. **166**(2): p. 133-143.
101. Beniash, E., J.P. Simmer, and H.C. Margolis, *The effect of recombinant mouse amelogenins on the formation and organization of hydroxyapatite crystals in vitro.* Journal of Structural Biology, 2005. **149**: p. 182-190.
102. Canham, L.T., *Bioactive silicon structure fabrication through nanoetching techniques.* Advanced Materials, 1995. **7**(12): p. 1033-1037.
103. Canham, L.T., et al., *Bioactive polycrystalline silicon.* Advanced Materials, 1996. **8**(10): p. 850-852.
104. Tanahashi, M. and T. Matsuda, *Surface functional group dependence on apatite formation on self-assembled monolayers in a simulated body fluid.* Journal of Biomedical Materials Research, 1997. **34**(3): p. 305-315.
105. Tarasevich, B.J., C.C. Chusuei, and D.L. Allara, *Nucleation and growth of calcium phosphate from physiological solutions onto self-assembled templates by a solution-formed nucleus mechanism.* Journal of Physical Chemistry B, 2003. **107**(38): p. 10367-10377.
106. Toworfe, G.K., et al., *Nucleation and growth of calcium phosphate on amine-, carboxyl- and hydroxyl-silane self-assembled monolayers.* Biomaterials, 2006. **27**(4): p. 631-642.
107. Chander, S. and F. DW, *Solubility and interfacial properties of*

hydroxyapatite: a review;. Adsorption on an surface chemistry of hydrixyapatite, ed. M. DN. 1984, New York: Plenum Press.
108. De Yoreo, J.J. and P.M. Dove, *Shaping crystals with biomolecules.* Science, 2004. **306**(5700): p. 1301-1302.
109. Dey, A., et al., *The role of prenucleation clusters in surface-induced calcium phosphate crystallization.* Nature Materials, 2010. **9**(12): p. 1010-1014.
110. Cullis, A.G., L.T. Canham, and P.D.J. Calcott, *The structural and luminescence properties of porous silicon.* Journal of Applied Physics, 1997. **82**(3): p. 909-965.
111. Mazzoleni, C. and L. Pavesi, *Application to optical-components of dieliectric porous silicon multilayers.* . Applied Physics Letters, 1995. **67**(20): p. 2983-2985.
112. Addadi, L., et al., *Mollusk shell formation: A source of new concepts for understanding biomineralization processes.* Chemistry-A European Journal, 2006. **12**(4): p. 981-987.
113. Falini, G., S. Weiner, and L. Addadi, *Chitin-silk fibroin interactions: Relevance to calcium carbonate formation in invertebrates.* Calcified Tissue International, 2003. **72**(5): p. 548-554.
114. Levi-Kalisman, Y., et al., *Structure of the nacreous organic matrix of a bivalve mollusk shell examined in the hydrated state using Cryo-TEM.* Journal of Structural Biology, 2001. **135**(1): p. 8-17.
115. Amos, F.F., C.B. Ponce, and J.S. Evans, *Formation of Framework Nacre Polypeptide Supramolecular Assemblies That Nucleate Polymorphs.* Biomacromolecules, 2011. **12**(5): p. 1883-1890.
116. Collino, S. and J.S. Evans, *Molecular specifications of a mineral modulation sequence derived from the aragonite-promoting protein n16.* Biomacromolecules, 2008. **9**(7): p. 1909-1918.
117. Metzler, R.A., et al., *Nacre Protein Fragment Templates Lamellar Aragonite Growth.* Journal of the American Chemical Society, 2010. **132**(18): p. 6329-6334.
118. Love, J.C., et al., *Self-assembled monolayers of thiolates on metals as a form of nanotechnology.* Chemical Reviews, 2005. **105**(4): p. 1103-1169.
119. Stewart, M.P. and J.M. Buriak, *New approaches toward the formation of silicon-carbon bonds on porous silicon.* Comments on Inorganic Chemistry, 2002. **23**(3): p. 179-203.
120. Zhang, Y.J. and J.J. Lu, *The transformation of single-crystal calcium phosphate ribbon-like fibres to hydroxyapatite spheres assembled from nanorods.* Nanotechnology, 2008. **19**(15).
121. Mullin, J., *Crystalization*. 3rd ed. 1992, Oxford: Buttersworth.
122. Wagman, D.D., et al., *The NBS tables of chemical thermodynamic properties - selected values for inorganic and C-1 and C-2 organic - substances in SI units* Journal of Physical and Chemical Reference Data, 1982. **11**: p. 1-&.
123. Brown, W.E., et al., *Crystallography of octacalcium phosphate.* Journal of the American Chemical Society, 1957. **79**(19): p. 5318-5319.
124. Brown, W.E., *Octalcalcium phosphate and hydroxyapatite.* Nature, 1962. **196**(4859): p. 1048-50.
125. Brown, W.E., et al., *Crystallographic and chemical relations between*

octacalcium phosphate and hydroxyapatite Nature, 1962. **196**(4859): p. 1050-55.
126. Eanes, E.D., J.D. Termine, and M.U. Nylen, *Electron-microscopic study of formation of amorphous calcium phosphate and its transformation to crystalline apatite.* Calcified Tissue Research, 1973. **12**(2): p. 143-158.
127. Termine, J.D. and E.D. Eanes, *Comparative chemistry of amorphous and apatitic calcium phosphate preparations.* Calcified Tissue Research, 1972. **10**(1): p. 171-197.
128. Eanes, E.D. and J.L. Meyer, *Maturation of crystalline calcium phosphates in aqueous suspensions at physiolocic pH.* . Calcified Tissue Research, 1977. **23**(3): p. 259-269.
129. Dorozhkin, S.V. and M. Epple, *Biological and medical significance of calcium phosphates.* Angewandte Chemie-International Edition, 2002. **41**(17): p. 3130-3146.
130. Heughebaert, J.C. and G. Montel, *Conversion of amorphous tricalcium phosphate into apatitic tricalcium phosphate* Calcified Tissue International, 1982. **34**: p. S103-S108.
131. Omelon, S.J. and M.D. Grynpas, *Relationships between Polyphosphate Chemistry, Biochemistry and Apatite Biomineralization.* Chemical Reviews, 2008. **108**(11): p. 4694-4715.
132. Brown, W.E., M. Mathew, and M.S. Tung, *Crystal-chemistry of octacalcium phosphate.* Progress in Crystal Growth and Characterization of Materials, 1981. **4**(1-2): p. 59-87.
133. Terpstra, R.A. and P. Bennema, *Crystal morphology of octacalcium phosphate - theory and observation* Journal of Crystal Growth, 1987. **82**(3): p. 416-426.
134. Nelson, D.G.A. and J.D. McLean, *High resolution eleectron-microscopy of octalcalcium phosphate and its hydrolysis products.* Calcified Tissue International, 1984. **36**(2): p. 219-232.
135. Vankemenade, M. and P.L. Debruyn, *The influence of casein on the kinetics of hydroxyapatite precipitation.* Journal of Colloid and Interface Science, 1989. **129**(1): p. 1-14.
136. Low, S.P., et al., *Evaluation of mammalian cell adhesion on surface-modified porous silicon.* Biomaterials, 2006. **27**(26): p. 4538-4546.
137. Moffat, K.L., et al., *Characterization of the structure-function relationship at the ligament-to-bone interface.* Proceedings of the National Academy of Sciences of the United States of America, 2008. **105**(23): p. 7947-7952.
138. Radhakrishnan, P., N.T. Lewis, and J.J. Mao, *Zone-specific micromechanical properties of the extracellular matrices of growth plate cartilage.* Annals of Biomedical Engineering, 2004. **32**(2): p. 284-291.
139. Zaslansky, P., A.A. Friesem, and S. Weiner, *Structure and mechanical properties of the soft zone separating bulk dentin and enamel in crowns of human teeth: Insight into tooth function.* Journal of Structural Biology, 2006. **153**(2): p. 188-199.
140. Wang, F., et al., *Histomorphometric analysis of adult articular calcified cartilage zone.* Journal of Structural Biology, 2009. **169**(3): p. 359-365.
141. Martin, I., et al., *Osteochondral tissue engineering.* Journal of Biomechanics, 2007. **40**(4): p. 750-765.

142. Mikos, A.G., et al., *Engineering complex tissues.* Tissue Engineering, 2006. **12**(12): p. 3307-3339.
143. Moffat, K.L., et al., *Orthopedic Interface Tissue Engineering for the Biological Fixation of Soft Tissue Grafts.* Clinics in Sports Medicine, 2009. **28**(1): p. 157-+.
144. Johnson, K. and R. Terkeltaub, *Inorganic pyrophosphate (PPI) in pathologic calcification of articular cartilage.* Frontiers in Bioscience, 2005. **10**: p. 988-997.
145. Kalya, S. and A.K. Rosenthal, *Extracellular matrix changes regulate calcium crystal formation in articular cartilage.* Current Opinion in Rheumatology, 2005. **17**(3): p. 325-329.
146. Terkeltaub, R.A., *Inorganic pyrophosphate generation and disposition in pathophysiology.* American Journal of Physiology-Cell Physiology, 2001. **281**(1): p. C1-C11.
147. Allan, K.S., et al., *Formation of biphasic constructs containing cartilage with a calcified zone interface.* Tissue Engineering, 2007. **13**(1): p. 167-177.
148. Tanaka, T., et al., *Use of a biphasic graft constructed with chondrocytes overlying a beta-tricalcium phosphate block in the treatment of rabbit osteochondral defects.* Tissue Engineering, 2005. **11**(1-2): p. 331-339.
149. Terkeltaub, R.A., *What does cartilage calcification tell us about osteoarthritis?* Journal of Rheumatology, 2002. **29**(3): p. 411-415.
150. Brown, E.H., et al., *Preparation and characterization of some calcium pyrophosphates.* Fertilizer Materials, 1963. **11**(3): p. 214-222.
151. Gamsjaeger, S., et al., *Cortical bone composition and orientation as a function of animal and tissue age in mice by Raman spectroscopy.* Bone, 2010. **47**(2): p. 392-399